Practical applications of unilateral models to Masonry Equilibrium

Maurizio Angelillo[‡]
[‡] Dipartimento di Ingegneria Civile, University of Salerno, Italy

Abstract This Chapter is devoted to the application of unilateral models to the stress analysis of masonry structures. Some 2d applications of what we call the simplified models for masonry, are discussed and studied. Though the essentially unilateral behaviour of masonry is largely recognized, some prejudices still persist on the possibility of making the No-Tension (NT) assumption a practical model for designing engineers. The results here presented demonstrate that the unilateral model for masonry can be a useful tool for modeling real masonry structures. In the exposition the critical points are emphasized and strategies to handle them are suggested, both for the most primitive model (namely the Rigid NT material), and for the more accurate Normal Elastic NT and Masonry-Like (ML)materials. The first tool here introduced for applying the No-Tension model to structures is the systematic use of singular stress and strain fields. Next a number of closed form solutions for NENT and ML materials is discussed. Finally a numerical approach based on descent is proposed for handling the zero-energy modes typical of unilateral materials. Some numerical solutions and comparisons with analytical solutions and test results are also presented.

This Chapter is dedicated to Giovanni Castellano who inspired most of my work on masonry since my early steps.

1 Basic tools

In this section the main notation and the basic notions of equilibrium and compatibility, in presence of singular stress and strain fields, are introduced. Singular strains are usually considered in perfect plasticity, and the use of singular stress fields (though in a mathematically unconscious way) has been around since the nineteenth century (see Mery (1840)). It is only fairly recently that Šilhavý, Lucchesi et al (see Lucchesi and Zani (2005)) , have put forward a rigorous mathematical formulation of stress field singularities. Chapters 2 and 3 of the present book are partly devoted to the mathematical exposition of these clever concepts within the theory of measures.

M. Angelillo (Ed.), *Mechanics of Masonry Structures*, CISM International Centre for Mechanical Sciences, DOI 10.1007/ 978-3-7091-1774-3_4, © CISM, Udine 2014

The formulation that is given here, instead, is rather informal and based mainly on geometrical arguments. A substantial knowledge of the mathematical theory of linear elasticity, such as that given in the monograph by Gurtin (1972), to which I refer for notations, is presumed. Familiarity with functional analysis is not strictly required, though some previous experience with elementary functional analysis in Sobolev spaces and variational methods (as can be found, for example, in the books by Kreyszig (1989) and Dym and Shames (1973)) would be of help.

The matter treated and analysed here is not entirely new. Much of what is reported, apart from the classical and more recent sources cited throughout the text, leans on a number of papers recently published, or under print or review, by myself or my reserch group. In particular, on singular stress: Angelillo et al. (2012) and Angelillo et al. (2013); on Limit Analysis for masonry: Angelillo and Fortunato (2013); on semianalitical solutions for panels: Fortunato (2010); on numerical methods for unilateral materials Angelillo et al. (2010).

1.1 Preliminaries

It is assumed that the body, a domain $\Omega \in \Re^n$ (here n=2), loaded by the given tractions $\underline{\mathbf{s}}$ on the part $\partial\Omega_N$ of the boundary, and subject to given displacements $\underline{\mathbf{u}}$ on the complementary, constrained part of the boundary $\partial\Omega_D$, is in equilibrium under the given surface displacements, tractions and body loads $(\underline{\mathbf{u}}; \underline{\mathbf{s}}, \mathbf{b})$[1] and undergoes displacements $\mathbf{u}$ and local deformations, so small that the infinitesimal strain $\mathbf{E}(\mathbf{u})$ is a proper strain measure.

Vectors and tensors are represented in Cartesian components, in a fixed frame $(0; x_1, x_2)$. Summation convention is adopted throughout the text.

1.2 Equilibrated stress fields, regularity of T

A stress field $\mathbf{T}$ is said to be *equilibrated* with $(\underline{\mathbf{s}}, \mathbf{b})$, if it satisfies the equilibrium equations

$$div\mathbf{T} + \mathbf{b} = \mathbf{0} \,,$$

and the traction boundary conditions

$$\mathbf{T}\mathbf{n} = \underline{\mathbf{s}} \,, \; on \; \partial\Omega_N \,,$$

$\mathbf{n}$ denoting the unit outward normal to $\partial\Omega$.

[1] Other possible data are the eigenstrains $\underline{\mathbf{E}}$; here I omit them from the analysis to simplify the exposition, though some special eigenstrains will be considered as data in some of the examples which follow.

$\mathbf{T}$ is a tensor function of $\mathbf{x} \in \Omega$, for which some kind of regularity must be assumed. If the differential equations of equilibrium are considered in a *strong sense*, the stress field $\mathbf{T}$ must be differentiable and its divergence must be continuous.

On adopting a variational formulation, if the material is linearly elastic, the minimal request for $\mathbf{T}$ is to be square summable, that is

$$\sqrt{\int_\Omega \mathbf{T} \cdot \mathbf{T} da} < \infty \, .$$

For some rigid perfectly plastic materials (such as rigid unilateral materials), less regular and even singular stresses may be admitted. The minimal request for such materials is that $\mathbf{T}$ be summable

$$\int_\Omega \sqrt{\mathbf{T} \cdot \mathbf{T}} da < \infty \, .$$

If one admits stress fields that are only summable, the set of competing functions enlarges to bounded measures, that is to summable distributions $\widetilde{\mathbf{T}}$:

$$\int_\Omega \left| \widetilde{\mathbf{T}} \right| < \infty \, ,$$

which, in general, can be decomposed into the sum of two parts

$$\widetilde{\mathbf{T}} = \widetilde{\mathbf{T}}_r + \widetilde{\mathbf{T}}_s \, ,$$

where $\widetilde{\mathbf{T}}_r$ is absolutely continuous with respect to the area measure (that is $\widetilde{\mathbf{T}}_r$ is a density per unit area) and $\widetilde{\mathbf{T}}_s$ is the singular part.

In the examples, the analysis will be restricted to bounded measures $\widetilde{\mathbf{T}}$ whose singular part is concentrated on a finite number of regular arcs, that is bounded measures admitting on such curves a density $\widetilde{\mathbf{T}}_s$ with respect to the length measure (that is special bounded measures with void Cantor part; for reference to these function spaces see Ambrosio et al. (2000)).

Remark 1. If the stress field is summable (and also if it is square summable), it is not differentiable in strong sense, and the equilibrium equations have to be reformulated in variational form (e.g. through the Virtual Work equation). Singular stresses require also special modifications of the boundary conditions; the trace of the stress $\mathbf{T}$ on the loaded part of the boundary is not given by $\mathbf{Tn}$ if $\mathbf{T}$ is singular. I shall come to this point later.$\diamond$

1.3 Compatible displacement fields, regularity of u

The displacement field $\mathbf{u}$ is said to be compatible if, besides being *regular enough* for the corresponding strain $\mathbf{E}(\mathbf{u})$ to exist [2], $\mathbf{u}$ satisfies the boundary conditions on the constrained part $\partial\Omega_D$ of the boundary

$$\mathbf{u} = \underline{\mathbf{u}} \ , \ on \ \partial\Omega_D \ .$$

For linearly elastic bodies, on adopting a variational formulation, the usual assumption is that $\mathbf{E}$ be square summable, that is

$$\sqrt{\int_\Omega \mathbf{E} \cdot \mathbf{E} da} < \infty \ .$$

For some rigid, perfectly plastic (or rigid unilateral) materials, it is sufficient to assume that $\mathbf{E}$ be summable

$$\int_\Omega \sqrt{\mathbf{E} \cdot \mathbf{E}} da < \infty \ .$$

As before, the set of competing functions enlarges to bounded measures, that is to summable distributions $\widetilde{\mathbf{E}}$; then the displacement $\mathbf{u}$ can admit finite discontinuities, i.e. $\mathbf{u}$ can be a function with bounded variation. If $\mathbf{E}$ were the whole gradient of $\mathbf{u}$, the summability of $\mathbf{E}$ would entail: $\mathbf{u} \in BV(\Omega)$, exactly. Since $\mathbf{E}$ is only the symmetric part of $\nabla\mathbf{u}$, $\mathbf{u}$ must belong to a larger space: $BD(\Omega)$. The strain corresponding to $\mathbf{u}$ is again a bounded measure

$$\int_\Omega \left|\widetilde{\mathbf{E}}\right| < \infty \ ,$$

which, in general, can be decomposed into the sum of two parts

$$\widetilde{\mathbf{E}} = \widetilde{\mathbf{E}}_r + \widetilde{\mathbf{E}}_s \ ,$$

where $\widetilde{\mathbf{E}}_r$ is absolutely continuous with respect to the area measure (that is $\widetilde{\mathbf{E}}_r$ is a density per unit area) and $\widetilde{\mathbf{E}}_s$ is the singular part.

$\widetilde{\mathbf{E}}_s$ has support on the union of a set of linear 1d measure (the jump set of $\mathbf{u}$) and a set of fractional measure.

For simplicity, in the examples, I shall restrict to bounded measures $\widetilde{\mathbf{E}}$ whose singular part is concentrated on a finite number of regular arcs, that is bounded measures admitting on such curves a density $\widetilde{\mathbf{E}}_s$ with respect

[2] Recall that, here, $\mathbf{E}(\mathbf{u})$ is the infinitesimal strain

to the length measure (that is special bounded measures with void Cantor part).

Remark 2. If $\mathbf{u} \in BD(\Omega)$, that is $\mathbf{u}$ can be discontinuous, the b.c. $\mathbf{u} = \underline{\mathbf{u}}$ on $\partial\Omega_D$ makes no sense. A way to keep alive the b.c. of Dirichelet type is to identify the masonry body rather than with the domain Ω (usually an open set) with the set $\Omega \cup \partial\Omega_D$ and to assume that $\mathbf{u}$ must comply with the constraint $\mathbf{u} = \underline{\mathbf{u}}$ on the *skin* $\partial\Omega_D$, admitting possible singularities of the strain at the constrained boundary. Then, from here on, I shall deviate from standard notation referring to Ω as to the set $\Omega \cup \partial\Omega_D$. $\diamond$

Given the displacement field $\mathbf{u}$ of $\mathbf{x}$, by taking the gradient of $\mathbf{u}$, in a classical sense if $\mathbf{u}$ is regular, and in a generalized sense if $\mathbf{u}$ is singular, the strain $\mathbf{E}(\mathbf{u})$ is derived. *Vice versa*, if $\mathbf{E}$ of $\mathbf{x}$ is given, the possibility of integrating the components $E_{\alpha\beta}$ to get the (possibly discontinuous) components u_α of $\mathbf{u}$, is submitted to the necessary compatibility conditions (also sufficient if Ω is simply connected)

$$E_{11,22} + E_{22,11} - 2E_{12,12} = 0 \ ,$$

where a comma followed by an index, say α, means differentiation with respect to x_α.

The reader will see in what follows, that, on admitting discontinuous displacements, this condition can be reinterpreted in a generalized sense and applied (with some care), also to discontinuous, and even singular, strains.

1.4 Dirac deltas: a familiar example

For the unilateral models that here are adopted for masonry materials, it makes sense to admit singular stresses and strains, that is stress fields $\mathbf{T}$ and strain fields $\mathbf{E}$ that can be concentrated on lines (line Dirac deltas). In mathematical terms these are not functions in a strict sense, since they assign finite values to all points $\mathbf{x} \in \Omega$, except to those belonging to a set of lines of $\Omega \cup \partial\Omega_D$, to which infinite values are associated. Anyway, these infinite values must be such that these stresses or strains be summable, that is

$$\int_\Omega |\mathbf{T}| < \infty \ , \ \int_\Omega |\mathbf{E}| < \infty \ ,$$

or, in other words, $\mathbf{T}$ and $\mathbf{E}$ must be bounded measures. Here I call $M(\Omega)$ the set of bounded measures on $\Omega \cup \partial\Omega_D$. Line Dirac deltas are special bounded measures; a simple example of a Dirac delta in 1d, is the concentrated load on a beam, that is a point Dirac delta (Figure 1).

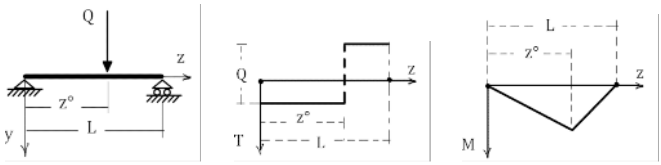

Figure 1. Concentrated transverse force Q on a beam: (a). Corresponding internal shear force T: (b), and bending moment M: (c).

From elementary beam theory the internal moment M, the shear force T and the transverse load per unit length q, are related by the differential equilibrium relations

$$M' = T\,,\ T' = -q\,,$$

where *prime* denotes differentiation with respect to z.

The previous equilibrium conditions admit also the following integral form

$$T(z) = T(0) - \int_0^z q\ ,\ M(z) = M(0) + \int_0^z T\ .$$

The second set of equations have sense also if q is a concentrated force, that is a Dirac delta:

$$q(z) = Q\delta(z^o)\ ,$$

Q being the intensity of the load, $\delta(.)$ the unit Dirac delta, z^o the point of application of the force.

The unit point Dirac delta applied at z^o is defined as follows

$$\int_{z^o-\epsilon}^{z^o+\epsilon} \delta(z^o) = 1\ ,\ \forall \epsilon > 0\ .$$

The differential equations can be extended to the case of singular loads by interpreting -q in Figure 1a as the generalized derivative of T in Figure 1b.

More generally, in 1d, the generalized derivative of a piecewise constant function f is a distribution whose regular part is zero and whose singular part has support on the jump set of f. Therefore a piecewise constant function is a special BV function whose singular part consists of point Dirac deltas applied at the points of discontinuity of f. The integral of such Dirac deltas across any point of discontinuity gives the value of the jump of f, at that point.

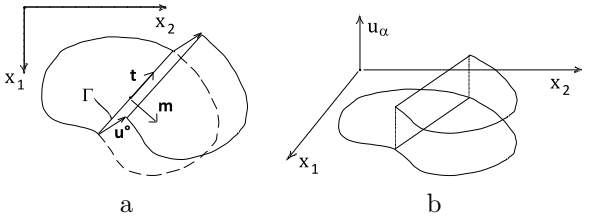

Figure 2. Discontinuous displacement alog a straight line Γ, unit tangent **t** and normal **m** to Γ: (a). Graph of the generic component u_α, a BV function: (b).

1.5 Singular stress and strain as line Dirac deltas

In what follows I will restrict to consider stress and strain fields that are special bounded measures, namely Dirac deltas with support on a finite number of regular arcs, and look at the restrictions imposed on these singular fields by equilibrium and compatibility, respectively.

Strain. In what follows, special displacement fields of bounded variation will be considered. In particular, restricting to discontinuous displacement fields **u** having finite discontinuities on a finite number of regular arcs Γ, the strain $\mathbf{E}(\mathbf{u})$ consists of a regular part $\mathbf{E}_r$, that is a diffuse deformation over $\Omega - \Gamma$, and a singular part $\mathbf{E}_s$ in the form of a line Dirac delta, concentrated on Γ.

The jumps of **u** along Γ, can be interpreted as fractures. In Figure 2a, to which I refer for notations, a crack separating the body Ω into two parts, $\wp_1$ and $\wp_2$, along a straight interface Γ, is represented. On such a line, the jump of **u**:

$$[[\mathbf{u}]] = \mathbf{u}^+ - \mathbf{u}^- \ .$$

due to a relative translation of the two parts, is considered. Here $\mathbf{u}^+$ is the displacement on the side of Γ where **m** points

The displacement field is a piecewise constant vector field, discontinuous on Γ; the graph of a generic Cartesian component of **u**, is depicted in Figure 2b.

The jump of **u** can be decomposed into normal and tangential components

$$\Delta v = [[\mathbf{u}]] \cdot \mathbf{m} \ , \ \Delta w = [[\mathbf{u}]] \cdot \mathbf{t} \ ,$$

where $\mathbf{t}, \mathbf{m}$ are the unit tangent and normal to Γ, represented in Figure 2a. Notice that, on any crack, incompenetrability of matter requires $\Delta v \geq 0$ (a unilateral restriction).

The strain $\mathbf{E}$ corresponding to the piecewise constant field $\mathbf{u}$ depicted in Figure 2b, is zero everywhere on $\Omega - \Gamma$ and is singular on Γ:

$$\mathbf{E}(\mathbf{u}) = \delta(\Gamma)(\Delta v \mathbf{m} \otimes \mathbf{m} + \frac{1}{2}\Delta w \mathbf{t} \otimes \mathbf{m} + \frac{1}{2}\Delta w \mathbf{m} \otimes \mathbf{t}) \ .$$

Stress. If the stress field $\mathbf{T}$ is non-singular (say $\mathbf{T} \in L^2(\Omega)$), on a possible discontinuity line Γ, for equilibrium, the stress emerging on Γ must be continuous. Then at any regular point of Γ, denoting $\mathbf{m}$ the unit normal to Γ, the stress $\mathbf{T}$ must satisfy the condition

$$(\mathbf{T}^+ - \mathbf{T}^-)\mathbf{m} = \mathbf{0} \ ,$$

$\mathbf{T}^+$ being the stress on the side of Γ where $\mathbf{m}$ points. Then, if $\mathbf{T} \in L^2(\Omega)$, the possible jumps of $\mathbf{T}$ must be restricted to the part of $\mathbf{T}$ non-emerging on Γ.

If $\mathbf{T}$ is singular, say a Dirac delta on Γ, also the part of $\mathbf{T}$ emerging on Γ can be discontinuous. The unbalanced emerging stress

$$\mathbf{q} = (\mathbf{T}^+ - \mathbf{T}^-)\mathbf{m} \ ,$$

in equilibrium, must be balanced by the stress concentrated on Γ (Figure 3). Referring for notations to Figure 3, the representation of the singular part $\mathbf{T}_s$ of $\mathbf{T}$ on Γ, is

$$\mathbf{T}_s = N\delta(\Gamma)\mathbf{t} \otimes \mathbf{t} \ .$$

For equilibrium, calling p, q the components of $\mathbf{q}$ in the tangential and normal directions, and denoting ρ the curvature of Γ, the following equations must hold

$$N' + p = 0 \ , \ N\,\rho + q = 0 \ .$$

Therefore q must be zero if Γ is straight.

Kinks. Though the singularity lines Γ, for the stress $\mathbf{T}$, that I consider are a.e. smooth, they can have kinks and multiple points. At such nodes the equilibrium of forces transmitted to the nodes must be satisfied; then if the node is inside the body and there are no concentrated external forces applied to the node there must be at least a triple junction.

Airy's stress function and singular stresses. In absence of body forces ($\mathbf{b}$=$\mathbf{0}$), the equilibrium equations admit the following solution in terms of a scalar function F:

$$T_{11} = F_{,22} \ , \ T_{22} = F_{,11} \ , \ T_{12} = -F_{,12} \ .$$

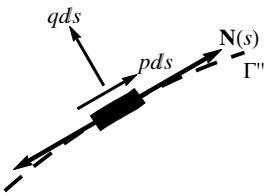

Figure 3. Stress singularity: forces acting on the curve Γ.

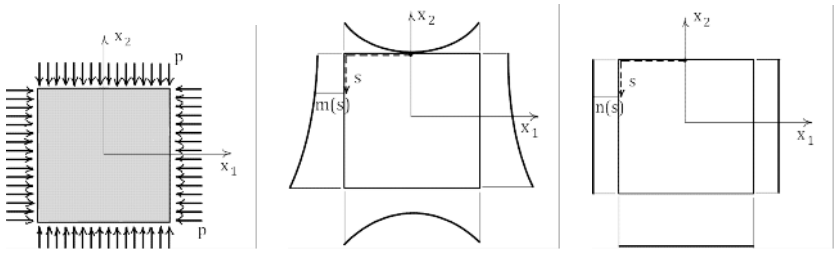

Figure 4. Square panel under uniform pressure: (a). Corresponding boundary value $m(s)$: (b), and normal slope $n(s)$: (c).

This is the general solution of the equilibrium equations, if the loads are *self-balanced* on any closed boundary delimiting Ω (see Gurtin (1972)).

The b.c. $\mathbf{T}\ \mathbf{n} = \underline{\mathbf{s}}$ on $\partial\Omega_N$, must be reformulated in terms of F. Denoting $\mathbf{x}(s)$ the parametrization of $\partial\Omega_N$ with the arc length, the b.c. on F are:

$$F(s) = m(s)\ ,\ \frac{dF}{d\nu} = n(s)\ ,\ on\ \partial\Omega_N\ ,$$

in which $dF/d\nu$ is the normal derivative of F at the boundary (that is the slope of F in the direction of $\mathbf{n}$) and $m(s)$, $n(s)$ are the moment of contact and the axial force of contact produced by the tractions $\underline{\mathbf{s}}(s)$, on a beam structure having the same shape of $\partial\Omega$, and cut at the point s=0.

A simple example is shown in Figure 4.

Regular and singular equilibrated stress fields can be derived by stress functions meeting the prescribed b.c. on F and $dF/d\nu$. A regular stress field is represented by a smooth F (see Figure 5a), a singular stress field by a continuous but folded F (Figure 5b). The projection of a fold of F on Ω is

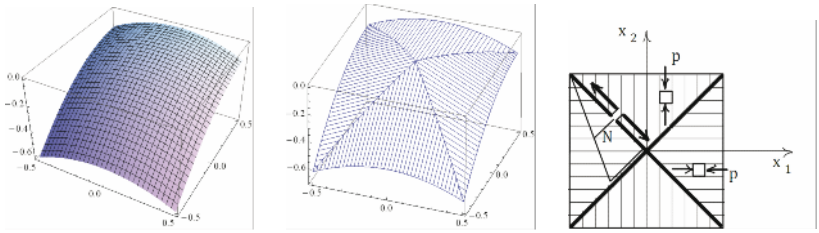

a b c

Figure 5. Square panel under uniform pressure. Smooth Airy's stress function giving homogeneous pressure inside the body: (a); folded Airy's function: (b); representation of the uniaxial and singular stress field corresponding to the folded Airy's function: (c).

called folding line and is denoted Γ. On a fold of F, the second derivative of F, with respect to the normal $\mathbf{m}$ to the folding line Γ, is a Dirac delta with support on Γ. Therefore, along Γ the Hessian $\mathbf{H}(F)$ of the stress function F is a dyad of the form

$$\mathbf{H}(F) = \Delta_m F \delta(\Gamma) \mathbf{m} \otimes \mathbf{m} \, ,$$

$\Delta_m F$ denoting the jump of slope of F in the direction of the normal $\mathbf{m}$ to Γ (see Figure 5c). Recalling the Airy's relation, the corresponding singular part of the stress is

$$\mathbf{T}_s = N \delta(\Gamma) \mathbf{t} \otimes \mathbf{t} \, ,$$

where the axial contact force N is given by

$$N = \Delta_m F \, .$$

2 Model *zero* (RNT)

In this section the main ingredients of the theory concerning the most primitive model for masonry materials, namely the Rigid No-Tension (RNT) material, are presented. After introducing the constitutive assumptions, the definitions of statically admissible and kinematically admissible fields are given, and the compatibility of loads and distortions is discussed. The RNT model allows for the application of the theorems of Limit Analysis: the formulation of the static and kinematic theorems for rigid-unilateral materials is given and a number of illustrative examples is developed.

2.1 Constitutive restrictions and equilibrium problem

It is assumed that the body $\Omega \in \Re^n$ (here $n = 2$), loaded by the given tractions $\underline{\mathbf{s}}$ on the part $\partial\Omega_N$ of the boundary, and subject to given displacements $\underline{\mathbf{u}}$ on the complementary, constrained part of the boundary $\partial\Omega_D$, is in equilibrium under the action of such given surface displacements and tractions, besides body loads $\mathbf{b}$ and distortions $\underline{\mathbf{E}}$ (the set of data being denoted: $(\underline{\mathbf{u}}, \underline{\mathbf{E}}; \underline{\mathbf{s}}, \mathbf{b})$), and undergoes small displacements $\mathbf{u}$ and strains $\mathbf{E}(\mathbf{u})$[3].

I point out that here the masonry structure is identified with the set: $\Omega = \Omega \cup \partial\Omega_D$, i.e. it is considered closed on $\partial\Omega_D$ and open on the rest of the boundary.

I consider that the body Ω is composed of Rigid No-Tension material, that is the stress $\mathbf{T}$ is negative semidefinite

$$\mathbf{T} \in Sym^{-} \ , \tag{1}$$

the effective strain $\mathbf{E}^* = \mathbf{E}(\mathbf{u}) - \underline{\mathbf{E}}$ is positive semidefinite

$$\mathbf{E}^* \in Sym^{+} \ , \tag{2}$$

and the stress $\mathbf{T}$ does no work for the corresponding effective strain $\mathbf{E}^*$

$$\mathbf{T} \cdot \mathbf{E}^* = 0 \ . \tag{3}$$

The effective strain E^* is a positive definite tensor field doing no work for the corresponding stress, and representing detachment fractures (that is type 1. fractures, see Sect.2, Chap.1). E^* is a sort of "reaction" deformation associated to the constraint on stress (1), and, therefore, is also called latent strain. In order to avoid trivial incompatible loads ($\underline{\mathbf{s}}$,$\mathbf{b}$), it is assumed that the tractions $\underline{\mathbf{s}}$ satisfy the condition

$$\underline{\mathbf{s}} \cdot \mathbf{n} < 0 \ , \ or \ \underline{\mathbf{s}} = \mathbf{0}, \ \forall \mathbf{x} \in \partial\Omega_N \ . \tag{4}$$

Notice that in the plane case (n=2) conditions (1), (2), can be rewritten as

$$tr\,\mathbf{T} \leq 0 \ , \ det\,\mathbf{T} \geq 0 \ , \tag{5}$$

$$tr\,\mathbf{E}^* \geq 0 \ , \ det\,\mathbf{E}^* \geq 0 \ . \tag{6}$$

[3]When eigenstrains are considered, under the small strain assumption, the total strain $\mathbf{E}(\mathbf{u})$ is decomposed additively as follows: $\mathbf{E}(\mathbf{u}) = \mathbf{E}^* + \underline{\mathbf{E}}$, $\mathbf{E}^*$ being the *effective* strain of the material.

2.2 Statically admissible stress fields

An equilibrated stress field $\mathbf{T}$ (that is a stress field $\mathbf{T}$ balanced with the prescribed body forces $\mathbf{b}$ and the tractions $\underline{\mathbf{s}}$ given on $\partial\Omega_N$) satisfying the unilateral condition (1) (that is conditions (5)), is said *statically admissible* for a RNT body. The set of statically admissible stress fields is denoted H and is defined as follows

$$H = \left\{ \mathbf{T} \in S(\Omega) \; s.t. \; div\mathbf{T} + \mathbf{b} = \mathbf{0} \; , \; \mathbf{Tn} = \underline{\mathbf{s}} \; on \; \partial\Omega_N \; , \; \mathbf{T} \in Sym^- \right\} \; , \quad (7)$$

$S(\Omega)$ being a function space of convenient regularity. Since for RNT materials, discontinuous and even singular stress fields will be considered, one can assume $S(\Omega) = M(\Omega)$, that is the set of bounded measures.

For Elastic No-Tension (ENT) materials a sensible choice is $S(\Omega) = L^2(\Omega)$, that is the function space of square summable functions.

Actually the space $M(\Omega)$ contains $L^2(\Omega)$ and is much larger than it, that is the set of functions which compete for equilibrium is richer for RNT than for ENT materials; this fact makes easier for RNT materials the search of s.a. stress fields.

The differential equations of equilibrium must be reformulated for non smooth $\mathbf{T}$, since the derivatives of $\mathbf{T}$ do not exist in a classical sense[4]. One way to do it is to impose equilibrium in a variational form, namely by using the Virtual Work Principle.

On introducing the set of virtual displacements

$$\delta K = \{ \delta\mathbf{u} \in S^*(\Omega) \; s.t. \; \delta\mathbf{u} = \mathbf{0} \; on \; \partial\Omega_D \} \; , \quad (8)$$

the stress field $\mathbf{T}$ is balanced with ($\underline{\mathbf{s}}$,$\mathbf{b}$) if and only if

$$\int_{\partial\Omega_N} \underline{\mathbf{s}} \cdot \delta\mathbf{u} + \int_\Omega \mathbf{b} \cdot \delta\mathbf{u} = \int_\Omega \mathbf{T} \cdot \mathbf{E}(\delta\mathbf{u}) \; , \; \forall \delta\mathbf{u} \in \delta K \, . \quad (9)$$

$S^*(\Omega)$ is a function space of convenient regularity. If $\mathbf{T} \in L^2(\Omega)$, then $S^*(\Omega) = H^1(\Omega)$ guarantees the finiteness of the internal work. If $\mathbf{T} \in M(\Omega)$, the choice $S^*(\Omega) = C^1(\Omega)$ ensures the possibility of computing the internal virtual work.

[4] For singular stress fields, even the b.c. on the emerging tractions must be changed, since the *Cauchy argument* leading to them, is restricted to absolutely continuous stress vectors.

2.3 Fundamental partition

To any statically admissible stress field $\mathbf{T}$ one can associate the following partition of the domain $\Omega = \Omega \cup \partial\Omega_D$:

$$\Omega_1 = \{\mathbf{x} \in \Omega \; s.t. \; tr\mathbf{T} \leq 0 \; , \; det\mathbf{T} \geq 0\} \; , \tag{10}$$

$$\Omega_2 = \{\mathbf{x} \in \Omega \; s.t. \; tr\mathbf{T} \leq 0 \; , \; det\mathbf{T} = 0\} \; , \tag{11}$$

$$\Omega_3 = \{\mathbf{x} \in \Omega \; s.t. \; \mathbf{T} = 0\} \; . \tag{12}$$

On introducing the spectral decomposition of $\mathbf{T}$:

$$\mathbf{T} = \sigma_1 \, \mathbf{k}_1 \otimes \mathbf{k}_1 + \sigma_2 \, \mathbf{k}_2 \otimes \mathbf{k}_2 \; ,$$

in Ω_1 the stress is of biaxial compression, that is $\sigma_1 < 0$, $\sigma_2 < 0$; in Ω_2 the stress is of uniaxial compression, that is $\mathbf{T}{=}\sigma \, \mathbf{k} \otimes \mathbf{k}$, $\sigma < 0$; Ω_3 is inert.

Notice that the form and the regularity of these regions depend on the smoothness of $\mathbf{T}$, and that such regions can be rather weird if one admits $\mathbf{T} \in M(\Omega)$. We will see in what follows that, on admitting only special bounded measures (i.e. Dirac deltas with support on a finite number of regular arcs), the regions Ω_i can degenerate, but the *fundamental partition* can be still easily identified.

Remark 3. In the Ω_2 regions, that is where the stress is of uniaxial compression, a classical theorem of *Tension Field Theory* (see *Subsection* 3.8 and Remark 9), states that (as the intuition suggests, see below and Figure 6) the lines of principal compression (tension in the case of TFT) form a family of straight lines if the body forces vanish.

A simple geometrical proof of this statement can be obtained by observing that, the equilibrium of a material tube contained in between two such infinitesimally spaced principal lines, is possible only if the tube is straight and the internal axial force of contact N is constant (see Figure 6).

If the two contiguous lines are parallel the stress itself is constant. If the two lines converge, on denoting R the distance between the point P and the point of intersection of the two lines, and introducing the arc length s along the ray from the origin P, calling $\sigma(s)$ and σ° the stress at Q and the stress at P, for equilibrium, the stress along the ray takes the form

$$\sigma(s) = \frac{R}{R-s}\sigma^\circ \; .$$

$\diamond$

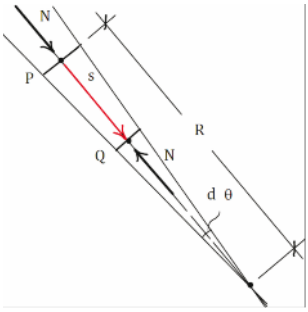

Figure 6. Stress along a compression ray.

2.4 Concavity of the Airy's stress function

In absence of body forces, a statically admissible stress field can be expressed[5] in terms of a scalar function F (called *Airy's solution*, see *subsection* 1.5).

The constraint (5), translated in terms of F, reads

$$tr\,\mathbf{T} = F_{,11} + F_{,22} \leq 0\ ,\ det\,\mathbf{T} = F_{,11}\,F_{,22} - F_{,12}^2 \geq 0\ , \tag{13}$$

then the Hessian $\mathbf{H}(F)$ of F, is negative semidefinite and the stress function F must be concave. Therefore, in absence of body forces $\mathbf{b}$, the equilibrium problem for a NT material, can be formulated as the search of a concave function F, taking on the part $\partial\Omega_N$ of the boundary, a specified value and a specified slope.

Example. As a simple example of an *equilibrium problem*, I consider the traction problem depicted in Figure 7a. Smooth and singular statically admissible stress fields can be easily derived from simple stress functions matching the given boundary data.

A smooth solution can be derived from the stress function (here L=1 is assumed):

$$F = \begin{cases} -\frac{3}{2}p + 2px_2\ ,\ x_2 < \frac{1}{2}(1-x_1^2)\ , \\ -\frac{1}{2}px_1^2 - 2p\frac{(1-x_2^2)^2}{1+x_1^2}\ ,\ x_2 \geq \frac{1}{2}(1-x_1^2)\ . \end{cases}$$

This F is a composite surface, flat in the region denoted Ω_3 in Figure 7c, and strictly concave in Ω_1. The graph of such F is depicted in Figure 7b. I

[5] Univocally, if the body is simply connected or loaded by self balanced tractions on any closed boundary.

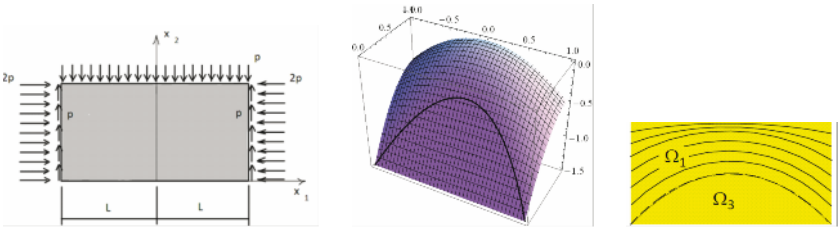

a b c

Figure 7. Wall beam under uniform transverse load: (a). Graph of the Airy's stress function, corresponding to the smooth solution: (b). Domain partition and one of the families of compression lines corresponding to the smooth solution: (c).

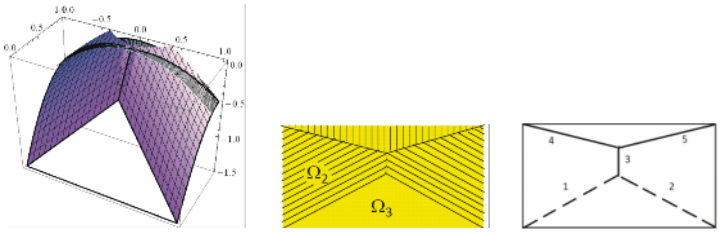

a b c

Figure 8. Graph of the folded Airy's function, showing the intersection of the generating surfaces: (a). Corresponding domain partition and principal lines of compression: (b). Support of the singular stress (solid lines 3, 4, 5): (c).

leave to the reader to verify that the corresponding $\mathbf{T}$ is statically admissible, that is that such $\mathbf{T}$ matches the boundary data and belongs to Sym^-.

A singular statically admissible stress field is derived from the stress function F depicted in Figure 8a. F is a continuous non-smooth function: the surface F, making (concave) folds along the lines indicated with 3, 4, 5 in Figure 8c, can be easily produced by prolongating the datum $F|_{\partial\Omega}$ with ruled surfaces having the prescribed slope $\frac{dF}{d\nu}|_{\partial\Omega}$ at the boundary. The intersections of the four ruled surfaces emanating from the boundary (see Figure 8a) give the folding lines; the jump of slope hortogonal to the folding line gives the value of the axial force along the line:

$$\mathbf{T}_s = N\delta(\Gamma)\mathbf{t} \otimes \mathbf{t} \, .$$

Since the fold is concave the jump of slope is negative, then

$$N = \Delta_m F \, < \, 0 \, .$$

In Figure 8b the principal lines of uniaxial compression corresponding to the non smooth solution are reported.

2.5 Kinematically admissible displacement fields

A compatible displacement field $\mathbf{u}$, that is a displacement $\mathbf{u}$ matching the given displacements $\underline{\mathbf{u}}$ on $\partial\Omega_D$ for which $(\mathbf{E}(\mathbf{u})$ - $\underline{\mathbf{E}}) \in Sym^+$, i.e. such that the *effective strain* satisfies the unilateral conditions (6), is said to be *kinematically admissible* for a RNT body.

The set of kinematically admissible displacement fields is denoted K and is defined as follows:

$$K = \left\{ \mathbf{u} \in T(\Omega) \; s.t. \; \mathbf{u} = \underline{\mathbf{u}} \; on \; \partial\Omega_D \; , \; \mathbf{(E(u)\text{-}\underline{E})} \in Sym^+ \right\} \; , \qquad (14)$$

where $\Omega = \Omega \cup \partial\Omega_D$ and $T(\Omega)$ is a function space of convenient regularity. Since for RNT materials, discontinuous displacements can be considered, one can assume $T(\Omega) = BV(\Omega)$, that is the set of functions of bounded variation (the functions whose gradient belongs to $M(\Omega)$, i.e. functions $\mathbf{u}$ admitting finite discontinuities). I restrict to the subset of $BV(\Omega)$, consisting of displacement fields $\mathbf{u}$ having finite jumps on a finite number of regular arcs. Actually, as we shall see, I will need only to consider discontinuous functions $\mathbf{u}$ whose jump set is the union of a finite number of segments.

The differential relation between $\mathbf{E}$ and $\mathbf{u}$, likewise the displacement b.c., must be reformulated in a weak form, since the derivative of $\mathbf{u}$ does not exist in a classical sense, and the trace of $\mathbf{u}$ on $\partial\Omega_D$ is not well defined. One way to do it is to impose compatibility in a variational form, namely by using the Complementary Virtual Work Principle.

On introducing the set of virtual stress fields

$$\delta H = \{ \delta\mathbf{T} \in T^*(\Omega) \; s.t. \; div\delta\mathbf{T} = \mathbf{0} \; , \; \delta\mathbf{T}\mathbf{n} = \mathbf{0} \; on \; \partial\Omega_N \} \; , \qquad (15)$$

the displacement field $\mathbf{u}$ is compatible with $(\underline{\mathbf{u}}, \underline{\mathbf{E}})$ if and only if

$$\int_{\partial\Omega_D} (\delta\mathbf{T}\mathbf{n}) \cdot \underline{\mathbf{u}} - \int_\Omega \delta\mathbf{T} \cdot \underline{\mathbf{E}} = \int_\Omega \delta\mathbf{T} \cdot \mathbf{E}(\mathbf{u}) \; , \; \forall \delta\mathbf{T} \in \delta H \, . \qquad (16)$$

$T^*(\Omega)$ is a function space of convenient regularity. If $\mathbf{u} \in H^1(\Omega)$ (as it is assumed in linear elasticity), then $T^*(\Omega) = L^2(\Omega)$ guarantees the finiteness of the internal virtual work. If $\mathbf{u} \in BV(\Omega)$, the choice $T^*(\Omega) = C^\circ(\Omega)$ ensures the possibility of computing the internal virtual work.

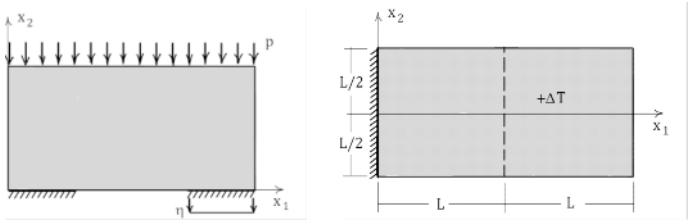

a b

Figure 9. Examples of kinematical problems. Wall loaded by uniform vertical load at the top and subjected to a given uniform settlement of the right foot: (a). Masonry panel subject to uniform thermal expansion of the right half: (b).

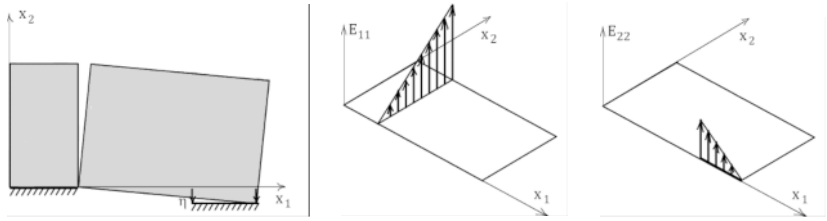

a b c

Figure 10. Compatible solution for the problem of Figure 9a: (a). Corresponding (singular) strain components: (b), (c).

Examples. As a simple illustration of typical *kinematical problems*, I construct some admissible deformations for the two example problems reported in Figure 9. In (a) the effect of a given settlement η of the right foot, is considered. In (b) the constraints are fixed and the effect of the distortion $\underline{\mathbf{E}} = \alpha \Delta T \, \mathbf{I}$, due to the uniform, positive increment of temperature ΔT, applied to the right half of the strip, is studied.

A kinematically admissible displacement, compatible with the given settlement, is shown in Figure 10a; in Figures 10b,c the strain components E_{11}, E_{22} are graphically represented.

A kinematically admissible displacement for the second example is

$$u_1 = \begin{cases} \alpha \Delta T x_1 (1 - x_2^2/L^2) \ , \ x_1 < L \ , \\ \alpha \Delta T x_1 \ , \ x_1 \geq L \ , \end{cases}$$

$$u_2 = \begin{cases} \alpha \Delta T x_2 x_1^2/L^2 \ , \ x_1 < L \ , \\ \alpha \Delta T x_2 \ , \ x_1 \geq L \ . \end{cases}$$

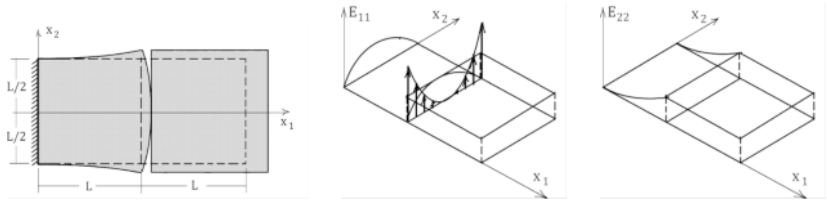

a b c

Figure 11. Compatible solution for the problem of Figure 10b: (a). Corresponding (regular and singular) strain components: (b), (c).

The corresponding deformation and the strain components E_{11}, E_{22}, are graphically represented in Figure 11. I leave to the reader to verify that the effective strain ($\mathbf{E}(\mathbf{u})$-$\underline{\mathbf{E}}$) belongs to Sym^{+}[6] and that the strain $\mathbf{E}$, whose non-vanishing components are depicted in Figures 11b c, satisfy the compatibility conditions (6) in a generalized sense.

2.6 Compatibility of loads and distortions

The data of a general BVP for a RNT body can be split into two parts

$$\ell \leftrightarrow (\underline{\mathbf{s}}, \mathbf{b}) \approx \textit{loads} ,$$

$$\ell^* \leftrightarrow (\underline{\mathbf{u}}, \underline{\mathbf{E}}) \approx \textit{distortions} .$$

The *equilibrium problem* and the *kinematical problem* for RNT materials, namely the search of admissible stress or displacement fields for given data, are essentially independent, in the sense that they are uncoupled but for condition (3).

It has to be pointed out that, for RNT bodies, there are non-trivial compatibility conditions, both on the loads and on the distortions; that is the existence of statically admissible stress fields for given loads, and the existence of kinematically admissible displacement fields for given distortions, is submitted to special conditions on the data (for a thorough study of compatibility conditions on the loads see Del Piero (1989) and Angelillo and Rosso (1995)).

[6] The assumption that the effective strain has to belong to Sym^{+}, implies that, on a crack Γ, the form of the singular strain be

$$\mathbf{E}^s = \delta(\Gamma)\Delta v \mathbf{m} \otimes \mathbf{m} , \ \textit{with} \ \Delta v > 0 ,$$

that is shearing discontinuities are forbidden.

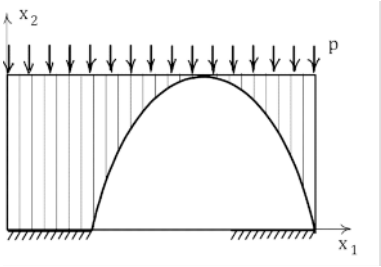

Figure 12. Statically admissible solution reconcilable with the compatible mechanism of Figure 11a, and corresponding to the BVP depicted in Figure 10a. An arch carrying a concentrated axial force is formed, springing from the two *hinges* of Figure 10a. The stress field is regular and uniaxial above the arch.

The definition of compatible loads and distortions is rather straightforward:

$$\{\ell \; is \; compatible\} \; \Leftrightarrow \{H \neq \emptyset\} \; , \tag{17}$$

$$\{\ell^* \; is \; compatible\} \; \Leftrightarrow \{K \neq \emptyset\} \; . \tag{18}$$

Therefore the more direct way to prove compatibility, both for loads and distortions, is to construct a s.a. stress field or a k.a. displacement field, as done in the previous examples.

To prove the existence of a solution to the BVP for a No-Tension body, the compatibility of ℓ and ℓ^* is necessary but not sufficient, since the further condition

$$\mathbf{T} \cdot \mathbf{E}^*(\mathbf{u}) = 0 \; ,$$

must be satisfied (this is the material restriction (3)). Then one can say that a possible solution to the BVP is given, if there exist a s.a. stress field and and a k.a. dispalcement field, which are reconcilable in the sense of condition (3).

As a simple example in Figure 12, a s.a. stress field giving, together with the mechanism of Figure 10a, a possible solution to the simple problem depicted in Figure 9a, is reported.

Examples. In the examples of Figure 13, the possible solution of two classical mixed BVP for RNT materials is pictorially presented. Notice that both the stress solution and the displacement solution present singularities.

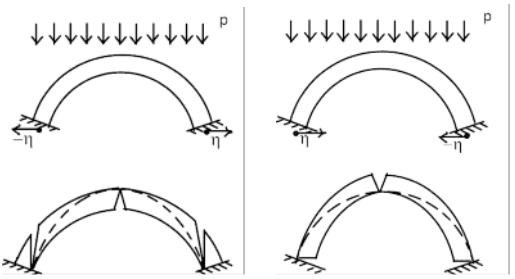

a b

Figure 13. Examples of solutions of typical BVP's for NENT materials. Arch loaded by a uniform (per-unit projection) vertical load at the extrados and subjected to a given uniform settlement of its abutments. In (a) the supports spread, in (b) they get closer. The strain is singular at the supports and at the key-stone; two different arches form in the two cases.

The examples reported in Figures 13, that can be found also in the milestone book by Heyman (1995), testify the need, in order to solve a BVP for Rigid No-Tension materials, to consider at the same time singular stress and strain fields, and call for an *extended* formulation of the theorems of Limit Analysis.

2.7 Incompatibility of loads and distortions

The way to verify the incompatibility of the data is less straightforward, requiring the definition of two new sets

$$H^\circ = \left\{ \mathbf{T}^\circ \in S(\Omega) \; s.t. \; div\mathbf{T}^\circ = \mathbf{0} \; , \; \mathbf{T}^\circ\mathbf{n} = \mathbf{0} \; on \; \partial\Omega_N \; , \; \mathbf{T}^\circ \in Sym^- \right\} \; ,$$

and

$$K^\circ = \left\{ \mathbf{u}^\circ \in T(\Omega) \; s.t. \; \mathbf{u}^\circ = \mathbf{0} \; on \; \partial\Omega_D \; , \; \mathbf{E}(\mathbf{u}^\circ) \in Sym^+ \right\} \; .$$

Both H° and K° can reduce to the sets $H^{\circ\circ}$ and $K^{\circ\circ}$ corresponding to null stress and strain fields, depending on the geometry of the boundary, of the loads and of the constraints.

Remark 4. The fact that $H^\circ - H^{\circ\circ}$ can be void and that $K^\circ - K^{\circ\circ}$ can be non-void is kind of peculiar of RNT materials; indeed we are used to think to 2d continua as overdetermined and deprived of rigid, *zero-energy*, internal modes.

One way to see overdeterminacy is to add to any s.a. stress field a, non zero, self balanced stress field $\mathbf{T}^\circ$. The fact that $H^\circ - H^{\circ\circ}$ can be void,

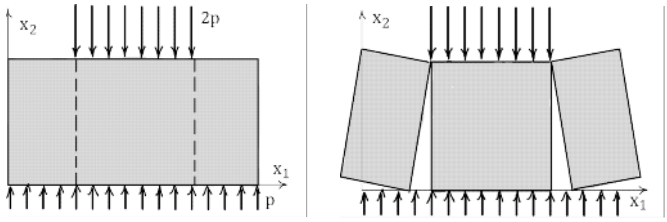

a b

Figure 14. Example of incompatible loads: in (a) wall loaded by uniform vertical loads at the top and bottom bases. K.a. displacement field for which the load performs positive work: (b).

means that overdeterminacy depends on the loads. There also can be loads for which the structure becomes statically admissible. The fact that the overdeterminacy/underdeterminacy of the structure depends on the load is typical also of *discrete* structures with unilateral constraints.

The absence of degrees of freedom is proved, for discrete structures, by denying the possibility of zero energy mechanisms. $\mathbf{u}^\circ \in K^\circ - K^{\circ\circ}$ is indeed a non trivial mechanism requiring, for the RNT body, zero energy expended. The underdeterminacy of the structure, descending from the fact that $K^\circ - K^{\circ\circ}$ can be non-void, demands for non trivial compatibility conditions on the loads. $\diamond$

The incompatibility of the data can be assessed as follows

$$\{\ell \; incompatible\} \Leftarrow \left\{\exists \mathbf{u}^\circ \in K^\circ \; s.t. \; \langle \ell, \mathbf{u}^\circ \rangle > 0\right\} \; , \tag{19}$$

$$\{\ell^* \; incompatible\} \Leftarrow \left\{\exists \mathbf{T}^\circ \in H^\circ \; s.t. \; \langle \ell^*, \mathbf{T}^\circ \rangle > 0\right\} \; , \tag{20}$$

where $\langle \ell, \mathbf{u}^\circ \rangle$, $\langle \ell^*, \mathbf{T}^\circ \rangle$ represent the work of the loads and distortions for $\mathbf{u}^\circ$, $\mathbf{T}^\circ$, respectively.

Examples. The load of Figure 14a is incompatible, since it makes positive work for the mechanism $\mathbf{u}^\circ$ depicted in Figure 14b.

The distortion represented in Figure 15a is incompatible, since it makes positive work for the self stress $\mathbf{T}^\circ$ depicted in Figure 15b.

Remark 5. The incompatibility of a given set of loads means that equilibrium is not possible and that acceleration of the structure must take place[7]. The incompatibility of a given set of distortions means that the given

[7] A trivial compatibility condition for all kinds of bodies, under pure traction conditions,

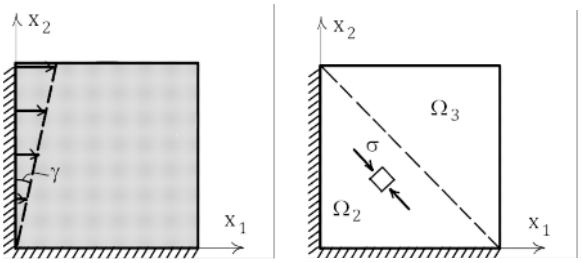

Figure 15. Example of incompatible distortions: in (a) panel subject to a given displacement of the left constraint. S.a. stress field for which the distortion performs positive work: (b).

kinematical data cannot be accomodated with a zero energy mechanism and demand for more complex material models (i.e. elastic NT, elastic NT-plastic, etc). ⋄

2.8 Limit Analysis

We have seen in the preceding sections that, for RNT bodies, both force and displacement data are subject to compatibility conditions, that is the existence of a statically admissible stress field and the existence of a kinematically admissible displacement field, are subordinated to some necessary or sufficient conditions on the given data. Here I concentrate on necessary or sufficient conditions for the compatibility of a given set of loads $(\underline{\mathbf{s}}, \mathbf{b})$, restricting to the case of zero kinematical data $(\underline{\mathbf{u}}, \underline{\mathbf{E}})$. The definition of safe, limit and collapse loads are given first, and the propositions defining the compatibility of the loads, that are essentially a special form of the theorems of Limit Analysis (LA), are then discussed.

Theorems of Limit Analysis. Recalling the definition of RNT materials, we can observe that the restrictions (2), (3) are equivalent to a rule of normality of the total strain to the cone of admissible stress states. Normality is the essential ingredient allowing for the application of the two theorems of Limit Analysis (see Del Piero (1998)). In order to avoid the possibility of trivial incompatible loads (and simplify the formulation of the two theorems), assumption (4) (i.e. that the tractions $\underline{\mathbf{s}}$ applied at the

is load balance. Load balance is only a necessary compatibility condition for unilateral bodies.

boundary are either compressive or zero) is made.

Admissible fields. The rigorous proof of the two theorems of Limit Analysis requires to set the problem in proper functions spaces. For RNT materials is appropriate and convenient to define the sets of statically admissible stress fields H and kinematically admissible displacement fields K, as follows

$$H = \left\{ \mathbf{T} \in S(\Omega) \; s.t. \; div\mathbf{T} + \mathbf{b} = \mathbf{0} \; , \; \mathbf{Tn} = \underline{\mathbf{s}} \; on \; \partial\Omega_N \; , \; \mathbf{T} \in Sym^- \right\} \; , \quad (21)$$

$$K = \left\{ \mathbf{u} \in T(\Omega) \; s.t. \; \mathbf{u} = \mathbf{0} \; on \; \partial\Omega_D \; , \; \mathbf{E}(\mathbf{u}) \in Sym^+ \right\} \; , \quad (22)$$

where a convenient choice for the function spaces $S(\Omega)$ and $T(\Omega)$ is

$$S(\Omega) = SMF(\Omega) \; ,$$

$$T(\Omega) = \{ \mathbf{u} \; s.t. \; grad\mathbf{u} \in SMF^*(\Omega) \} \; ,$$

SMF being the set of Special Measures (that is measures with null Cantor part) whose jump set is Finite, in the sense that the support of their singular part consists of a finite number of regular $(n-1)$d arcs[8].

With SMF^* I denote the subset of SMF for which the support of the singular part is restricted to a finite number of $(n-1)$d segments.

Notice that, depending on the geometry of the structure $\Omega = \dot{\Omega} \cup \partial\Omega_N$ and on the given loads, the set H can be void. If H is void the load $(\underline{\mathbf{s}}, \mathbf{b})$ is incompatible, in the sense previously specified (no possibility of equilibrium with purely compressive stresses).

Strictly admissible stress fields and load classification. In order to formulate the theorems of Limit Analysis, I need to introduce the following definitions.

On denoting$\langle \ell, \mathbf{u} \rangle$ the work of the load $\ell = (\underline{\mathbf{s}}, \mathbf{b})$ for the displacement $\mathbf{u}$, the load can be classified as follows:

1. (ℓ is a collapse load)$\Leftrightarrow$ ($\exists \mathbf{u}^* \in K s.t. \langle \ell, \mathbf{u}^* \rangle > 0$),
2. (ℓ is a limit load)$\Leftrightarrow$ ($\langle \ell, \mathbf{u} \rangle \leq 0$, $\forall \mathbf{u} \in K$ and $\exists \mathbf{u}^* \in K - K^{\circ\circ}$ s.t. $\langle \ell, \mathbf{u}^* \rangle = 0$),
3. (ℓ is a safe load)$\Leftrightarrow$ ($\langle \ell, \mathbf{u} \rangle < 0 \; , \; \forall \mathbf{u} \in K$).

[8] We suggest the reader to consult the book (Ambrosio et al., 2000)for a complete essay on SBV functions and measure spaces.

I now introduce a useful definition. A stress field $\mathbf{T} \in H$ such that $tr\mathbf{T} < 0$ and $det\mathbf{T} > 0$, $\forall \mathbf{x} \in \Omega$, is said to be *strictly admissible*.

Notice that, if $\mathbf{T}$ is strictly admissible, then at each point of Ω (that is the open set $\dot{\Omega}$ to which the fixed part of the boundary $\partial\Omega_D$ is added) it results:

$$\sigma_1 < 0 \ , \ \sigma_2 < 0 \ ,$$

σ_1, σ_2 being the eigenvalues of $\mathbf{T}$ at the point $\mathbf{x}$.

Kinematic Theorem. If ℓ is a collapse load (in the sense of item (1) above) then H is void.

Static Theorem. If a strictly admissible stress field $\mathbf{T}$ exists, then the load ℓ is safe (in the sense of item (3) above).

Limit Theorem. If H is not void and there exists $\mathbf{u}^* \in K - K^{\circ\circ}$ $\langle \ell, \mathbf{u}^* \rangle = 0$, then the load ℓ is limit (in the sense of item (2) above).

For the proof of these theorems I refer to the paper (Del Piero, 1998). The reader must be warned that the proofs given by Del Piero refer to a similar function space for the displacement but to a different functional setting for the stress (namely $L^2(\Omega)$). In the present paper I assume that these theorem are still valid in the present larger setting for the stress and smaller setting for the displacement[9].

2.9 Simple applications of the theorems of Limit Analysis

Example 1. Compressed wall/pier. The two simple BVP depicted in Figure 16 are considered. The first one (Figure 16a) refers to a rectangular wall compressed at the two bases by uniform normal tractions. The second example (Figure 16b) is a wall compressed at the top base by a uniform pressure load and fixed at the bottom base. By employing the Airy's representation and by using the static and kinematic theorems, it can be shown that in case (a) the load is limit and in the second case the load is safe.

The data for F and $dF/d\nu$ at the boundary, in case (a), are shown in Figure 16c. In this case the only concave surface that can possibly satisfy

[9]For general stress and strain fields that can be line Dirac deltas on a finite number of regular arcs the internal work $\int_\Omega \mathbf{T} \cdot \mathbf{E}$ is not defined. Considering the restrictions which define the sets H and K, that is taking into account the constraints on $\mathbf{T}$ and $\mathbf{E}$, the only case in which there are troubles in computing the internal work (if $\mathbf{T}$ and $\mathbf{E}$ are so restricted) is when both the stress and the strain are singular on the same line Γ, the line is curved and there is a stress discontinuity in the direction of the normal $\mathbf{m}$ to Γ. A way to avoid this is to allow stress singularities on curved lines but to assume that the support of the jumps of $\mathbf{u}$ is a segmentation, that is a line formed by the union of a finite number of straight arcs.

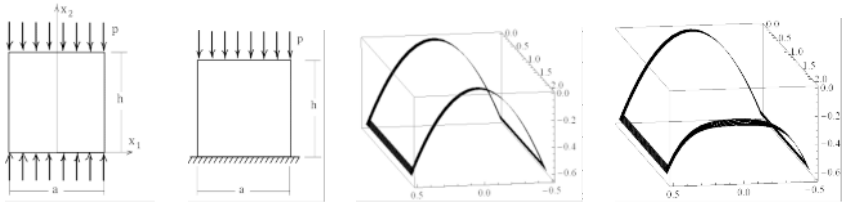

a b c d

Figure 16. Compressed pier (wall). Pure traction problem: (a), Mixed problem: (b). Corresponding data for F and dF/ν for the two cases.

the data shown in Figure 16c is the parabolic cylinder defined by

$$F = -\frac{px_1^2}{2} .$$

The uniqueness of this F can be proved by observing that the surface defined by it coincides with the upper part of the convex hull of the curve carrying the boundary datum for F. The properties of minimality of the convex hull ensure the uniqueness of F and of the corresponding stress (see Angelillo and Rosso (1995)), that is of the uniform uniaxial stress

$$\{\mathbf{T}\} = \left\{ \begin{array}{cc} 0 & 0 \\ 0 & -p \end{array} \right\} .$$

Since this is the only statically admissible stress field, H is a singleton and we can say that the structure, with this load, is statically determined (see Remark 4). Notice that based on the definition (3) above and on the theorems of LA, the load is not safe. It is actually limit (see Limit Theorem above) since by splitting the panel into two parts along any vertical line Γ with a normal crack, the strain corresponding to this mechanism is a horizontal uniaxial Dirac delta whose intensity has the value of the displacement jump along Γ: the work of the load for this non-zero mechanism is zero. Notice that the strain corresponding to this mechanism and the unique statically admissible stress field are reconcilable in the sense of condition (3), that is they represent a possible solution for the BVP. The fact that, under these conditions, strain can increase indefinitely at constant load is a typical feature of limit loads.

In case (b) the previous stress function can be corrected by adding a term to it. Notice that the boundary is loaded only on the lateral sides and on the top base (with the same load of case (a)), and that both the value and the slope of the stress function can be modified along the bottom base

of the panel (see Figure 16d). The simplest correction with polinomia one can think of, is

$$F = -\frac{p\,x_1^2}{2} - \beta\,\frac{(a^2 - x_1^2)^2\,x_2^2}{a^4}\ .$$

The corresponding stress is

$$\{\mathbf{T}\} = \left\{ \begin{array}{cc} -\beta\,\frac{2(a^2-x_1^2)^2}{a^4} & -\beta\,\frac{8(a^2-x_1^2)x_1x_2}{a^4} \\ -\beta\,\frac{8(a^2-x_1^2)x_1x_2}{a^4} & -p+\beta\,\frac{4(a^2-3x_1^2)x_2^2}{a^4} \end{array} \right\}\ .$$

The trace and the determinant of $\mathbf{T}$ are then

$$tr\mathbf{T} = -p + \beta\,\left(-2 + \frac{4a^2x_1^2 + 4a^2x_2^2 - 2x_1^4 - 12x_1^2x_2^2}{a^4}\right)\ ,$$

$$det\mathbf{T} = \beta\frac{2(a^2 - x_1^2)^2}{a^8}\left(pa^4 - \beta(4a^2 + 20x_1^2)x_2^2\right)\ .$$

If $h \leq \frac{\sqrt{2}}{2}\,a$ then $tr\mathbf{T}$ is always negative. If $h > \frac{\sqrt{2}}{2}\,a$ then $tr\mathbf{T}$ is negative on Ω if

$$\beta < \frac{pa^2}{4h^2 - 2a^2}\ ,$$

and $det\mathbf{T}$ is positive on Ω if

$$\beta < \frac{pa^2}{24h^2}\ .$$

Then $\mathbf{T}$ is negative definite on Ω, and the load is safe, on the base of the Static Theorem of LA, if the second inequality holds. For example, for a square panel, if one takes $\beta < \frac{p}{96}$, then the stress given by the above expression is strictly admissible and the load is safe. In Figure 17 the stress functions emploied for cases (a) and (b) are shown side by side for comparison, in the special case $h = 2a$, and putting for case (b), $\beta = \frac{p}{400}$.

Notice that the negative definiteness of $\mathbf{T}$ in case (b) is not uniform, since on the lateral sides we must have $det\mathbf{T} = 0$ and one of the two eigenvalues of $\mathbf{T}$ must tend to zero as that part of the boundary is approached.

Remark 6. The bounds found on β give values of β vanishingly small with respect to p, as the ratio h/a increases; if one takes β/p as a sort of measure of the safety level of the load with respect to collapse: then slender walls, under this kind of loading, tend to become less and less safe, as the ratio h/a is increased.$\diamond$

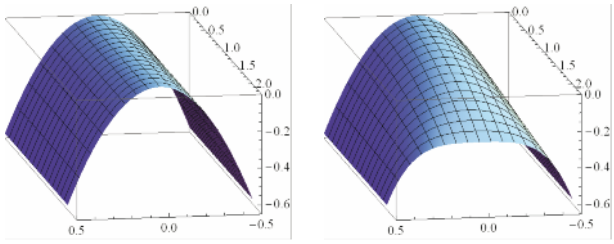

a b

Figure 17. Compressed pier (wall): in (a) Airy's stress function for the traction problem. In (b) Airy's stress function adopted for the mixed case.

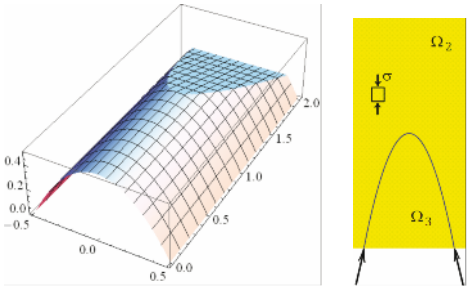

a b

Figure 18. In (a) Airy's folded stress function for the mixed problem. In (b) a scheme of the corresponding stress is reported.

Remark 7. It is worth pointing out that the existence of a strictly admissible stress field does not imply that the actual state of stress in the body be of biaxial compression. If the material is rigid in compression, any statically admissible stress has the same dignity and is theoretically admissible for equilibrium.

The choice among these fields requires the introduction of more advanced constitutive restrictions, allowing for shortening strains. When elasticity is assumed it happens that s.a. stress fields which are not strictly admissible are preferable, on an energetic ground, to strictly admissible ones. Therefore the material exhibits both biaxial and uniaxial stress states (and fractures) despite the existence of a strictly admissible stress field (see *Exact solution 4*, *Subsection* 3.7).◇

By using the Airy's formulation singular s.a. stress fields can be easily generated. By modifying, with some care, these singular fields, strictly

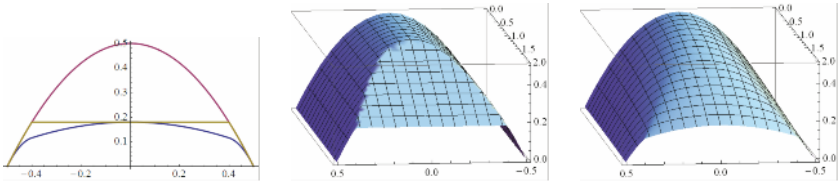

a b c

Figure 19. Smoothing of the folded stress function of Figure 18. Sections of the folded surface and its smoothed transformation at $x_2 = 0$: (a); the section of the parabolic cylinder corresponding to the solution of the traction problem is reported for reference. In (b), (c) a 3d view of the folded and smoothed surfaces is shown

admissible stress fields can be obtained. A non smooth F satisfying the b.c. for case (b) of Figure 16 is depicted in Figure 18a.

The stress field corresponding to the non smooth Airy's function depicted in Figure 18a, is reported schematically in Figure 18b. The way in which such a composite surface can be generated by the boundary data is explained in detail in the next example. Notice that the half-span αa and the rise βh of the arch-like structure depicted in Figure 18b can be chosen arbitrarily provided that α, β vary in the interval $[0, 1]$.

The process through which the singular statically admissible stress field depicted in Figure 18 can be smoothed out and transformed into a strictly admissible stress field is not discussed here for brevity. A 3d view of the folded F and of its strictly admissible modification (together with the stress function of case (a) used as a reference surface) is shown pictorially in Figure 19.

Example 2. Rocking of a rectangular panel. This is perhaps the most classical problem for unilateral masonry-like materials, for which the determination of the limit load under a horizontal force is trivial; therefore this is the ideal example to understand how the theorems of limit analysis can be applied to NT materials and how one can take advantage of singular stress fields and of the stress function formulation.

The vertical load is fixed to the value $q = \frac{P}{L}$ and the intensity of the concentrated horizontal force is taken as $H = \alpha P$, α being a load parameter. A trivial upper bound for α ($\alpha^\circ = \frac{1}{3}$) in the case shown in Figure 20a, is found by considering the rocking mechanism of the panel (shown in Figure 20b) and applying the kinematic theorem. If one can find a statically admissible stress field for the same value of α then α° is the limit value of the load parameter.

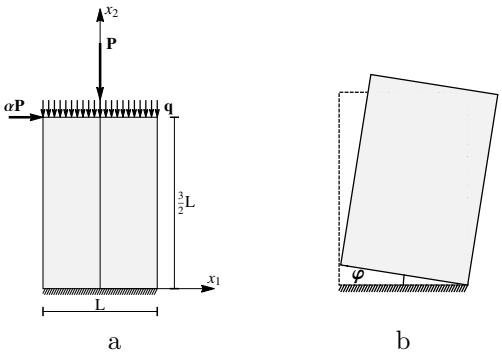

Figure 20. Rectangular panel loaded by vertical and horizontal forces. Loading scheme: (a). Rocking mechanism: (b)

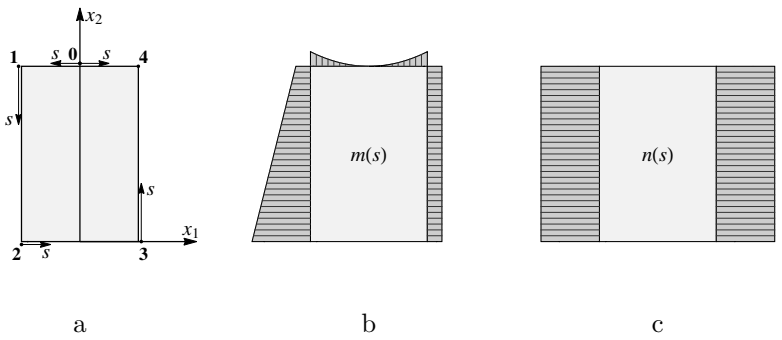

Figure 21. Rectangular panel loaded by vertical and horizontal forces. Parametrization of the boundary: (a). Boundary value for F (moment $m(s)$): (a). Boundary value for the normal derivative of F (axial force $n(s)$): (c)

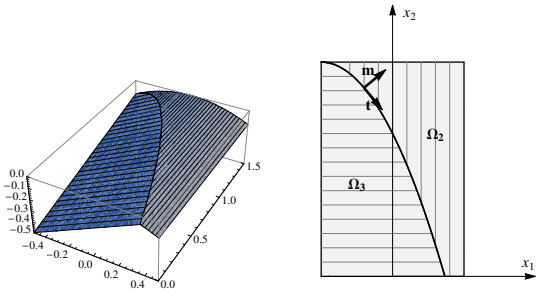

Figure 22. Rectangular panel loaded by vertical and horizontal forces for $\alpha = 1/4$. Composite stress function: (a). Corresponding support of the singular stress on the planform and domain partition: (b).

For $\alpha < \frac{1}{3}$, say $\alpha = \frac{1}{4}$, a strictly admissible stress field can be constructed. To use the Airy's formulation the loaded boundary is divided into five parts (see Figure 21a where $L = 1$ is set).

1. The boundary is parametrized with the arc length s. The data $m(s)$ and $n(s)$ are defined in terms of the load on the segments 0-1 and 1-2 (see Figure 21b, c). From them the curve carrying the datum for F and the gradient $gradF$ at the boundary are computed.

Segment 0-1.

Parametrization: $\mathbf{x}(s) = \{-s, \frac{3}{2}\}$;

Moment: $m(s) = -\frac{qs^2}{2}$;

Axial force: $n(s) = 0$;

Curve of boundary data: $\mathbf{X}(s) = \{-s, \frac{3}{2}, -\frac{qs^2}{2}\}$;

Gradient of F at the boundary: $gradF^{\circ}(s) = \{-m'(s), n(s)\} = \{qs, 0\}$.

Segment 1-2.

Parametrization: $\mathbf{x}(s) = \{-\frac{1}{3}, \frac{3}{2} - s\}$;

Moment: $m(s) = -\frac{q}{8} - \frac{qs}{4}$;

Axial force: $n(s) = -\frac{q}{2}$;

Curve of boundary data: $\mathbf{X}(s) = \{-\frac{1}{2}, \frac{3}{2} - s, -\frac{q}{8} - \frac{qs}{4}\}$;

Gradient of F at the boundary: $gradF^{\circ}(s) = \{-n(s), m'(s)\} = \{\frac{q}{2}, \frac{q}{4}\}$.

2. The data are extended inside the body with a uniaxial prolongation. Such a prolongation is obtained by constructing on each part γ_i of the boundary, a ruled surface having as generating curve, the curve $\mathbf{X}(s)$ carrying the Dirichelet data, and formed by the straight lines r directed as the given loads and whose slope is specified by $gradF^{\circ}(s)$. If the load is zero, the direction of the line r is taken as the inward normal -**n**.

Segment 0-1
Load direction: $\mathbf{k} = \{0, -1\}$;
Propagation vector: $\mathbf{v}(s) = \{k_1, k_2, gradF \cdot \mathbf{k}\} = \{0, -1, 0\}$;
Parametric form of F^1: $\mathbf{y}(s, \nu) = \mathbf{X}(s) + \nu\mathbf{v}(s) = \{-s, \frac{3}{2} - \nu, -\frac{qs^2}{2}\}$;
F^1 in terms of x_1, x_2: $F^1(x1, x_2) = -\frac{qx_1^2}{2}$.
Segment 1-2
Load direction: $\mathbf{k} = \{1, 0\}$;
Propagation vector: $\mathbf{v}(s) = \{k_1, k_2, gradF \cdot \mathbf{k}\} = \{1, 0, \frac{q}{2}\}$;
Parametric form of F^2: $\mathbf{y}(s, \nu) = \mathbf{X}(s) + \nu\mathbf{v}(s) =$
$\{-\frac{1}{2} + \nu, \frac{3}{2} - s, -\frac{p}{8}(1 - 2qs + 4\nu q)\}$;
F^2 in terms of x_1, x_2: $F^2(x1, x_2) = -\frac{q}{4}(1 - 2x_1 - x_2)$.

3. The two surfaces F^1 and F^2 intersect along a curve (represented in Figure 22a) whose projection Γ on the "planform" is determined, in explicit form. By solving the equation $F^1 = F^2$, one obtains the following equation for Γ:

$$x_2 = 1 - 2x_1 - 2x_1^2 \, .$$

The curve Γ is a parabola, passing through the point $\{-\frac{1}{2}, \frac{3}{2}\}$ and intersecting the base at $x_1^\circ = \frac{1}{2}(\sqrt{3} - 1)$. Γ splits the rectangle into two parts Ω_2, Ω_3(Figure 22b).

4. Along Γ the stress is singular: it is a concentrated axial force N whose intensity is determined by the jump of slope ΔF of the composite surface F in the direction of $\mathbf{h}$ (Figure 22ab). Since the gradient jump across Γ is $gradF^1 - gradF^2 = -q\{\frac{1}{2} + x_1, \frac{1}{4}\}$ and the unit normal $\mathbf{h}$ to Γ is $\mathbf{h} = \{2 + 4x_1, 1\}/\sqrt{5 + 16x_1 + 16x_1^2}$, we have

$$\Delta F = (gradF^1 - gradF^2) \cdot \mathbf{h} = -\frac{1}{4} q \sqrt{5 + 16x_1 + 16x_1^2} \, .$$

The stress corresponding to this composite F is zero in Ω_1, uniaxial inside Ω_2, and a Dirac delta stress of intensity $N = \Delta F$, balancing the stress jump on Γ due to the stress discontinuity, at the interface between Ω_1 and Ω_2 (Figure 23a). The graph of N along the curve Γ, in the interval $\left[-\frac{1}{2}, \frac{1}{2}(\sqrt{3} - 1)\right]$, is shown in Figure 23b.

Remark 8. Notice that the concentrated force emerging at the bottom edge is the trace of the singular stress field $\mathbf{T}(x_1) = N(x_1)\delta(\Gamma)\mathbf{t}(x_1) \otimes \mathbf{t}(x_1)$, $\mathbf{t}$ being the unit tangent vector to Γ: $\{\mathbf{t}\} = \{h_2, -h_1\}$. The value of such force is $\mathbf{R} = N(x_1^\circ)\delta(x_1^\circ)\mathbf{t}(x_1^\circ)$, i.e. it is not given by the Cauchy formula $\mathbf{s}(\mathbf{n}) = \mathbf{T}\mathbf{n}$, valid for absolutely continuous stress vectors $\mathbf{s}$.$\diamond$

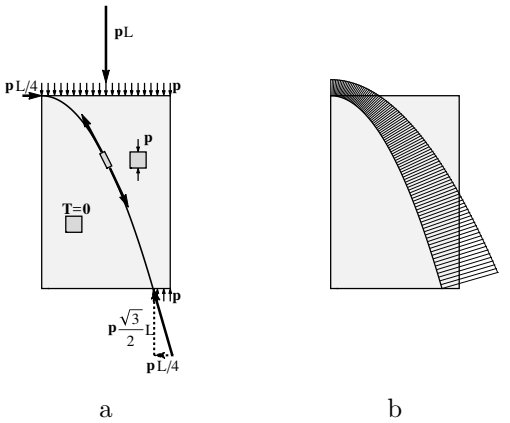

a b

Figure 23. Rectangular panel loaded by vertical and horizontal forces for $\alpha = 1/4$. Stress corresponding to the stress function of Figure 22: (a). Graph of the axial force along the arch: (b).

A s.a. stress field for $\alpha = \frac{1}{3}$ is obtained by following the same steps as before. The two functions F^1 and F^2 are in this case:

$$F^1(x_1, x_2) = -q\frac{x_1^2}{2} \, , F^2(x_1, x_2) = -\frac{1}{24}q(9 - 12x_1 - 8x_2) \, .$$

They intersect along the curve Γ depicted in Figure 24a, whose projection on the planform is given by the equation:

$$x_2 = \frac{3}{8}(3 - 4x_1 - 4x_1^2) \, .$$

Γ is a parabola passing through the points $[-1/2, 3/2]$, $[1/2, 0]$ (thus is the two opposite top and bottom corners of the rectangle: Figure 24b). The jump of slope along Γ is

$$\Delta F(x_1) = (gradF^1 - gradF^2)|_\Gamma \cdot \mathbf{h}(x_1) = -\frac{1}{6}q\sqrt{13 + 36x_1 + 36x_1^2} \, .$$

the corresponding axial force N along Γ, in the interval $[-0.5, 0.5]$, is reported in Figure 24d.

In Figure 24c the stress field corresponding to the composite surface F^1, F^2 is reported. Such a field is not strictly admissible and does zero work for the mechanism of Figure 20b, therefore $\alpha = 1/3$ is the limit load.

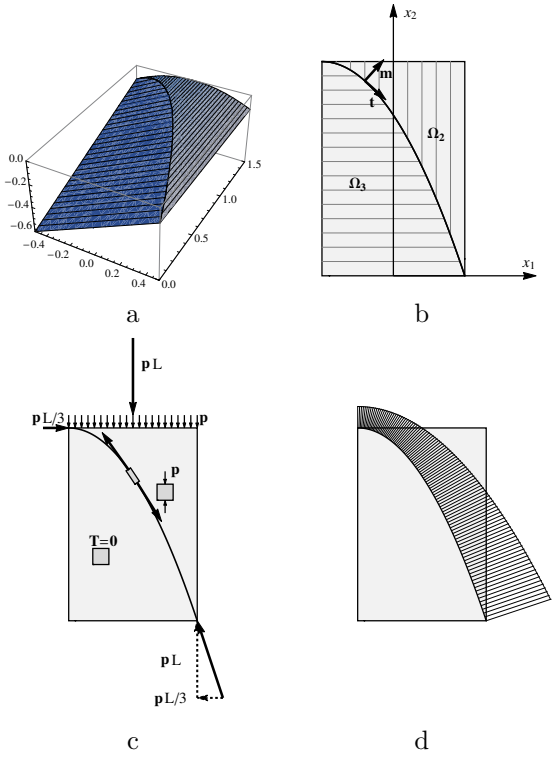

Figure 24. Rectangular panel loaded by vertical and horizontal forces for $\alpha = 1/3$. Strees function: (a). Support of the singular stress on the planform and domain partition: (b). Stress corresponding to the stress function depicted in (a): (c). Graph of the axial force along the arch: (d).

The stress field that was constructed for $\alpha = 1/4$ is not strictly admissible (actually the stress that we derived from the folded stress function is on the boundary of the cone Sym^- all over Ω), but, for any value of the load parameter $\alpha < \frac{1}{3}$, the previous construction can be used to generate a strictly admissible stress field. The method proceeds as follows:

Assume that a value of the parameter, say $\widetilde{\alpha} < \frac{1}{3}$, is given. If one removes a portion $p = q(1 - 3\widetilde{\alpha})$ from the given uniform load, the load becomes limit, that is the parabola hits the right corner of the rectangle and, as before, a stress field $\mathbf{T}^1$ can be constructed. Now I consider the panel under the action of the uniform vertical load p applied at the top base, and take the strictly admissible solution, say $\mathbf{T}^2$, constructed for the

previous example (the compressed wall). The sum of the two stress fields $\mathbf{T}^1 + \mathbf{T}^2$ is strictly statically admissible, since Sym^- is convex, the second stress state is strictly inside the cone, and then the sum of the two stress fields is also strictly inside the cone for any $\mathbf{x} \in \Omega$.

Remark 9. In the previous example statically admissible stress fields were produced through the stress function formulation. The overdetermined problem of equilibrium was reduced to a determined problem by restricting the search to a special class of stress functions, namely that of ruled surfaces (that is surfaces composed of straight lines). The stress fields corresponding to these surfaces are either uniaxial or null, that is the stress is limit *almost everywhere* in the body and the equilibrium problem is determined, since to the two differential equations of equilibrium the algebraic condition that the stress is uniaxial ($det\mathbf{T} = 0$) is added[10]. Any statically admissible uniaxial stress field balanced with zero body forces $\mathbf{b}$, has one family of isostatic lines (the ones corresponding to the negative eigenvalue) composed of straight lines (see Remark 3 and Figure 6). These straight lines, being actually the projections of the straight lines generating the ruled stress surface associated to $\mathbf{T}$, are called *compression rays* [11].

The differential problem is parabolic, and the stresses inside Ω are determined by the boundary data. By propagating the loads from opposite parts of the boundary the corresponding stress fields are usually unbalanced at the interface between the two fields: singular stress fields must be admitted along the interface. Both the value of the singular stress and the shape and location of the interface is determined by equilibrium. With the stress function formulation both the form and the location of the interface, besides the intensity of the axial contact force along Γ, are derived by intersecting two contiguous stress surfaces.$\diamond$

Example 3. Lintel under vertical and horizontal loads. A rectangular wall beam, supported at the bottom corners A, B, submitted to vertical and horizontal loads applied along its top edge, is shown in Figure 25a to which I refer for notations. This element can be representative of lintels, that is the transverse structures connecting the piers in masonry portals or in sequences of arches, when the effect of the loads transmitted to the arch from other parts of the structure, prevails on the self load, and

[10] This assumption is the basic hypothesis of the *Tension Field Theory* (see (Mansfield, 1969)), a simplified unilateral model for thin elastic membranes, analogous to the NT model for masonry structures (see Remark 3 and *Subsection* 3.8).

[11] This is a terminology similar to that adopted in *Tension Field Theory*, see Fortunato (2010).

the diffuse effect of body forces will be neglected. In Example 5 below the effect of uniform vertical body forces is considered.

The lintel's lower edge is actually often curved (see dashed line in Figure 25a), this feature being in keeping with the kind of stress state that I wish to consider in the element, as we shall see below. The presence of this arched intrados is necessary for equilibrium, if vertical body forces are considered.

By adopting the previous approach, in the case at hand I formulate the equilibrium problem of the lintel as follows.

The loads acting on Ω consists of a distributed load $\mathbf{q}$, applied along the top edge of Ω and having two components $\{q_1, q_2\}$ (see Figure 25b). The supports A, B reacts with two forces $\mathbf{R}_A, \mathbf{R}_B$, whose components are denoted $\{H(A), V(A)\}$, $\{-H(B), V(B)\}$; the lateral and the lower edges are unloaded.

Restricting to at most uniaxial stress fields and denoting $g = q_1/q_2$ the slope of the applied load with respect to x_2, the stress field, in the upper part of the domain, is a uniaxial field in the direction of the compression rays emanating from the top edge, whose slope with respect to x_2 is g. Calling τ the length along the (straight) top edge of the domain, measured from O, I also assume that the slope g is so restricted:

$$g(0) = 0 \ , \ g(L) = 0 \ , \ -\frac{\tau}{h^\circ} \leq g(\tau) \leq \frac{L-\tau}{h^\circ} \ , \ |g(\tau)| \ ,$$

that is the initial and final slopes are zero (then the two extreme compression rays run along the lateral edges), and the compression rays go from base to base and do not cross each other inside the rectangle enclosing Ω.

The stress field in the lower part of the domain is zero. The upper and the lower regions are separated by a common boundary Γ, passing through A and B, that is parametrized in terms of τ as follows

$$\Gamma = \{\{\mathbf{x}_\Gamma\} = \{\tau + g(\tau)y(\tau), y(\tau)\} \ , \ \tau \in \{0, L\}\} \ ,$$

carrying a concentrated axial force.

We denote H and V the horizontal and vertical components of the axial contact force N, arising on Γ in order to equilibrate the stress jump [12]. By imposing the equilibrium of the piece $\wp$ of Ω represented in Figure 25a, the following set of differential equations is obtained

$$H' = q_1 \ , \ V' = q_2 \ , \ V = H\frac{y'}{1 + gy' + g'y} \ ,$$

[12] For the positive sign of these two components I refer to the choice reported in Figure 25a.

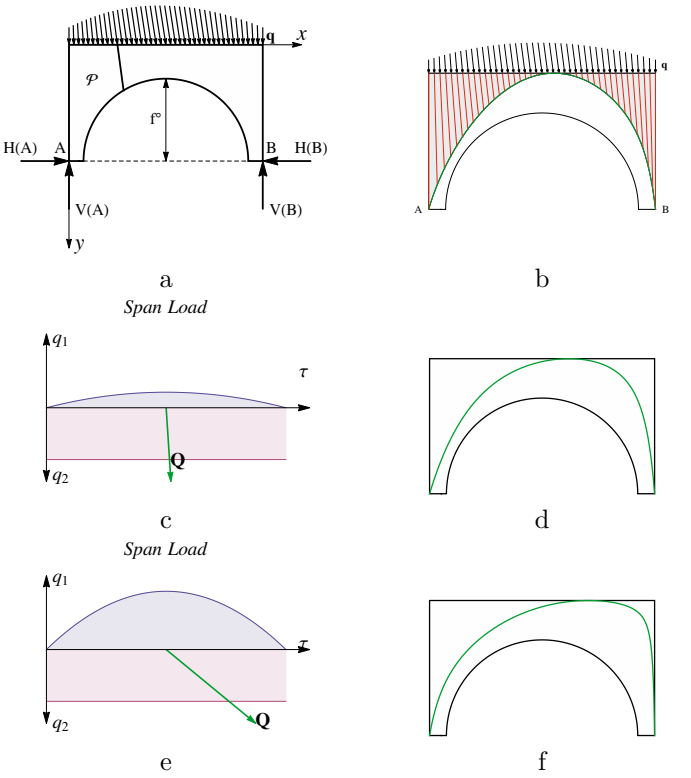

Figure 25. Lintel loaded by vertical and horizontal forces. Geometry of the panel: (a). Forces acting on the panel, compression rays and arch: (b). Horizontal and vertical load for two special cases (c, e) corresponding to the equilibrium solutions (d, f).

to be solved for H, V, y with the boundary conditions

$$y(0) = h^\circ \ , \ y(L) = h^\circ \ , \ y(\tau^\circ) = 0 \ , \ y'(\tau^\circ) = 0 \ ,$$

τ° being an unknown position along the upper edge. In the special case in which the horizontal and vertical loads have the form

$$q_1(\tau) = \frac{6q^\circ(L-\tau)^2\tau}{L^3} \ , \ q_2(\tau) = q^\circ \ ,$$

that is the vertical load is uniform, the horizontal load is parabolic, and the horizontal load resultant is half of the vertical resultant, the solution is

$$H = q^\circ \left(\frac{(h^\circ - L)^2}{8h^\circ} + \frac{6L^2\tau^2 - 8L\tau^3 + 3\tau^4}{2L^3} \right) ,$$

$$V = \frac{1}{2} q^\circ (h^\circ - L + 2\tau) ,$$

$$y = \frac{h^\circ L^3 (h^\circ - L + 2\tau)^2}{L^5 + (h^\circ)^2 a(\tau) - 2h^\circ b(\tau)} ,$$

where

$$a(\tau) = L^3 - 24L^2\tau + 48L\tau^2 - 24\tau^3 ,$$
$$b(\tau) = L^4 - 12L^3\tau + 36L^2\tau^2 - 44L\tau^3 + 18\tau^4 .$$

The solution of this special case for $h^\circ = \frac{L}{2}$ is reported in Figure 25.

Example 4. Lintel under a vertical uniform load and a horizontal concentrated force. Here I apply the stress function method to solve a problem similar to the previous one, namely the equilibrium of a rectangular, simply supported panel under a vertical uniform load applied along the top edge and a horizontal concentrated force acting at the left upper corner (Figure 26a). Again it is assumed that the supports in A and B react with two concentrated forces passing through A and B. These two forces are expressed in the form

$$\{\mathbf{R}(A)\} = \left\{ H, \frac{q^\circ L}{2} - \frac{Fh^\circ}{L} \right\} ,$$

$$\{\mathbf{R}(B)\} = \left\{ -H - F, \frac{q^\circ L}{2} + \frac{Fh^\circ}{L} \right\} ,$$

The corresponding boundary data for the stress function are reported pictorially in Figure 26b. Prolongating the data with ruled surfaces having the prescribed slope and direction at the boundary, a surface composed by three parts, a parabolic cylinder and two planes, is generated. Notice that the value of the thrust H could be chosen arbitrarily, within some limits, and that, in Figure 26b, it is set to a value such that the intersection of the lower plane with the parabolic cylinder, touches the upper boundary (minimal thrust).

The intersection of the three surfaces (Figure 26c) determines the 1d structure depicted in Figure 26d. The stress is uniaxial between the top edge and the structure Γ, null below the estrados of the arch; the singular part of it is concentrated on the support of the folds of F, that is on the structure Γ.

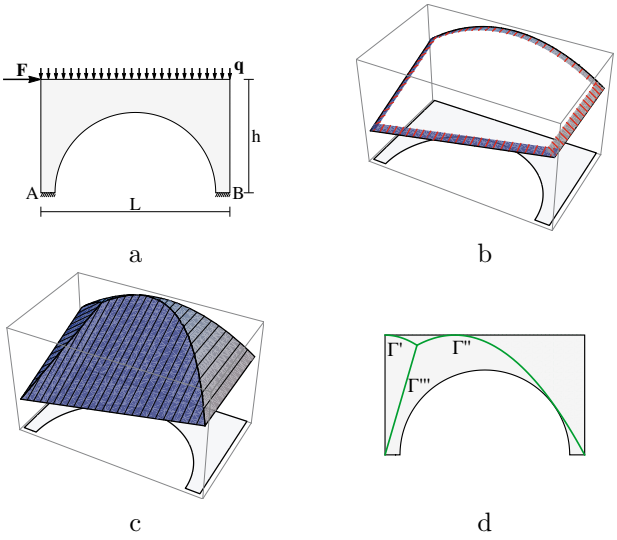

Figure 26. Lintel loaded by vertical and horizontal forces: (a). Boundary data: (b). Composite stress function: (c). Support of the singular stress, arch structure: (d).

Example 5. Lintel under homogeneous vertical body forces. A rectangular wall beam of heigth h° and width L, supported at the bottom corners A, B and submitted to homogeneous vertical body forces, is shown in Figure 27a, to which I refer for notations. This element is representative of lintels for which the effect of body forces is not negligible. The parameter $p^\circ = \frac{2h^\circ}{L}$ defines the aspect ratio of the lintel.

The lintel's lower edge is actually considered as symmetric (with respect to the center line) and curved (see dashed line in Figure 27a). For now the shape of this symmetric curve Γ is not specified, whilst its rise is fixed and called $f^\circ = (1-\alpha)h^\circ$, α being a parameter ranging in the open interval $(0,1)$. Notice that αh° is the thickness of the arch at the keystone.

The curve is described parametrically, in the Cartesian frame depicted in Figure 27a, as follows

$$\Gamma = \{\{\mathbf{x}_\Gamma\} = \{x, f(x)\}\ ,\ x \in [-L/2, L/2]\}\ ,$$

with

$$f(L/2) = f(-L/2) = 0, f(0) = (1-\alpha)h^\circ\ .$$

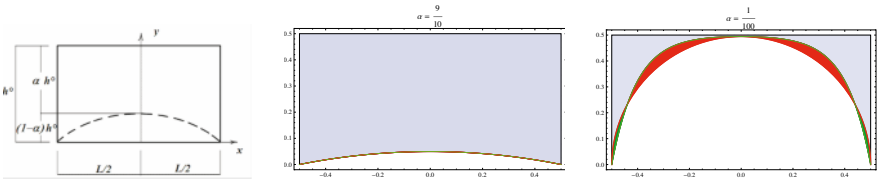

a b c

Figure 27. Lintel loaded by uniform body forces. Geometry of the panel: (a). Lower arch for $\alpha = 9/10$: (b) and for $\alpha = 1/100$: (c).

I construct two different statically admissible solutions for the equilibrium problem of the lintel as described in what follows.

First solution: maximal thrust. With the first solution I assume that inside the body the stress field is a.e. uniaxial and vertical, and an arch, on which the normal stress is concentrated, forms along the bottom boundary curve Γ. The loads acting on the wall produce a resultant vector $\mathbf{Q}$, having components $\{0, -Q\}$, with $Q = -\gamma\ area(\Omega)$, and located at the center of the wall. The supports A, B react with two forces $\mathbf{R}_A, \mathbf{R}_B$, whose components are denoted $\{H(A), V(A) = Q/2\}$, $\{-H(B), V(B) = Q/2\}$, where $H(A) = H(B) = H$, H being the unknown thrust of the arch; the rest of the boundary is unloaded.

The uniaxial stress field of simple compression in the vertical direction, has a non-vanishing component of the form

$$\sigma = -\gamma(h^\circ - y)\ .$$

Therefore the arch Γ is subjected to the vertical distributed load (per unit horizontal length) $q = -\gamma(h^\circ - f(x))$, $f(x)$ being the vertical coordinate of the arch Γ. For equilibrium the shape of the arch must satisfy the equation

$$f'' = -\gamma\frac{h^\circ - f}{H}\ .$$

that one can solve (for f and H) with the boundary conditions

$$f(L/2) = f(-L/2) = 0, f(0) = (1-\alpha)h^\circ\ .$$

The solution is

$$f = \frac{\left(1 + e^{L\sqrt{\frac{\gamma}{H}}} - e^{\frac{(L-2x)}{2}\sqrt{\frac{\gamma}{H}}} - e^{\frac{(L+2x)}{2}\sqrt{\frac{\gamma}{H}}}\right)\mathrm{h}^\circ}{1 + e^{L\sqrt{\frac{\gamma}{H}}}}\ ,$$

$$H = \gamma \frac{L^2}{\mathrm{Log}^2\left(\frac{2-\alpha^2-2\sqrt{1-\alpha^2}}{\alpha^2}\right)} \ .$$

The value of the force resultant is then

$$Q = \gamma p^\circ \frac{2L^2\left(1-\alpha^2+\sqrt{1-\alpha^2}\right)\left(\mathrm{Log}\left(2-\alpha^2-2\sqrt{1-\alpha^2}\right)-2\mathrm{Log}(\alpha)\right)}{\left(-1+\sqrt{1-\alpha^2}\right)\mathrm{Log}^2\left(\frac{2-\alpha^2+2\sqrt{1-\alpha^2}}{\alpha^2}\right)} \ .$$

In Figures 27b,c the shape of the lower curve determined through equilibrium is compared to the actual shape of the intrados of the lintel, for two extreme special cases ($\alpha = 0.9$, $\alpha = 0.01$). From these two pictures one can see that, in the first case, the statically admissible stress field here constructed can be accepted as an approximate equilibrated solution (by neglecting the slight geometrical difference between the two curves); whilst, in the second case, there is a large portion of the domain (located below the arch) that remains out of the picture.

It is to be pointed out that for $\alpha \to 1$, the thrust force tends to $+\infty$.

Second solution: reducing the thrust.The domain Ω is divided into two parts: the part Ω' comprised between the curve Γ and the curve

$$\Gamma' = \{\{\mathbf{x}_\Gamma\} = \{\{x, g(x)\} \ , \ x \in [-L/2, L/2]\}\} \ ,$$

with

$$g(x) = \frac{1}{1-\alpha} f(x) \ ,$$

and the part Ω'', that is the part of Ω located above Γ' (see Figure 28). A solution of the equilibrium problem for the region Ω' is constructed first; the problem of equilibrium of the region Ω'' is solved in a second phase, and superimposed to the previous stress field.

Again I restrict to at most uniaxial stress fields, assuming that the stress field is convected to one of the two families of curvilinear lines $\vartheta^1 = x, \vartheta^2 = \lambda$, defined by

$$x_1 = x \ , \ x_2 = h(x, \lambda) \ ,$$

with

$$h(x, \lambda) = (1 - \alpha + \lambda\alpha)\, g(x) \ ,$$

where, $x \in [-L/2, L/2]$, $\lambda \in (0, 1)$ and

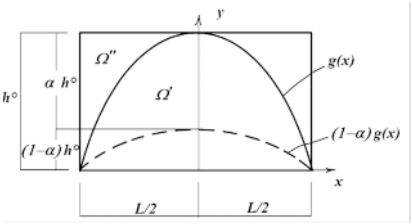

Figure 28. Lintel loaded by uniform body forces: geometry of the panel and domain partition for the second solution.

$$g(x) = \frac{1}{1-\alpha} f(x)$$

is the function describing the upper curve Γ'.

The natural and reciprocal base vectors associated to this curvilinear system, in components in the Cartesian reference depicted in Figure 28, are

$$\{\mathbf{a}_1\} = \{1, h_{,1}\} \ , \ \{\mathbf{a}_2\} = \{0, h_{,2}\} \ ,$$

$$\left\{\mathbf{a}^1\right\} = \{1, 0\} \ , \ \left\{\mathbf{a}^2\right\} = \left\{-\frac{h_{,1}}{h_{,2}}, \frac{1}{h_{,2}}\right\} \ .$$

The uniaxial stress field here considered has the form

$$\mathbf{T} = \sigma \mathbf{a}_1 \otimes \mathbf{a}_1 \ ,$$

σ being a function of (x, λ), describing the intensity of the stress field, to be found, together with f, by solving the equilibrium equation

$$\frac{\partial}{\partial \vartheta^\alpha} \left(\sigma \mathbf{a}_1 \otimes \mathbf{a}_1\right) \mathbf{a}^\alpha + \mathbf{b} = \mathbf{0} \ .$$

By projecting this vector equation along the natural bases, after some algebra, the following system of second order differential equations, is obtained:

$$\sigma_{,1} + \sigma \frac{h_{,12}}{h_{,2}} = 0 \ ,$$

$$-\frac{\gamma}{h_{,2}} + \sigma \frac{h_{,11}}{h_{,2}} = 0 \ ,$$

Recalling that $h_{,2} = \frac{\partial h}{\partial \lambda} = \alpha g$, since $h_{,2}$ is always different from zero inside Ω', integrating the first equation, one obtains

$$\sigma = \frac{m(\lambda)}{h_{,2}} \ ,$$

$m(\lambda)$ being an unknown function of λ. Substituting into the second equation one obtains

$$\gamma = m(\lambda)\frac{h_{,11}}{h_{,2}} \ .$$

Therefore, taking into account that $h_{,2} = \frac{\partial h}{\partial \lambda} = \alpha g$ and $h_{,11} = \frac{\partial^2 h}{\partial x^2} = (1 - \alpha + \alpha\lambda)g''$, the following two conditions are obtained:

$$g'' = -kg \ , \ m(\lambda) = -\gamma \frac{\alpha}{k(1 - \alpha + \alpha\lambda)} \ ,$$

k being a constant that I will assume positive.

By solving the first equation with the boundary conditions $g(-L/2) = 0, g(0) = h^\circ$ the following solution is obtained

$$g^\circ = \mathrm{h}^\circ \left(\cos\left(\sqrt{k}x\right) + \cot\left(\frac{\sqrt{k}L}{2}\right) \sin\left(\sqrt{k}x\right) \right) \ .$$

By imposing the condition $g'(0) = 0$ the value of the constant k is determined:

$$k = \frac{\pi^2}{L^2} \ ,$$

and then the form of the curve Γ' is given by

$$g^\circ = h^\circ cos\left(\frac{\pi x}{L}\right) \ ,$$

that is

$$\Gamma' = \left\{ \{\mathbf{x}\} = \left\{ x, h^\circ cos\left(\frac{\pi x}{L}\right) \right\} \ , \ x \in \left[-\frac{L}{2}, \frac{L}{2} \right] \right\} \ .$$

The *physical* uniaxial stress component

$$\sigma = T_{(11)} = \mathbf{T} \cdot \left(\frac{\mathbf{a}_1}{|\mathbf{a}_1|} \otimes \frac{\mathbf{a}_1}{|\mathbf{a}_1|} \right) = -\frac{L^2 \gamma \mathrm{Sec}\left(\frac{\pi x}{L}\right)}{\mathrm{h}^\circ \pi^2 (1 + \alpha(-1 + \lambda))} \ ,$$

along the ϑ^1 curves, is depicted in the graphic of Figure 29.

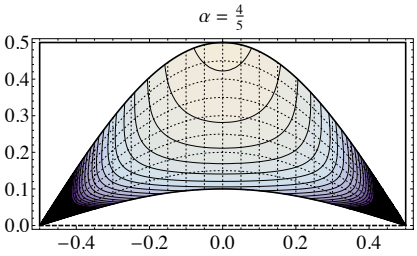

Figure 29. Contour plot of the stress σ in the region Ω'.

It is assumed that the load which is given above the curve Γ', is taken by an arch Γ'', that is by a concentrated stress with support on Γ''. The form of this curve, springing from the points A, B, determined by the form of the load through equilibrium, should be located below the load (that is below the curve Γ') and contained inside the masonry (that is above the curve Γ). In this way, the load can be transmitted to the arch by compressive uniaxial vertical stresses, linearly varying inside Ω'', and constant outside it.

The vertical load that I consider acting on Γ''' is then

$$q = \gamma(s + h^\circ - g^\circ) \ ,$$

γs being the effect of a given uniform over-load. By solving the equilibrium equation for the arch, with the conditions that the arch passes through the points A and B, and through the point P of coordinates $\{0, \mathrm{h}_y\}$, one obtains

$$\Gamma''' = \left\{ \left\{ x, \frac{\mathrm{h}_y \left(\pi^2 (L\mathrm{p}^\circ + 2s)\left(L^2 - 4x^2\right) - 8L^3 \mathrm{p}^\circ \cos\left(\frac{\pi x}{L}\right)\right)}{L^2 \left(L\left(-8 + \pi^2\right)\mathrm{p}^\circ + 2\pi^2 s\right)} \right\}, \right.$$
$$\left. x \in (-L/2, L/2) \right\} \ ,$$

where $p^\circ = \frac{2h^\circ}{L}$ is the *aspect ratio* of the lintel. In Figure 30 the form of the arch for $p^\circ = 1$, $s = L/8$ and three special cases is reported.

Finally the values of the vertical reactions and of the thrust forces in A and B, due to the compound effect of the first and the second equilibrium solutions are:

$$Q/2 = \frac{(\pi - 4p^\circ + 2\pi p^\circ)\gamma}{8\pi} + \frac{p^\circ \alpha \gamma}{2\pi} \ , \tag{23}$$

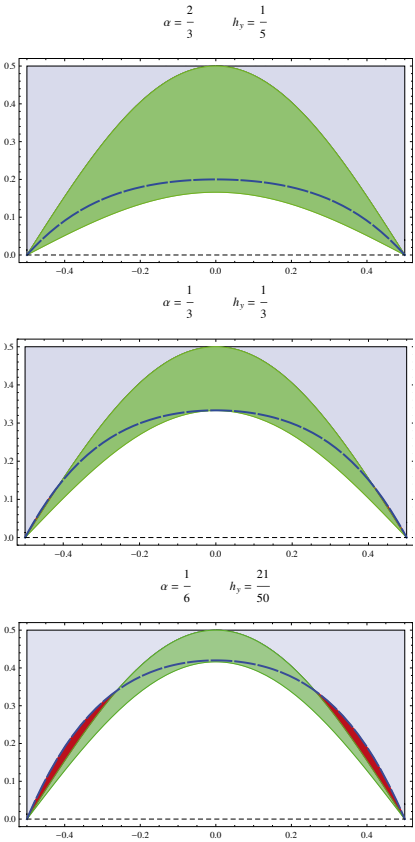

Figure 30. Lintel loaded by uniform body forces: geometry of the arch Γ''' carrying the load of the part Ω'' for three special cases: from top top to bottom, $\alpha = 2/3$, $\alpha = 1/3$, $\alpha = 1/6$.

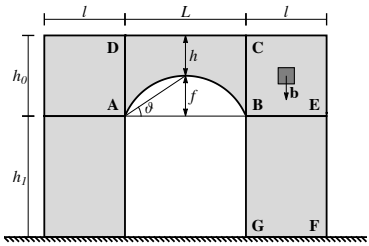

Figure 31. Typical masonry portal. L: span of the arch, f: rise, h: thickness. $ABCD$: lintel, $h_\circ$: height of the lintel. $GFEB$: pier, h_1: height of the pier, ℓ: width of the pier.

$$H = \frac{\left(-16p^\circ + \pi^2(1+2p^\circ)\right)\gamma}{32h_y\pi^2} - \frac{\gamma \mathrm{Log}(1-\alpha)}{\pi^2}\,. \tag{24}$$

2.10 Derand's rule

Based on the unilateral model the safety of the structure is a matter of geometry rather than of strength of materials, in keeping with the spirit of the "rules of proportion" used by the ancient architects for masonry design. The essential characteristic of all these rules is that they are proportional and that they control the overall form of the structure of the building, regardless of its size.

Most of these rules, being not written, have faded and progressively been forgotten, but it is evident that the great buildings of the past could not have been built without some kind of rich and complex knowledge, because its application resulted in astonishing realizations such as the Pantheon and the Gothic cathedrals. One of the rules that is survived, is the Derand's rule (see Benvenuto (1991) and Huerta (2008)), and here I try to assess the safety margins it assures on the basis of singular stress fields for the masonry-like model. The results here obtained confirm that this often criticized rule is actually a sharp technical tool.

The rule applied to a portal. In 1643 François Derand published his monumental work on vaults (Derand (1643)), where the rule for determining the thickness of the walls, needed to support the thrust of the vaults, appears. Here I apply the rule to a simple masonry portal.

If Figure 31, a masonry panel Ω, having the form of a portal, fixed at the base and unloaded on the rest of the boundary, is depicted. The panel

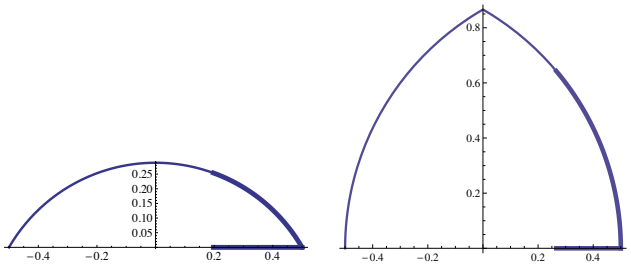

Figure 32. Derand's rule for shallow and pointed arches.

is loaded by its own weight **b**, considered uniform and acting vertically downward, and by a small uniform vertical load applied along the top edge. The main nomenclature concerning such a typical structure is reported in Figure 31, to which I refer for notations. For simplicity I take the unit of length and force in such a way that $L = 1$ and $|\mathbf{b}| = \gamma = 1$.

Derand's rule applies both to segmental and pointed arches as illustrated in Figure 32a,b, to which I refer for notations. Based on this rule the thickness of the wall is the segment ℓ_c indicated as a thick line in Figure 32a,b, that is given by the projection of the arch segment, reported in the same figure, on the horizontal line. The rule is that the arch segment whose projection determines ℓ_c, is $\frac{1}{3}$ of the total length of the intrados.

On introducing the angle $\vartheta = artan(2(1-\alpha)h^\circ)$ (in which α is the parameter introduced in the previous example) and noticing that the radii for the segmental ($\vartheta < \pi/4$) and pointed ($\vartheta > \pi/4$) arches are

$$r' = \frac{L}{2sin2\vartheta} \ , \ r'' = \frac{L}{2(1+cos2\vartheta)} \ ,$$

the rule gives

$$\ell_c = \begin{cases} \frac{L}{2} - r' sin\frac{2}{3}\vartheta \ , \\ r'' \left(1 - cos\frac{2}{3}(\pi - 2\vartheta)\right) \ . \end{cases} \tag{25}$$

Limit Analysis solution We analyze the equilibrium of the portal considering separately the equilibrium of the lintel ABCD and of the pier BEFG, and then assembling the two parts.

Lintel. The effect of the dead load **b** on the lintel depicted in Figure 33a is analyzed by adopting the second s.a. stress field, introduced in the previous Section. Based on this solution the forces transmitted to the piers at

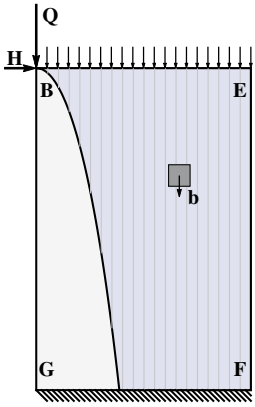

Figure 33. Forces acting of the pier. **Q**, **H** are the vertical and horizontal forces trasmitted by the lintel; the uniformly distributed load at the top base is the effect of the weight of the part BEC; **b** is the body force.

the points A, B, have the vertical and horizontal components given by (23) and (24).

The concentrated and distributed forces acting on the right pier of the portal, are depicted in Figure 33a.

Pier. These forces and their slope can be used as data for the equilibrium of the pier, as shown in Figure 33. In the pier $BEFG$ I consider an arch Γ springing from the point B with the slope given by $2H/Q$. The arch Γ is represented by its graph $z(x)$ in a right handed reference $\{O; x, y\}$ with origin in B and y directed vertically, downward. The arch Γ carries the inclined thrust force coming from the lintel and the weight of the part of the wall above it, besides the over-load s. A uniaxial stress field, linearly varying with y, and balancing the, constant, vertical load $\mathbf{b}$ ($|\mathbf{b}| = \gamma = 1$), is considered both above and below the arch: the upper part is sustained by the arch; the part below is supported by the soil. The equilibrium conditions give, in this case, the following equation for z:

$$z'' = \frac{1}{H}(s + h^\circ + z) \, .$$

This equation can be integrated with the conditions

$$z(0) = 0, z'(0) = \frac{2H}{Q} \, .$$

The solution is

$$z^\circ = \frac{1}{2}\left((p^\circ\frac{L}{2}+s)(1-e^{-\beta x})(-1+e^{\beta x})+\frac{2H}{Q\beta^2}(1+e^{\beta x})\right) ,$$

where $\beta = \sqrt{1/H}$. The form taken by the arch Γ depends on the aspect ratio, p°, of the lintel, and on the parameter α defining the thickness of the arch at the key stone. To compare the results with the rule of Derand, I introduce the parameter

$$\lambda = tan(\vartheta) ,$$

and notice that

$$\lambda = \frac{(1-\alpha)2h^\circ}{L} = (1-\alpha)p^\circ .$$

Then z° can be expressed as a function of p° and λ and the limit length ℓ_c, that is the intersection of the arch Γ' with the base, can be determined for different values of the heigth h.

Effect of the heigth: Gil's rule. Derand'rule makes no reference to the heigth of the pier, though other rules of proportion relating the shape of the arch to the heigth of the piers are known. One of these is the seventh rule of Gil (Rodrigo Gil de Hontanon, see Huerta (2004)) for which the heigth of the pier is approximately twice the rise of the arch.

In Figure 34 a comparison between the values of ℓ_c given by Derand's rule with that obtained with the RNT model under Gil's prescription (that is by putting for the heigth: $h = 2f$), is presented. The values of ℓ_c are plotted against the parameter λ, for a few values of the parameter p°, in the range of practical interest: $\{\frac{1}{10}, \frac{9}{10}\}$. The different curves refer to different values of p°.

The values of ℓ_c predicted with the unilateral model (which being obtained with the static theorem of LA are *safe* and then upper bounds to the limit length ℓ_c) are always smaller than the values prescribed by Derand in the range of values of the aspect ratio p° here explored. Notice that the range considered covers both the cases of shallow and pointed arches and that, based on the NT theory, Derand's prescription appears as a rather sharp rule.

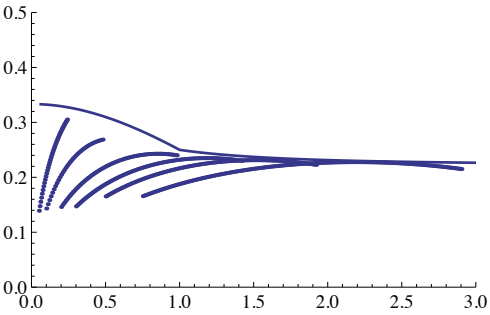

Figure 34. Comparison of Derand's (and Gil's) rule with LA predictions. The continuous upper curve represents the graphic of Derand's rule (25). The sequence of curves represents the LA predictions of ℓ_c for (from left to right) $p^\circ = \{\frac{1}{8}, \frac{1}{4}, \frac{1}{2}, 1, 2, 3\}$.

3 Model *one* (NENT)

In this section the main ingredients of the theory concerning model *one* for masonry materials, namely the Normal Elastic No-Tension (NENT) material, that is the $n > 1$ version of the 1d model introduced in Chapter 1, are presented. The constitutive assumptions, the balance equations and the boundary conditions are introduced and the boundary value problem for NENT materials is formulated. On introducing a proper form of stored elastic energy, the minimum problem for the potential energy functional provides the existence of the solution for this boundary value problem. The main issues connected with energy minimization and a number of illustrative exact solutions and examples are discussed.

3.1 A Premise on Minimum problems and the peculiarity of NT materials

Several problems in physics and Engineering can be formulated as a minimum search: a functional describing the energy of the system and depending on an unknown function has to be minimized over the set of all admissible functions. In the context of elasticity, denoting $\mathbf{u}$ the displacement vector describing the deformation from a given configuration Ω, of a material body subject to a system of applied forces and given boundary displacements, the energy can be written in the form

$$E(\mathbf{u}) = -\langle \ell, \mathbf{u} \rangle + U(\mathbf{u}) \,, \tag{26}$$

where -$\langle \ell, \mathbf{u} \rangle$ is the linear form describing the potential energy of the load, that is minus the work of the load $\ell = (\underline{\mathbf{s}}, \mathbf{b})$ for the displacement $\mathbf{u}$, and U($\mathbf{u}$) is the stored energy functional. The simplest case in which existence theorems for the minimum problem

$$\min_{\mathbf{u} \in K} E(\mathbf{u}) \ , \tag{27}$$

K being the subset of a convenient Banach space $T(\tilde{\Omega})$, occurs when $E(\mathbf{u})$ is lower semicontinuous and coercive, in the sense that $E(\mathbf{u}) \to \infty$ as $\|\mathbf{u}\|_S \to \infty$. Unfortunately, as we shall see, the energy functional for masonry-like materials is not coercive (see also the form that the strain energy density takes in the 1d case (see Figure 10.a of Chapter 1) and therefore some supplementary hypotheses have to be added in order to get existence. For instance, existence of solution in the case of Normal Elastic No-Tension materials, under small strains and in the 2d context, has been established by Giaquinta and Giusti (in Giaquinta and Giusti (1985)), under a so called *safe load condition*. Specifically the form of energy to be minimized in the case of NENT materials is

$$E(\mathbf{u}) = -\int_{\partial\Omega_N} \underline{\mathbf{s}} \cdot \mathbf{u} - \int_{\Omega} \mathbf{b} \cdot \mathbf{u} + \int_{\Omega} \Phi(\mathbf{E}(\mathbf{u})) \ , \tag{28}$$

where $\mathbf{E}(\mathbf{u})$ is the infinitesimal strain associated to $\mathbf{u}$, $\Phi(\mathbf{E}(\mathbf{u}))$ is the elastic energy density, and the stress $\mathbf{T}$ is related to $\mathbf{E}$ through the relation

$$\mathbf{T} = \frac{\partial \Phi}{\partial \mathbf{E}} \ . \tag{29}$$

The minimizer of $E(\mathbf{u})$ is searched for $\mathbf{u} \in S(\Omega)$ (a Banach space) and $\mathbf{u} = \underline{\mathbf{u}}$ on $\partial\Omega_D$. Concerning the nature of such Banach space, that is the regularity of $\mathbf{u}$, actually it seems reasonable to expect, based on the non coercivity of Φ (see Figure 10.a of Chapter 1) and on the at most linear growth of the energy $E(\mathbf{u})$, that $\mathbf{u}$ be possibly discontinuous and the corresponding deformation not to be absolutely continuous. A popular choice for $S(\Omega)$ is the space $BD(\Omega)$ of bounded deformations, though one expects that, apart from very special cases and away from the case of collapse loads, the minimizers should be much more regular. We shall return to the variational formulation of equilibrium for masonry materials after the BVP in its strong form is considered.

3.2 The Boundary Value Problem for NENT materials

Constitutive restrictions. It is assumed that the structure $\Omega \in \Re^n$ (here $n = 2$), loaded by the given tractions $\underline{\mathbf{s}}$ on the part $\partial\Omega_N$ of the boundary, and

subject to given displacements $\underline{\mathbf{u}}$ on the complementary, constrained part of the boundary $\partial\Omega_D$, is in equilibrium under the action of the given surface and body loads ($\underline{\mathbf{s}}$, $\mathbf{b}$) and distortions $\underline{\mathbf{E}}$, and undergoes small displacements $\mathbf{u}$ and strains $\mathbf{E}(\mathbf{u})$[13].

Notice again that Ω is considered closed on $\partial\Omega_D$ and open on the rest of the boundary.

We consider that the structure Ω is composed of Normal Elastic No-Tension material, that is the stress $\mathbf{T}$ is negative semidefinite

$$\mathbf{T} \in Sym^{-} \ , \tag{30}$$

the effective strain, that is the total infinitesimal strain $\mathbf{E}(\mathbf{u})$ minus the eigenstrains $\underline{\mathbf{E}}$, is decomposed additively into the sum of an elastic part $\mathbf{E}^e$ and an anelastic part $\mathbf{E}^a$, namely:

$$\mathbf{E}(u) = \mathbf{E}^e + \mathbf{E}^a + \underline{\mathbf{E}} \ , \tag{31}$$

the elastic part being linearly related to the stress $\mathbf{T}$:

$$\mathbf{E}^e = \mathbf{A}\,[\mathbf{T}] \ , \tag{32}$$

the latent anelastic part (a measure for fracture) being positive semidefinite

$$\mathbf{E}^a \in Sym^{+} \ , \tag{33}$$

and the stress $\mathbf{T}$ doing no work for the corresponding latent strain $\mathbf{E}^a$

$$\mathbf{T} \cdot \mathbf{E}^a = 0 \ . \tag{34}$$

Notice that in the plane case (n=2) conditions (30), (33), can be rewritten as

$$tr\,\mathbf{T} \leq 0 \ , \ det\,\mathbf{T} \geq 0 \ , \tag{35}$$

$$tr\,\mathbf{E}^a \geq 0 \ , \ det\,\mathbf{E}^a \geq 0 \ . \tag{36}$$

Remark 10. It is to be pointed out that a NENT material, that is a material defined by the restrictions (30) through (34), is elastic in the sense that, given the total strain $\mathbf{E}(\mathbf{u})$, the stress can be univocally determined. The material is actually hyperelastic as we shall see later in what follows.$\diamond$

[13]When eigenstrains are considered, under the small strain assumption, the total strain $\mathbf{E}(\mathbf{u})$ is decomposed additively as follows: $\mathbf{E}(\mathbf{u})=\mathbf{E}^* + \underline{\mathbf{E}}$, $\mathbf{E}^*$ being the *effective* strain of the material.

Equilibrium problem. In order to avoid trivial incompatible loads ($\underline{\mathbf{s}}$,$\mathbf{b}$), I assume again that the tractions $\underline{\mathbf{s}}$ satisfy condition (4).

In equilibrium, the stress field $\mathbf{T}$ must be balanced with $\mathbf{b}$, that is

$$div\mathbf{T} + \mathbf{b} = \mathbf{0} \,, \tag{37}$$

and the stress $\mathbf{T}$ and the displacement $\mathbf{u}$ must comply with the boundary conditions

$$\mathbf{T}\mathbf{n} = \underline{\mathbf{s}} \,, \; on \; \partial\Omega_N \,, \mathbf{u} = \underline{\mathbf{u}} \,, \; on \; \partial\Omega_D \,. \tag{38}$$

Boundary Value Problem. The boundary value problem for NENT materials can be formulated as follows:

Given a bounded open set Ω *and the partition* $\partial\Omega = \partial\Omega_D \cup \partial\Omega_N$, *find the fields* $\mathbf{u}$, $\mathbf{T}$ *defined over* $\Omega \cup \partial\Omega_D$, *such that the material restrictions* (30) through (34), *the balance equations* (37) *and the b.c.* (38) *are satisfied.*

Peculiar features of the fracture field for NENT materials, in the three sets of the Fundamental Partition. As it was already observed in the previous Chapter concerning the RNT model, to each statically admissible stress field $\mathbf{T}$ defined over $\Omega \cup \partial\Omega_D$, is associated a Fundamental Partition of the domain: $\Omega = \Omega_1 \cup \Omega_2 \cup \Omega_3$, of biaxial, uniaxial and zero stress (see Section 2.3).

In Ω_2 the equilibrium equations and the condition $det\mathbf{T} = 0$, form a system of three equations in the three unknown independent components of $\mathbf{T}$. The differential problem is parabolic and the stress is determined by equilibrium regardless of the material response.

In Ω_1 fractures are not possible, that is $\mathbf{E}^a = \mathbf{0}$.

In Ω_3, where $\mathbf{T} = \mathtt{0}$, any positive semidefinite fracture field is possible.

Also in Ω_2 the material can be fractured. The necessity of fractures is naturally produced by the problem being statically determined: the elastic strain associated to the statically determined stress is generally not compatible and fracture strains are required to restore compatibility. The normality condition requires that in Ω_2 the fractures must open up orthogonally to the isostatic compression lines, therefore, as a consequence of normality, on a crack line (that is a line where the strain is a line Dirac delta) the jump of displacement must be purely orthogonal to the crack line. If the strain is regular, in a curvilinear frame with natural bases $\mathbf{a}_1, \mathbf{a}_2$ coincident with the eigenvectors of $\mathbf{T}$, $\mathbf{T}$ admits the representation

$$\mathbf{T} = \sigma \frac{\mathbf{a}_1 \otimes \mathbf{a}_1}{\mathbf{a}_1 \cdot \mathbf{a}_1} ,$$

σ being the only non zero, negative eigenvalue of $\mathbf{T}$. Normality implies the following form for the fracture strain $\mathbf{E}^a$:

$$\mathbf{E}^a = \lambda \frac{\mathbf{a}_2 \otimes \mathbf{a}_2}{\mathbf{a}_2 \cdot \mathbf{a}_2} ,$$

λ being the only non zero, non negative eigenvalue of $\mathbf{E}^a$. Then, regardless of the possible elastic anisotropy of the material, the principal directions of stress and anelastic strain of a NENT material are always coincident all over Ω.

3.3 Strain energy density in 2d

Most of the features illustrated by the 1d ENT model (that is *Model 1* introduced in *Chapter* 1) are transposed to the 2d case, except that to obtain hyperelasticity there is a price to pay: the assumption of normality (that is the constituitve assumptions (33), (34)) must be made on the total latent strain $\mathbf{E}^a$. Such an assumption implies that on a discontinuity line Γ for the displacement $\mathbf{u}$, that is on the support of a concentrated fracture, the jump of displacement must be orthogonal to Γ. Therefore sliding is forbidden on fracture lines. It is shown by Del Piero in Del Piero (1989) that, for NENT materials, the major symmetry of $\mathbf{A}$ is necessary and sufficient to get existence of an elastic energy function. In the isotropic case the form of the energy density Φ can be constructed explicitly[14] in terms of the eigenvalues e_1, e_2 of $\mathbf{E}$ (here $e_1 < e_2$ is assumed). In the case of generalized plane stress, one has (see Figure 35)

$$\Phi = \begin{cases} 0 , & e_1 \geq 0 \text{ and } e_2 \geq 0 , \\ \frac{1}{2} E e_1^2 , & e_1 < 0 \text{ and } e_2 \geq -\nu e_1 , \\ \frac{1}{2} \frac{E}{1-\nu^2} \left(e_1^2 + e_2^2 + 2\nu e_1 e_2 \right) & e_1 < 0 \text{ and } e_2 < -\nu e_1 , \end{cases}$$

E, ν being the Young modulus and the Poisson ratio. Notice that the stress $\mathbf{T}$ derived from Φ satisfies identically the no-tension restriction (30), that is there is no need to impose it as a constraint.

[14] In the general anisotropic case the explicit symbolic form of Φ is not known and must be constructed numerically, case by case.

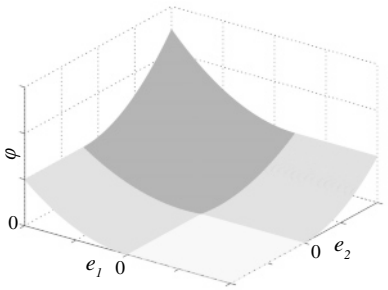

Figure 35. Strain energy density of isotropic NENT materials: zero energy region: light grey; parabolic energy region: grey; elliptic energy region: dark grey.

3.4 Function spaces for the potential energy functional.

For hyperelastic materials equilibrium states of the body can be searched as minimizers of the total potential energy (28)

$$\min_{\mathbf{u}\in K} E(\mathbf{u}) \ , \tag{39}$$

K being the set of kinematically admissible displacement fields for NENT materials, defined as follows

$$K = \{\mathbf{u} \in T(\Omega) \ s.t. \ \mathbf{u} = \underline{\mathbf{u}} \ on \ \partial\Omega_D \ \} \ , \tag{40}$$

where $\Omega = \dot{\Omega} \cup \partial\Omega_D$ and $T(\Omega)$ is a convenient Banach space. As it is evident from the picture of Figure 35, the strain energy function characterizing NENT materials is not coercive.

Coercivity of the total potential energy can be restored by considering the following *supersafe load condition* on the applied forces (here I consider for simplicity the case of fixed boundary constraints: $\mathbf{u} = 0$, *on* $\partial\Omega_D$)

Supersafe load condition. The load $\mathbf{p}, \mathbf{b}$ is said to be *supersafe* if there exists at least one stress field $\overline{\mathbf{T}} \in H$, H being the set of statically admissible stress fields for NT materials defined in (7):

$$H = \left\{\mathbf{T} \in S(\Omega) \ s.t. \ div\mathbf{T} + \mathbf{b} = \mathbf{0} \ , \ \mathbf{Tn} = \underline{\mathbf{s}} \ on \ \partial\Omega_N \ , \ \mathbf{T} \in Sym^{-}\right\} \ , \tag{41}$$

such that

$$(\overline{\mathbf{T}} + \beta \mathbf{I}) \in Sym^{-} \ , \tag{42}$$

for some constant $\beta > 0$. In other words the load is supersafe if $\overline{\mathbf{T}}$ is strictly statically admissible over the set Ω in a uniform way, that is independently of $\mathbf{x}$. The definition of supersafe loads depends on the choice of the function space $S(\Omega)$. For NENT materials one can assume

$$S(\Omega) \equiv L^2(\Omega) \ . \tag{43}$$

If the load is supersafe then the potential energy associated to the external forces can be expressed in terms of $\overline{\mathbf{T}}$ and of any displacement $\mathbf{u} \in K$, in the form

$$-\int_{\partial\Omega_N} \underline{\mathbf{s}} \cdot \mathbf{u} - \int_{\Omega} \mathbf{b} \cdot \mathbf{u} = -\int_{\Omega} \overline{\mathbf{T}} \cdot \mathbf{E}(\mathbf{u}) \ .$$

Then the total potential energy can be rewritten in terms of this super safe s.a. stress field $\overline{\mathbf{T}}$ as

$$E(\mathbf{u}) = -\int_{\Omega} \overline{\mathbf{T}} \cdot \mathbf{E}(\mathbf{u}) + \frac{1}{2} \int_{\Omega} \mathbf{C}[\mathbf{E}^e(\mathbf{u})] \cdot \mathbf{E}^e(\mathbf{u}) \ .$$

Recalling that $\mathbf{E}(\mathbf{u}) = \mathbf{E}^e(\mathbf{u}) + \mathbf{E}^a(\mathbf{u})$, on using the safe load assumption one can write

$$E(\mathbf{u}) \geq -\int_{\Omega} \overline{\mathbf{T}} \cdot \mathbf{E}^e(\mathbf{u}) + \frac{1}{2} \int_{\Omega} \mathbf{C}[\mathbf{E}^e(\mathbf{u})] \cdot \mathbf{E}^e(\mathbf{u}) + \beta \int_{\Omega} |\mathbf{E}^a(\mathbf{u})| \ ,$$

that is the energy has at least a linear growth with respect to the norm of the space $BD(\Omega)$: the space of functions $\mathbf{u}$ whose corresponding infinitesimal deformation $\mathbf{E}$ is a bounded measure. For full information on this function space I refer to the paper by Temam and Strang (1994). Here I notice only that, since the infinitesimal strain $\mathbf{E}$ can be a bounded measure, then $\mathbf{u}$ can be discontinuous and $\mathbf{E}$ can be decomposed in its absolutely continuous and singular parts with respect to the 2d Lebesgue measure:

$$\mathbf{E}(\mathbf{u}) = \mathbf{E}_r + \mathbf{E}_s \ .$$

Recalling the decomposition of $\mathbf{E}$ into its elastic and fracture parts, since the potential energy grows quadratically with respect to the elastic part of the deformation, then only the fracture part $\mathbf{E}^a$ can be singular,

that is only fracture discontinuities are admitted. In other words the elastic deformation must be regular and the anelastic deformation can be either regular or singular. In Giaquinta and Giusti (1985) (theorem 6.8, p 381), the authors show the existence of the solution for the minimum problem with $T(\Omega) = BD(\Omega)$ under the supersafe load condition (and some supplementary technical conditions) in the special case of traction problems and isotropic elastic behaviour. Since the energy is not strictly convex the solution is in general non unique.

3.5 Complementary energy functional.

Also a dual energy principle based on the Complementary Energy can be proved (see Giaquinta and Giusti (1985)). The stress state $\mathbf{T}^\circ$ that corresponds to the solution of the boundary value problem for NENT materials can be characterized as the minimizer of the energy functional

$$E_c(\mathbf{T}) = -\int_{\partial\Omega_D} \mathbf{T}\mathbf{n}\cdot\underline{\mathbf{u}} + \frac{1}{2}\int_\Omega \mathbf{A}[\mathbf{T}]\cdot\mathbf{T}\ , \tag{44}$$

over the set H of statically admissible stress fields

$$H = \left\{\mathbf{T}\in S(\Omega)\ s.t.\ div\mathbf{T}+\mathbf{b}=\mathbf{0}\ ,\ \mathbf{T}\mathbf{n}=\underline{\mathbf{s}}\ on\ \partial\Omega_N\ ,\ \mathbf{T}\in Sym^-\right\}\ , \tag{45}$$

$S(\Omega)$ being a convenient Banach space. $S(\Omega)$ can be assumed as the Hilbert space $L^2(\Omega)$: in other words H is represented by the symmetric second order tensors $\mathbf{T}$ of $L^2(\Omega)$, such that $\mathbf{T}$ is negative semidefinite and balanced with $\underline{\underline{\mathbf{s}}}, \mathbf{b}$. Obviously on considering $\mathbf{T}\in L^2(\Omega)$ the balance conditions must be considered in a generalized sense (see (8), (9)).

The choice of $L^2(\Omega)$ as the function space for the stress field seems natural considering the quadratic term which represents the stress energy in the complementary energy (44). Since the Complementary Energy functional is strictly convex over the convex set H, the existence and the uniqueness of the minimizer $\mathbf{T}^\circ$ of such functional is guaranteed whenever H is not void (that is there exist at least one square summable stress field $\mathbf{T}$ such that $\mathbf{T}$ is negative semidefinite and balanced with $\underline{\underline{\mathbf{s}}}, \mathbf{b}$, or, in other words, the loads are compatible in the sense of definition (17)). Therefore though the solution $\mathbf{u}^\circ$ may be non unique the elastic part $\mathbf{E}^e$ of the strain solution is unique. Non uniqueness is restricted to the anelastic part $\mathbf{E}^a$ of the deformation $\mathbf{E}$, and to special arrangements of the boundary conditions. This circumstance makes the displacement and stress approach to the equilibrium of NENT materials non symmetric, in the sense that existence of the minimizer $\mathbf{T}^\circ$ for the complementary energy. is not sufficient for the existence of the minimizer $\mathbf{u}^\circ$ of the potential energy E. The existence of $\mathbf{T}^\circ$

requires only the existence of an admissible stress field, existence of $\mathbf{u}^\circ$, with the known theorems, requires instead the existence of a uniformly strictly admissible stress field. There are indeed counterexamples for the existence of $\mathbf{u}^\circ$ in the case the loads do not satisfy the safe load condition, in which a s.a. stress field $\mathbf{T}^\circ$ can be found; two of them are reported in the next *Subsection*.

3.6 Examples of non-existence.

To my knowledge there are no examples of non existence, for traction problems, in the case in which the loads do not satisfy the safe load condition but there exists a strictly admissible stress field $\mathbf{T}$. The only known counterexamples refer to the case in which the loads do not satisfy the safe load condition and there exists a balanced and admissible, but not strictly admissible, stress field $\mathbf{T}$. In the known examples there are parts of the domain that can be taken away and transplaced rigidly, without paying any energy price. Therefore $E = 0$ as $|\mathbf{u}| \to +\infty$, and I can say that the loads are collapse loads, in the sense that the deformation can increase indefinitely at constant load. Some trivial examples of non-existence are considered in what follows.

Two examples of non existence. The NENT material is a peculiar model for a continuum, some care in the imposition of the data must be exercised to avoid nasty results, that is lack of solution or very large displacements for small loads. The idea is that the material is rather delicate and loads and displacements must be applied cautiously to allow for the material to accept them. This aspect is somehow in keeping with the behaviour of real masonry structures which suffer from the application of concentrated loads or from the abrupt changes of loads or given displacements. The message is that the data of a BVP relative to a body made of NENT material must be specially disposed and coordinated.

The two following examples are two, more or less famous, examples of non existence. The first case (Figure 36a) refers to a traction problem, the second (Figure 36b) to a mixed BVP.

These two examples suggest that a *finite* normal crack develops on a line: the assumption of infinitesimal displacements and strains is violated.

3.7 Elementary analytical solutions

A number of closed form solutions for NENT materials were first presented in Angelillo and Giliberti (1988); here I report some of them.

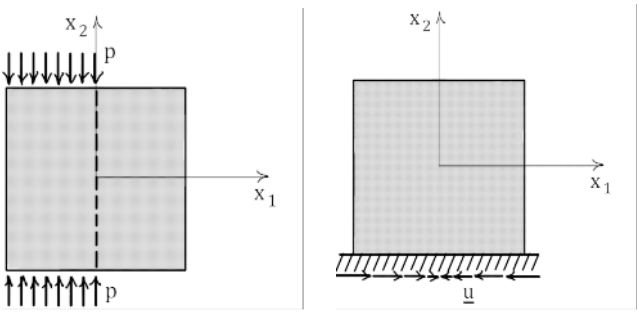

Figure 36. Examples of non existence of the solution for the NENT BVP. (a) : the displacement corresponding to the only statically admissible state cannot possibly verify the normality condition at the interface Γ (the vertical center line), unless the normal displacement jump on Γ tends to $+\infty$. (b): since the only statically admissible stress field is $\mathbf{T} = \mathbf{0}$, any k.a. displacement field cannot possibly satisfy the normality condition at the base for the given tangential displacements, unless the normal displacement jump at the base tends to $+\infty$.

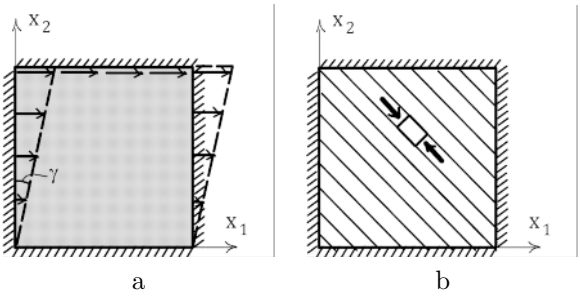

Figure 37. Pure shear: (a). Stress field solution: (b).

Exact solution 1: Pure shear. The very first simple, non trivial solution (i.e. distinct from elementary solutions of linear elasticity), for NENT materials is pure shear (Figure 37).

The solution, in terms of displacements, is identical to the universal solution for homogeneous linearly elastic materials, that is

$$u_1 = \gamma x_2 \ , \ u_2 = 0 \ .$$

The corresponding strain decomposition into elastic and anelastic strains: $\mathbf{E} = \mathbf{E}^e + \mathbf{E}^a$, for a homogeneous and isotropic NENT material, is

$$\left\{ \begin{array}{cc} 0 & \frac{\gamma}{2} \\ \frac{\gamma}{2} & 0 \end{array} \right\} = \left\{ \begin{array}{cc} -\frac{\gamma}{4} & \frac{\gamma}{4} \\ \frac{\gamma}{4} & -\frac{\gamma}{4} \end{array} \right\} + \nu \left\{ \begin{array}{cc} \frac{\gamma}{4} & \frac{\gamma}{4} \\ \frac{\gamma}{4} & \frac{\gamma}{4} \end{array} \right\} + (1-\nu) \left\{ \begin{array}{cc} \frac{\gamma}{4} & \frac{\gamma}{4} \\ \frac{\gamma}{4} & \frac{\gamma}{4} \end{array} \right\} ,$$

where

$$\{\mathbf{E}^a\} = (1-\nu) \left\{ \begin{array}{cc} \frac{\gamma}{4} & \frac{\gamma}{4} \\ \frac{\gamma}{4} & \frac{\gamma}{4} \end{array} \right\} .$$

The associated stress field, trivially balanced with zero body loads inside Ω is (see Figure 37b)

$$\{\mathbf{T}\} = E \left\{ \begin{array}{cc} -\frac{\gamma}{4} & \frac{\gamma}{4} \\ \frac{\gamma}{4} & -\frac{\gamma}{4} \end{array} \right\} .$$

With this solution the whole domain is of the Ω_2 type, the material being uniformly compressed along a family of compression rays parallel to a diagonal of the square panel; uniformly distributed fractures open up in the direction of the other diagonal. Therefore, in a real masonry panel, one may expect a pattern of parallel cracks in the direction of the compression rays.

Exact solution 2: Simple flexure. The second problem I consider is the flexure of a rectangular strip. The geometry and the boundary conditions are depicted in Figure 38a to which I refer for notations. A simple solution of the problem exists if the material is isotropic and one assumes $\nu = 0$ (an assumption that, though far from being realistic, produces easy analytical solution that one can use as benchmark problems for numerical approximations).

In this case the displacement field $\mathbf{u} = u\hat{\mathbf{e}}_1 + v\hat{\mathbf{e}}_2$ with

$$u = \frac{\varphi}{L}(L - 2x_1)x_2 ,$$

$$v = -\frac{\varphi}{L}(L - x_1)x_1 ,$$

solves all the field and boundary equations, for a homogeneous and isotropic NENT material, with $\nu = 0$. Indeed the corresponding total strain is

$$\{\mathbf{E}\} = \left\{ \begin{array}{cc} -2\frac{\varphi x_2}{L} & 0 \\ 0 & 0 \end{array} \right\} ,$$

that is easily decomposed into the elastic and fracture parts:

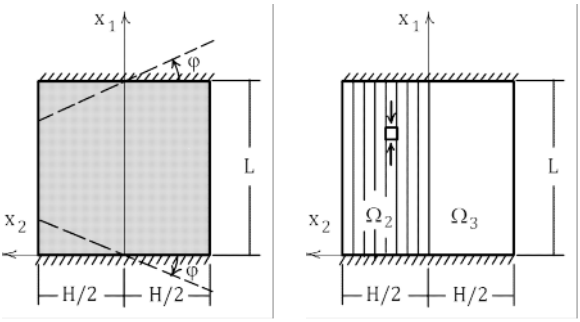

Figure 38. Pure flexure of a rectangular strip. Boundary data: (a), stress and domain partition corresponding to the first solution: (b).

$$\{\mathbf{E}^e\} = \begin{cases} \left\{ \begin{array}{cc} -2\frac{\varphi x_2}{L} & 0 \\ 0 & 0 \end{array} \right\} & , \; x_2 > 0 \, , \\ \left\{ \begin{array}{cc} 0 & 0 \\ 0 & 0 \end{array} \right\} & , \; x_2 \leq 0 \, , \end{cases} \tag{46}$$

$$\{\mathbf{E}^a\} = \begin{cases} \left\{ \begin{array}{cc} 0 & 0 \\ 0 & 0 \end{array} \right\} & , \; x_2 > 0 \, , \\ \left\{ \begin{array}{cc} -2\frac{\varphi x_2}{L} & 0 \\ 0 & 0 \end{array} \right\} & , \; x_2 \leq 0 \, . \end{cases} \tag{47}$$

The corresponding stress field is

$$\{\mathbf{T}\} = E \begin{cases} \left\{ \begin{array}{cc} -2\frac{\varphi x_2}{L} & 0 \\ 0 & 0 \end{array} \right\} & , \; x_2 > 0 \, , \\ \left\{ \begin{array}{cc} 0 & 0 \\ 0 & 0 \end{array} \right\} & , \; x_2 \leq 0 \, . \end{cases} \tag{48}$$

This stress field is obviously balanced with the prescribed body load $\mathbf{b} = \mathbf{0}$ at the interior and with the surface tractions $\underline{\mathbf{s}} = \mathbf{0}$ given at the loaded part of the boundary ($x = \mp H/2$). Based on this solution for the

stress, the domain Ω is divided into two zones of the type Ω_2, Ω_3, as depicted in Figure 38b.

For this example I can also give a different solution, namely the same stress field but a different fracture field, under the same boundary conditions. The second solution (see Figure 39) to the same problem is defined by the displacement field $\mathbf{u} = u\hat{\mathbf{e}}_1 + v\hat{\mathbf{e}}_2$, as follows

$$u = \begin{cases} \frac{\varphi}{L}(L - 2x_1)x_2 & , \ x_2 > 0 \ , \\ \varphi x_2 & , \ x_2 < 0 \text{ and, } \ x_1 < L/2 \ , \\ -\varphi x_2 & , \ x_2 < 0 \text{ and, } \ x_1 > L/2 \ , \end{cases}$$

$$v = \begin{cases} -\frac{\varphi}{L}(L - x_1)x_1 & , \ x_2 > 0 \ , \\ -\varphi x_1 & , \ x_2 < 0 \text{ and, } \ x_1 < L/2 \ , \\ \varphi(x_1 - L) & , \ x_2 < 0 \text{ and, } \ x_1 > L/2 \ . \end{cases}$$

The corresponding total strain is composed of absolutely continuous and singular parts: $\mathbf{E} = \mathbf{E}_r + \mathbf{E}_s$ with

$$\{\mathbf{E}_r\} = \begin{cases} \left\{ \begin{array}{cc} -2\frac{\varphi x_2}{L} & 0 \\ 0 & 0 \end{array} \right\} & , \ x_2 > 0 \ , \\ \left\{ \begin{array}{cc} 0 & 0 \\ 0 & 0 \end{array} \right\} & , \ x_2 \leq 0 \ , \end{cases}$$

$$\{\mathbf{E}_s\} = \begin{cases} \left\{ \begin{array}{cc} -2\varphi x_2 & 0 \\ 0 & 0 \end{array} \right\} \delta & , \ x_1 = L/2 \text{ and } x_2 \leq 0 \ , \\ \left\{ \begin{array}{cc} 0 & 0 \\ 0 & \frac{\varphi x_1^2}{L} \end{array} \right\} \delta & , \ x_1 < L/2 \text{ and } x_2 = 0 \ , \\ \left\{ \begin{array}{cc} -2\varphi x_2 & 0 \\ 0 & \frac{\varphi(x_1 - L)^2}{L} \end{array} \right\} \delta & , \ x_1 > L/2 \ \& \ x_2 = 0 \ . \end{cases}$$

where δ denotes the unit Dirac delta. The total strain is then decomposed in its elastic and anelastic parts as follows:

$$\mathbf{E}^e = \mathbf{E}_r \ , \ \mathbf{E}^a = \mathbf{E}_s \ .$$

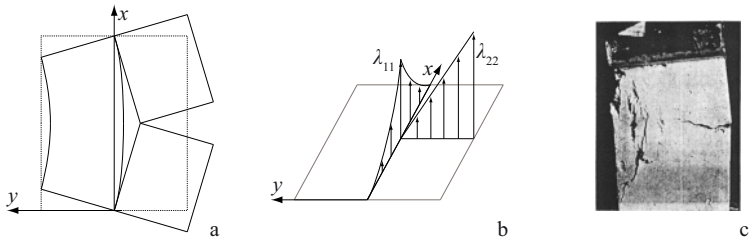

Figure 39. Deformed configuration corresponding to the second solution: (a). Graph of the non zero Cartesian components of $\mathbf{E}^a$:(b). Flexure test on a masonry panel (courtesy G. Castellano): (c).

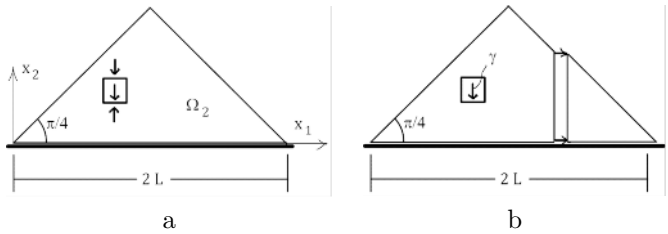

Figure 40. Heap under uniform body forces resting on a smooth foundation: (a). Mechanism for which the load does zero work: (b).

Therefore the stress $\mathbf{T}$ coincides with that of the first solution and determines the same partition of the domain Ω, as described in Figure 38b.

The fracture strain is singular and describes the cracks exhibited by the deformed configuration depicted in Figure 39a. A graph of the E_{11} and E_{22} components of $\mathbf{E}^a$ is reported in Figure 39b. In the absence of any energy price to pay to open up fractures, the two solutions reported are perfectly equivalent and the body can choose any of the two. It could be of some interest to look at the result of the flexure test performed on a masonry-like material (a mixture of lime and gypsum with a ratio between tensile and compressive strength of $\frac{1}{20}$) shown in Figure 39c.

Exact solution 3: 2d heap of masonry stones on a smooth foundation. The third problem I consider concerns a triangle of NENT material, simply supported at the base on a rigid, perfectly smooth interface (see Figure 40). The only external forces I consider are represented by a uniform gravitational load $\mathbf{b} = -\gamma \hat{\mathbf{e}}_2$ directed vertically.

A solution to this problem can be easily found since there exists only

one admissible stress field for this geometry and for these data.

The load is a collapse load since the resultant stress across any vertical section of the triangle (see Figure 40b) is zero and any two parts divided by a vertical section, can be separated horizontally with a vertical crack, corresponding to a zero energy mode and consisting into a horizontal uniaxial strain, concentrated on the line of separation.

Setting the length scale in such a way that $L = 1$, the one and only s.a. stress field, negative semidefinite and in equilibrium with the load, is written as follows

$$\{\mathbf{T}\} = \left\{ \begin{array}{cc} 0 & 0 \\ 0 & \sigma(x_1, x_2) \end{array} \right\} ,$$

with

$$\sigma(x_1, x_2) = \left\{ \begin{array}{cc} \gamma(x_2 - x_1) & , \; x_1 \leq 1 \, , \\ \gamma(x_2 + x_1 - 2) & , \; x_1 \geq 1 \end{array} \right\} .$$

To this stress field (considering for simplicity the case $\nu = 0$) is associated the elastic strain

$$\{\mathbf{E}^e\} = \left\{ \begin{array}{cc} 0 & 0 \\ 0 & \epsilon(x_1, x_2) \end{array} \right\} ,$$

with

$$\epsilon(x_1, x_2) = \left\{ \begin{array}{cc} \frac{\gamma}{E}(x_2 - x_1) & , \; x_1 \leq 1 \, , \\ \frac{\gamma}{E}(x_2 + x_1 - 2) & , \; x_1 \geq 1 \end{array} \right\} .$$

Therefore, taking into account the normality condition $\mathbf{T}.\mathbf{E}^a$, the anelastic strain takes the form

$$\{\mathbf{E}^a\} = \left\{ \begin{array}{cc} \lambda(x_1, x_2) & 0 \\ 0 & \end{array} \right\} ,$$

the total strain being

$$\{\mathbf{E}\} = \left\{ \begin{array}{cc} \lambda(x_1, x_2) & 0 \\ 0 & \epsilon(x_1, x_2) \end{array} \right\} .$$

Such total strain is compatible if and only if

$$\frac{\partial^2 \lambda(x_1, x_2)}{\partial x_2^2} + \frac{\partial^2 \epsilon(x_1, x_2)}{\partial x_1^2} = 0 \, .$$

The function $\epsilon(x_1, x_2)$ is not smooth and its second derivatives must be interpreted in a generalized sense. The 3d graph of $\epsilon(x_1, x_2)$ depicted in

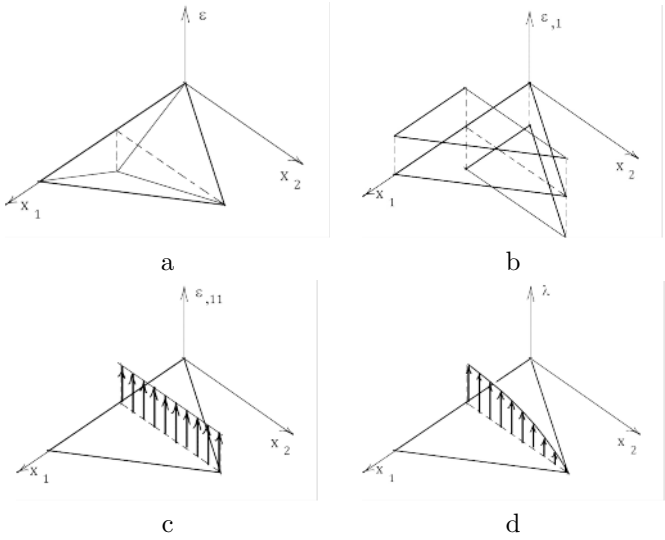

Figure 41. 3d plot of the elastic uniaxial strain $\epsilon(x_1, x_2)$: (a). In (b): first derivative of $\epsilon(x_1, x_2)$ with respect to x_1: piecewise constant field. In (c): second derivative; a constant line Dirac delta with support on the center line Γ. In (d) the anelastic strain $\lambda(x_1, x_2)$ restoring compatibility: a parabolic line Dirac delta with support on the center line Γ

Figure 41a, can help to visualize the first and second derivatives of $\epsilon(x_1, x_2)$ with respect to x_1 reported in Figures 41b,c.

A function $\lambda(x_1, x_2)$ that solves the compatibility equation and is non negative is

$$\lambda(x_1, x_2) = \frac{\gamma}{E}(L - x_2^2)\,\delta(\Gamma)\,,$$

where $\delta(\Gamma)$ is the line Dirac delta defined on the line Γ of equation $x_1 = 1$ (see the graph depicted in Figure 41d).

The displacement $\mathbf{u} = u\hat{\mathbf{e}}_1 + v\hat{\mathbf{e}}_2$ is then obtained integrating the total deformation. In components

$$u = \begin{cases} \frac{\gamma}{2E}(x_2^2 - 1) & ,\ x_1 < 1\,, \\ \frac{\gamma}{2E}(1 - x_2^2) & ,\ x_1 > 1\,, \end{cases}$$

$$v = \begin{cases} \frac{\gamma}{2E}x_2(x_2 - x_1) & ,\ x_1 < 1\,, \\ \frac{\gamma}{2E}x_2(x_2 + x_1 - 2) & ,\ x_1 > 1\,, \end{cases}$$

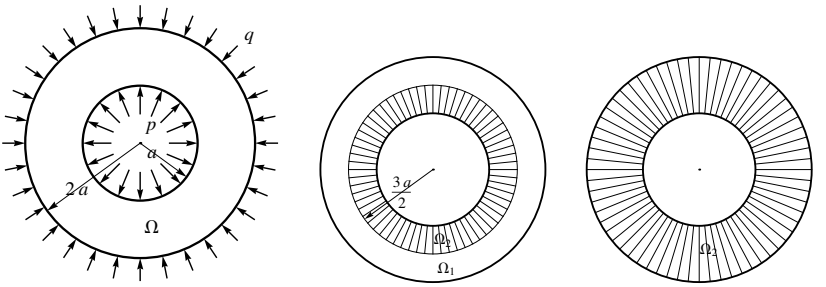

Figure 42. Ring under external and internal pressures: (a). Fundamental partition of the domain corresponding to the solution for $\alpha = 25/48$: (b). Fundamental partition corresponding to $\alpha = 1/2$: (c).

The deformation corresponding to this discontinuous displacement field, singular on the center line Γ, gives a concentrated fracture varying parabolically with x_2.

Exact solution 4: Ring under internal and external pressures. The fourth problem I consider concerns a ring of internal radius a and external radius $2a$, composed of NENT material and subjected to an internal pressure p and an external pressures $q = \alpha\, p$ (see Figure 42).

The real number α is a load parameter varying in the interval $[1/2, 1]$. Notice that the case $\alpha = 1$ corresponds to the elastic solution of uniform pressure.

First Case: supersafe load. First I consider the case in which $1/2 < \alpha < 1$. To fix the ideas I consider the special case $\alpha = \frac{25}{48}$.

In this case the load is *supersafe* since there exists a strictly s.a. stress field, uniformly bounded from above by a uniform compression of value $-p/18$. Such s.a. stress field, in physical components in the polar coordinate system $\{r, \vartheta\}$ with origin in the center of the ring, takes the form

$$T_{rr} = -p\left(\frac{a}{r} + \frac{r^2 - a^2}{36r^2}\right) ,$$

$$T_{\vartheta\vartheta} = -p\frac{r^2 + a^2}{36r^2} ,$$

$$T_{r\vartheta} = 0 .$$

The existence of a purely compressive s.a. stress field does not imply that the solution of the BVP is necessarily of pure biaxial compression. In the case at hand we shall see that both uniaxial and biaxial stress states, and fractures open up in the inner part of the domain.

With reference to the linear elastic solution for an isotropic pressurized ring, recalling the formula for the stress (see Timoshenko and Goodier (1951)), one easily finds that: in the region $\Omega_1 = \{\{r, \vartheta\}\ s.t.\ \frac{3}{2}a < r < 2a\}$, the stress coincides with the classical elastic solution; in the region $\Omega_2 = \{\{r, \vartheta\}\ \text{ s.t. } \ a < r < \frac{3}{2}a\}$, the stress is uniaxial and radial (see Figure 42b). Namely:

$$T_{rr} = \begin{cases} -\frac{p\,a}{r} & , \ a \le r \le \frac{3}{2}a \ , \\ -\frac{p\left(9a^2+4r^2\right)}{12r^2} & , \ \frac{3}{2}a \le r \le 2a \ , \end{cases}$$

$$T_{\vartheta\vartheta} = \begin{cases} 0 & , \ a \le r \le \frac{3}{2}a \ , \\ -\frac{p\left(4r^2-9a^2\right)}{12r^2} & , \ \frac{3}{2}a \le r \le 2a \ , \end{cases}$$

$$T_{r\vartheta} = 0 \ .$$

We leave to the reader to verify that this stress field verifies the balance equations with zero body forces, matches the given pressures at the inner and outer boundary, and is compressive. In the region Ω_1 the stress field being coincident with the elastic solution, gives compatible strains and the physical components$\{u_r, 0\}$ of the displacement $\mathbf{u}$, can be easily found through the relations:

$$E_{\vartheta\vartheta} = T_{\vartheta\vartheta} - \nu T_{rr} \ , \ E_{\vartheta\vartheta} = \frac{u_r}{r} \ .$$

In Ω_2, u_r can be found, modulo a constant, through the equations

$$E_{rr} = T_{rr} - \nu T_{\vartheta\vartheta} \ , \ E_{rr} = \frac{\partial u_r}{\partial r} \ .$$

The constant is finally determined by imposing the continuity condition

$$u_r\left(r^-\right) = u_r\left(r^+\right) \ ,$$

at $r = \frac{3}{2}a$. Then the displacement u_r takes the following form

$$u_r = \begin{cases} \frac{p\,a}{E}\left(log\left(\frac{3a}{2r}\right) + \nu\right) & , \ a \le r \le \frac{3}{2}a \ , \\ \frac{p\left(4r^2(-1+\nu)+9a^2(1+\nu)\right)}{12Er} & , \ \frac{3}{2}a \le r \le 2a \ , \end{cases}$$

In Ω_2 the elastic deformations $E^e_{rr} = T_{rr}$, $E^e_{\vartheta\vartheta} = -\nu T_{rr}$, left alone, are not compatible. To restore compatibility I must add the fracture field

$$E^a_{\vartheta\vartheta} = \frac{\partial u_r}{\partial r} - E^e_{\vartheta\vartheta} \ ,$$

that is

$$E^a_{\vartheta\vartheta} = \begin{cases} \frac{p\,a}{Er}\, log\left(\frac{3a}{2r}\right) & , \ a \le r \le \frac{3}{2}a \ , \\ 0 & , \ \frac{3}{2}a \le r \le 2a \ . \end{cases}$$

Then the fracture field is described by a regular deformation consisting into a diffuse uniaxial circumferential strain taking place in the internal ring Ω_2, of outer radius $\frac{3}{2}a$, and becoming vanishingly small at the boundary between Ω_1 and Ω_2 (as shown pictorially in Figure 42b).

Second case: Limit load. Consider now the case in which $\alpha = \frac{1}{2}$ (see Figure 42c).

In this case the load is *limit* since there exists at the same time, a stress field belonging to H, that is a statically admissible (but not strictly admissible) stress field, and also a non-zero displacement field belonging to K° for which the load does zero work.

This s.a. stress field, in physical components in the polar coordinate system $\{r, \vartheta\}$ with origin in the center of the ring, is

$$T_{rr} = -p\frac{a}{r} \ ,$$

$$T_{\vartheta\vartheta} = 0 \ ,$$

$$T_{r\vartheta} = 0 \ .$$

Notice that, in this case, this is also the unique statically admissible solution, that is the set H of s.a. stress fields is a singleton (with the language of Structural Mechanics one may say that the *structure*, with this kind of load, is statically determined).

The given loads do zero work for the *mechanism* described by the following physical components of displacement:

$$u_r = \overline{u} \ , \ u_\vartheta = 0 \ ,$$

where $\overline{u}$ is an arbitrary positive constant.

The solution of the BVP in terms of displacements reads

$$u_r = \overline{u} + \frac{p\,a}{E}\left(log\left(\frac{2a}{r}\right) + \nu\right) \ , \ u_\vartheta = 0 \ ,$$

and the corresponding fracture strain is

$$E^a_{\vartheta\vartheta} = \frac{\overline{u}}{r} + \frac{p\,a}{Er}\, log\left(\frac{2a}{r}\right) .$$

We point out that, being $\overline{u}$ an unknown positive parameter, the solution, in terms of strains and displacements, is not unique.

3.8 Masonry-like panels under flexure, shear and compression: Mansfield-Fortunato semi-analytical solutions

The problem of equilibrium for normal elastic no-tension materials can be formulated as a minimum problem for the complementary energy functional over the set of statically admissible stress fields H.

Masonry facades are often formed by an assembly of units in the form of rectangular panels; an example of a wall with openings in which rectangular panels can be devised in the masonry, is shown in Figure 43. A special class of mixed boundary value problem for such units can be solved by minimizing the complementary energy over the subset $\tilde{H}$ of H defined by the admissible stress fields that are of rank one. These minimal uniaxial stress states represent often the exact solution of such BVP's in some parts of the domain. This can be verified by deriving the corresponding fracture strains through the compatibility equations and checking the boundary conditions for the associated displacements.

These approximate solutions for rectangular panels have some relevance both for masonry structures as well as for elastic membranes due to simplified models which impose unilateral constraints on the normal stress, namely the No-Tension theory (NT-T) for masonry (see Fortunato (2010))and the *Tension Field Theory* (TF-T) for membranes (see Mansfield (1969) and Steigmann (1990) and references therein). Solutions of similar problems, consisting of uniaxial stress fields directed along a one parameter family of rays[15], can be found in the technical literature dating back to sixties.

The first to analyze the *shearing* problem, under the ad hoc assumptions of TF-T, in mathematically rigorous terms, was Mansfield (Mansfield, 1969). In Mansfield (1989) he considers more general boundary conditions. For NT materials, the shearing case was also studied with a variational approach by Angelillo and Olivito (1995) in the general case of unilateral, anisotropic elastic materials.

In a recent paper, Fortunato (2010), a comprehensive study, valid for any relative rigid displacements of the bases (including rotations), is presented;

[15] We recall that (see Remark 3, Remark 9 and Figure 6), in the regions of uniaxial stress and under vanishing body forces, a classical result of TF-T is that the lines of principal traction (compression for NT-T) form a family of straight lines.

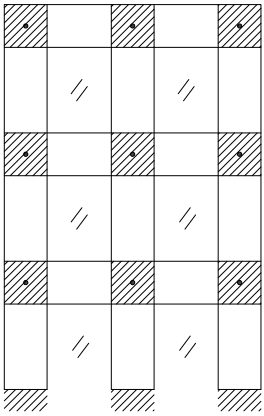

Figure 43. Structural scheme of a masonry wall with openings (in a simplified model dashed parts can be considered as rigid).

on introducing a curvilinear coordinate system convected with the compression rays, the problem is reduced to an ordinary differential equation for the ray distribution (that is the Euler equation of the minimum problem for the complementary energy over the set $\tilde{H}$), without the need of any ad hoc assumptions besides energy minimization. The basic tension field assumption (that is the restriction to $\tilde{H}$), in the present context, reduces the compression ray solution to an approximate solution of the minimum problem for the complementary energy, and gives a lower bound for the *stiffness* of the panel. A definition of the partition of the domain Ω into uniaxial stress part Ω_2 and slack part Ω_3, explicit in terms of the relative displacement parameters, is given. Simple ordinary differential equations are obtained from the compatibility condition, from which the anelastic strain (that is the fracture strain for NT-T and the wrinkling strain for TF-T) can be computed through integration.

Unilateral models for masonry and wrinkling. The last result has significant relevance for the problem of wrinkling of thin membranes. When a thin panel is forced into the post-buckling range by loads applied to its edges, load is transmitted primarily along one of the principal axes of stress, while bending effects remain secondary. The panel deforms into a wavy or wrinkly surface, the crests of the waves coinciding approximately with the trajectories of the tensile stresses (see Figure 44b).

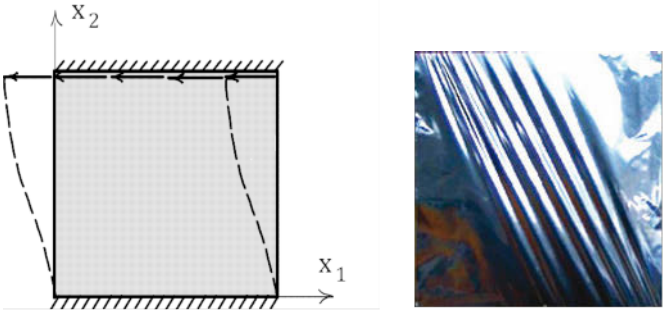

a b

Figure 44. Wrinkling of a rectangular sheet under relative shearing of the bases and free on the lateral sides. Boundary conditions: (a) . In (b) wrinkles developing in an alluminium sheet subject to the b.c. described in (a).

TF-T defines approximately the magnitude and direction of the stress in the wrinkled zone. The anelastic strains, in TF-T, are a measure of wrinkling, in the sense that they may be viewed as limits of sequences of ordinary deformations whose gradients oscillate finely on any interval. The definition of the wave length and the amplitude of the wrinkles is of vital importance in many applications (such as sails or space solar panels). In recent works, some authors (Epstein (1999), Wong and Pellegrino (2006)) propose approximate formulas for estimating the amplitude as well as the wave length of wrinkles, based on the knowledge of the TFT stress field and the corresponding anelastic strain. Then the knowledge of the anelastic strain can be used to test the adherence of such formulas to the description of known experimental results on panels.

Basic Boundary Value Problem for a Masonry Panel In this Section I summarize the main results of the analysis given by Fortunato in (Fortunato, 2010). Consider a masonry-like rectangular panel, traction free on the lateral sides and subject to zero body forces and prescribed rigid body displacements of the top and bottom bases. A Cartesian frame of reference $\{O;\ x_1 = x,\ x2 = y\}$ (Figure 45a) is introduced, with associated unit base vectors $(\mathbf{e}_1, \mathbf{e}_2)$; let us define $\{u_A,\ v_A,\ \varphi_A\}$ as the translation and rotation parameters of the block R_A relative to the pole A°, $\{u_B,\ v_B,\ \varphi_B\}$ as the translation and rotation parameters of the block R_B relative to the pole B°, $\{U, V, \Phi\}$ as the relative rigid displacement parameters between the top and bottom bases.

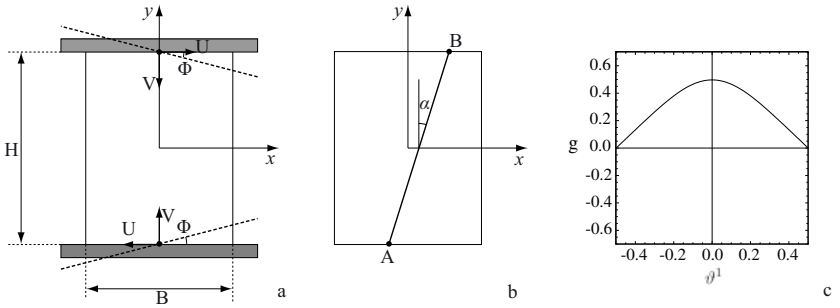

Figure 45. Masonry panel undergoing rigid relative displacements of the bases: a. Slope g of a compression ray: (b). Typical minimizing slope g as a function of $\vartheta^1 = x$: (c).

Modulo an ineffective rigid body displacement, it is straightforward to relate the displacement components at the top and bottom bases a, b with the relative (rigid) displacement parameters, written

$$\mathbf{u}_a = u_a\mathbf{e}_1 + v_a\mathbf{e}_2 = U\mathbf{e}_1 + (V + \Phi x)\mathbf{e}_2 \ ,$$

$$\mathbf{u}_b = u_b\mathbf{e}_1 + v_b\mathbf{e}_2 = -U\mathbf{e}_1 - (V + \Phi x)\mathbf{e}_2 \ .$$

Based on the complementary energy principle stated in *Subsection* 3.5, the equilibrium solution can be searched by minimizing the complementary energy over the set H defined in (45). In keeping with the spirit of TF-T, an approximate solution is looked for in the restricted set $\tilde{H}$ obtained by considering stress fields $\mathbf{T} \in H$ such that $\mathbf{T}$ is of rank-one.

Remark 11. As shown by some of the elementary solutions previously discussed, the displacement solution, in the closure of the regions $\Omega_2 \cup \Omega_3$, can exhibit singularities affecting the latent strain. These singularities correspond to discontinuities in the displacement through lines that can be interpreted as fracture lines. The normality assumptions (34), (36), imply that displacement discontinuities be orthogonal to the discontinuity line. ⋄

Remark 12. On the interface between Ω_2 and Ω_3 the stress must be continuous in order to avoid shear discontinuities (violating the normality rule). As a consequence the stress along the interface between the regions Ω_2 and Ω_3 must be zero, the interface itself a straight unextended line. ⋄

The minimizer $\mathbf{T}^\circ$ of the complementary energy over the restricted set $\tilde{H}$ is generally not the exact solution of the problem, rather an approximate solution.

For any $\mathbf{T} \in \tilde{H}$ one has $\Omega = \Omega_2 \cup \Omega_3$, that is $\Omega_1 = \emptyset$. Once the free boundary between Ω_2 and Ω_3 is identified, the solution of the equilibrium problem is reduced to the search of the stress field solution in Ω_2. As already remarked, in Ω_2 one of the two families of principal stress curves (i.e., the integral curves of the stress eigenvectors) is made of straight lines, that are called *compression rays*. The compression rays carry the non zero stress and do not overlap. Since the lateral sides of the panel are stress free the compression rays intersect the boundary along the bases. Therefore the definition of the behaviour of a single panel, under the above assumptions, is reduced to finding in Ω_2 the optimal compression ray distribution, with the optimal choice being determined by energy convenience.

In what follows, I summarize the results of the analysis given by Fortunato in (Fortunato, 2010), omitting all the proofs and referring to the cited paper for the detailed derivations. The main results contained in Fortunato (2010) concern: 1. the explicit definition of the partition $\Omega = \Omega_2 \cup \Omega_3$, in terms of the data $\{U, V, \Phi\}$. 2. The explicit definition of the stress and complementary energy to be minimized, in terms of the slope of the rays g. 3. The formalization of the Euler equations and boundary conditions for all the possible data. 4. The explicit definition of the anelastic strains (fractures) in terms of the slope g.

Partition of the panel and free boundary between Ω_2 and Ω_3 Consider the rectangular panel of base $B_\circ$ and height $H_\circ$. In the sequel a rectangular normalized panel is considered, which is a rectangular panel whose base is of unit length and whose height is $H = H_\circ/B_\circ$. The slope function g of a compression ray is introduced; the compression ray intersects the bottom and top bases at the abscissae x_A, x_B and the horizontal axis at $\vartheta_1 = \frac{x_A + x_B}{2}$, and the slope is defined as a function of ϑ^1

$$[-1/2, 1/2] \ni \vartheta^1 \to g(\vartheta^1) := tan(\alpha(\vartheta^1)$$

where α is the angle between such ray and the y axis, as shown in Figure 45b, to which I refer for notations.

In order that the rays belong entirely to Ω, the geometrical constraints on g

$$-\frac{1-2\vartheta^1}{H} \leq g(\vartheta^1) \leq \frac{1-2\vartheta^1}{H} \; s.t. \; \vartheta^1 > 0 \,, \tag{49}$$

$$-\frac{1+2\vartheta^1}{H} \leq g(\vartheta^1) \leq \frac{1+2\vartheta^1}{H} \; s.t. \; \vartheta^1 \leq 0 \,, \tag{50}$$

must be satisfied.

On observing that, for compatibility (that is in order that the strain satisfies the elasticity relations for shortening and the normality conditions for lengthening), the interface between the regions Ω_2, Ω_3, if any, must be an unextended ray, the following equation definining such class of rays is derived:

$$g(\vartheta^1) = -\frac{V}{U} - \frac{\Phi}{U}\vartheta^1 \ . \tag{51}$$

The free boundary must be chosen in this class.

It is easy to show that all the rays satisfying the constraint (51) pass through a common centre C whose coordinates $\{x_\circ, y_\circ\}$ depend only on the parameters $\{U, V, \Phi\}$. The expressions for the coordinates of the centre C are

$$x_\circ = -\frac{V}{\Phi} \ , \ y_\circ = \frac{U}{\Phi} \ .$$

The partition of the panel into the disjoint regions Ω_2 and Ω_3, and in particular their free boundary (necessarily made by rays that satisfy the constraint (51)), can be obtained by the position of the center C, and is independent of the size of the rigid displacement parameters, provided the ratios $\frac{U}{\Phi}$ and $\frac{V}{\Phi}$ stay constant.

If $U > 0$ the inequality

$$g(\vartheta^1) < -\frac{V}{U} - \frac{\Phi}{U}\vartheta^1 \ . \tag{52}$$

defines the ray passing through the points P and Q on the top and bottom bases which are shortened for the given rigid displacements parameters $\{U, V, \Phi\}$ of the bases.

This is a kinematic constraint on the slope g for the existence of the compression rays, that is for the existence of the region Ω_2.

In the case $U = 0$, $g(\vartheta^1)$ is not restricted and the rays are shortened, as long as $\vartheta^1 > -\frac{V}{\Phi}$ if $\Phi > 0$ and $\vartheta^1 < -\frac{V}{\Phi}$ if $\Phi < 0$. In the case $U < 0$ then $g(\vartheta^1) > -\frac{V}{\Phi} - \frac{\Phi}{U}\vartheta^1$.

Summing up, the restrictions on $g(\vartheta^1)$ that have been introduced can be reformulated as follows:

Given the rigid boundary displacement parameters $\{U, V, \Phi\}$, find the pair $\{\vartheta^1, g(\vartheta^1)\}$, so that the geometrical constraints (49), (50) and the kinematical constraint (52) hold.

These five inequalities define a feasible region for the pair $(\{\vartheta^1, g(\vartheta^1)\}$ that can be easily visualized with a graph through which the interface between the Ω_2 and Ω_3 regions can be located.

Depending on the values of the triplet $\{U, V, \Phi\}$, the feasible region for g can be either empty or not empty. In the latter case the region is a polygon with three to five sides whose extrema, with respect to the ϑ^1 component, define the boundary of the Ω_2 region. These extrema are called $\underline{\vartheta}^1$ and $\overline{\vartheta}^1$.

Based on the values of U, V, Φ, there are essentially five representative cases to be considered:

(i) Shearing, shortening, flexure: $U \neq 0\ , V > 0,\ \Phi \neq 0$;
(ii) Shearing, elongation, flexure: $U \neq 0\ , V < 0,\ \Phi \neq 0$;
(iii) Shortening: $U = 0\ , V > 0,\ \Phi = 0$;
(iv) Shearing: $U \neq 0\ , V = 0,\ \Phi = 0$;
(v) Shortening, flexure: $U = 0\ , V < 0,\ \Phi \neq 0$.

Figure 46 shows the admissible repertoire of $g(\vartheta^1)$ in the range $[-1/2, 1/2]$ for one of these cases.

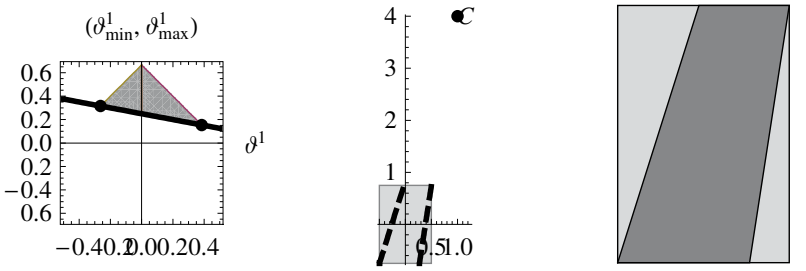

Figure 46. Definition of the taut region for the case of shearing, elongation, flexure. Restrictions on g and limit slopes: (a). Position of the center C: (b). Taut region: (c).

Curvilinear Coordinates in Ω_2 In Ω_2 it is convenient to introduce a system of curvilinear coordinates $\{\vartheta^1, \vartheta^2\}$ with one of the curvilinear lines, say ϑ^2, convected to the compression rays. In terms of the Cartesian coordinates $x_1 = x, x_2 = y$, with associated base vectors $\mathbf{e}_1, \mathbf{e}_2$, the curvilinear coordinates $\{\vartheta^1, \vartheta^2\}$ are defined as follows

$$x_1 = \vartheta^1 + g\vartheta^2\ ,\ x_2 = \vartheta^2\ ,$$

g being the slope of the rays, a function of ϑ^1 alone.

A physical reference system, that is a variable orthonormal base $\{\mathbf{e}_{1'}, \mathbf{e}_{2'}\}$, with $\mathbf{e}_{2'}$ tangent to the compression rays at any point of Ω_2, is also introduced.

Strain and Stress in Ω_2 Calling u_α, the covariant components of the displacement field $\mathbf{u}$ in the curvilinear system $\{\vartheta^1, \vartheta^2\}$, the local infinitesiamal strain $\mathbf{E}$ has the following covariant components in the same curvilinear system

$$E_{11} = u_{1,1} - \frac{g''\vartheta^2}{1 + g'\vartheta^2} u_1 \ ,$$

$$E_{22} = u_{2,2} \ ,$$

$$E_{12} = \frac{1}{2}(u_{1,2} - u_{2,1}) - \frac{g'}{1 + g'\vartheta^2} u_1 \ .$$

The physical component of strain in the ray direction, that is the strain component in the direction of $\mathbf{e}_{2'} \otimes \mathbf{e}_{2'}$, is related to the covariant component E_{22} through the relation

$$E_{(2'2')} = E_{22} \frac{1}{1 + g^2} \ .$$

Notice that the total strain $\mathbf{E}$, in the variable hortonormal base $\{\mathbf{e}_{1'}, \mathbf{e}_{2'}\}$, is described by the matrix

$$\{\mathbf{E}\} = \left\{ \begin{array}{cc} \lambda(\vartheta^1, \vartheta^2) - \nu\epsilon(\vartheta^1, \vartheta^2) & 0 \\ 0 & \epsilon(\vartheta^1, \vartheta^2) \end{array} \right\} \ .$$

where ν is the Poisson ratio, $\epsilon = E_{(2'2')}$ is the elastic strain component and λ is the unknown fracture field.

The decomposition of the total strain into its anelastic and elastic parts is then

$$\{\mathbf{E}^a\} = \left\{ \begin{array}{cc} \lambda(\vartheta^1, \vartheta^2) & 0 \\ 0 & 0 \end{array} \right\} \ ,$$

$$\{\mathbf{E}^e\} = \left\{ \begin{array}{cc} -\nu\epsilon(x_1, x_2) & 0 \\ 0 & \epsilon(x_1, x_2) \end{array} \right\} \ .$$

The uniaxial stress $\mathbf{T}$, in order to satisfy the equilibrium with zero body forces, must take the form (for a pictorial description of equilibrium along a compression ray see Remark 3 and Figure 6)

$$\mathbf{T} = \sigma \mathbf{e}_{2'} \otimes \mathbf{e}_{2'} \ ,$$

with

$$\sigma = \frac{f(1+g^2)}{1+g'\vartheta^2} \ .$$

The elastic part ϵ of the deformation, is easily obtained, through the Hooke's law, in the form

$$\epsilon = \frac{\sigma}{E} \ ,$$

E being the Young modulus of the material.

Energy The complementary energy (44) can be written in the form

$$E_c = -\int_{\underline{\vartheta}^1}^{\overline{\vartheta}^1} 2f(Ug+V+\Phi\vartheta^1)d\vartheta^1 + \frac{1}{2}\int_{\underline{\vartheta}^1}^{\overline{\vartheta}^1}\int_{-\frac{H}{2}}^{\frac{H}{2}} \frac{f^2}{E}\frac{(1+g^2)^2}{1+g'\vartheta^2}d\vartheta^1 d\vartheta^2 \ . \quad (53)$$

The complementary energy, depending parametrically on $\{U, V, \Phi\}$ is a functional of f, g, that is of two unknown numeric functions of ϑ^1. The function f can be determined explicitly by pre-minimizing E_c with rewspect to f. Such a minimizer is

$$f = \frac{Eg'}{(1+g^2)^2}\frac{2(Ug+V+\Phi\vartheta^1}{log(1-g'\frac{H}{2}) - log(1-g'\frac{H}{2})} \ .$$

By substituting the previous expression into the stress, one has

$$\sigma = \frac{1}{1+g'\vartheta^2}\frac{Eg'}{1+g^2}\frac{2(Ug+V+\Phi\vartheta^1}{log(1-g'\frac{H}{2}) - log(1-g'\frac{H}{2})} \ ,$$

and substituting back into the energy, after some algebra, the following reduced expression of E_c is obtained

$$E_c = -2E\int_{\underline{\vartheta}^1}^{\overline{\vartheta}^1} \frac{(Ug+V+\Phi\vartheta^1)^2 g'^2}{(1+g^2)^2 \log\frac{1+g'\frac{H}{2}}{1-g'\frac{H}{2}}}d\vartheta^1 \ . \quad (54)$$

This is a functional of the sole unknown function g, to be minimized for g with the boundary conditions

$$g(\underline{\vartheta}^1) = \underline{g} \ , \ g(\overline{\vartheta}^1) = \overline{g} \ .$$

The solution, that is called $g_\circ$, can be determined by finding the zeroes of the derivative (the Euler equation) associated to the minimum problem for (54) (see equation (58), p.101 of Fortunato (2010)). The Euler equation

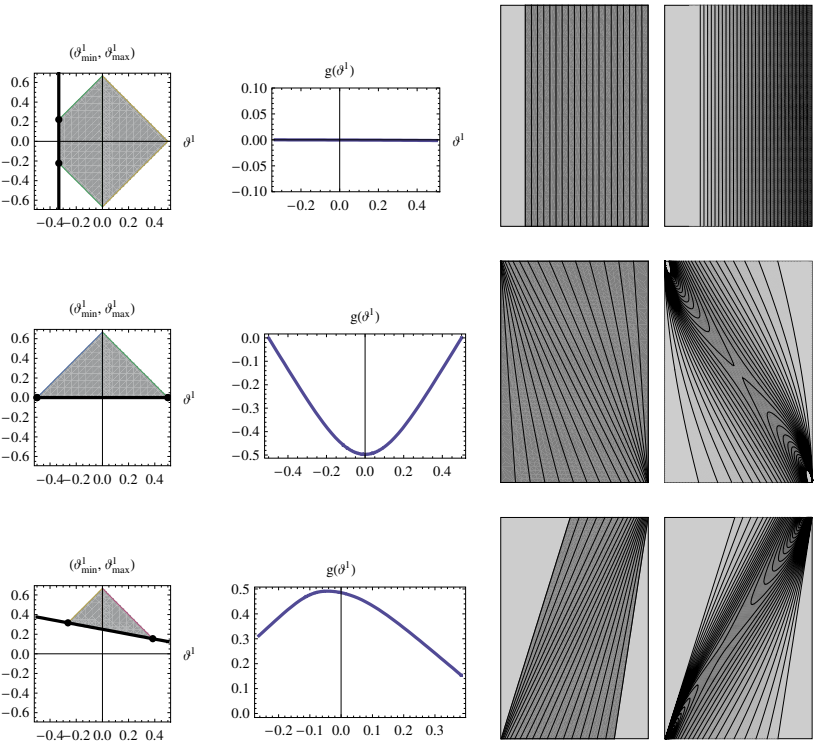

Figure 47. Numerical solution of three special cases. In column a: fundamental partition and minimizing slope g. In column b: compression rays corresponding to the minimizing g and level curves of the principal stress. First row: shortening and flexure. Second row: pure relative shearing. Third row: shearing, elongation and flexure.

is a second order non-linear differential equation for g that, due to the precence of *log* terms in g', results rather stiff. The equation is integrated by Fortunato in (Fortunato, 2010) for some special cases, by employing a multi-shooting technique and a Gauss-Kronrod quadrature formula.

Compatibility, Anelastic Deformation The stress field $\mathbf{T}_\circ$ corresponding to the minimizer $g_\circ$, that is the uniaxial stress field directed as the compression rays for which the principal stress component is

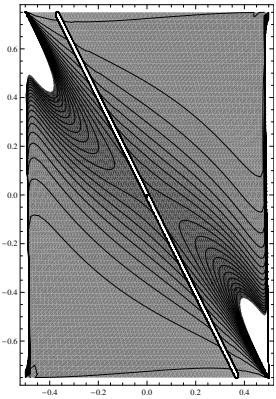

Figure 48. Level curves for of the fracture strain for the case of pure relative shearing.

$$\sigma = \frac{1}{1+g'_\circ\vartheta^2}\frac{Eg'_\circ}{1+g_\circ^2}\frac{2(Ug_\circ+V+\Phi\vartheta^1}{log(1-g'_\circ\frac{H}{2})-log(1-g'_\circ\frac{H}{2})}\ ,$$

can be either an approximation to the exact solution or the solution of the BVP. In order to check that $\mathbf{T}_\circ$ is the exact solution of the BVP, compatibility of the strain $\mathbf{E}$, and compatibility of the corresponding displacements on the part $\partial\Omega_D$ of the boundary, must be verified. Actually a continuous displacement field $\mathbf{u}$ of which $\mathbf{E}$ is the symmetric part of its gradient exists in Ω_2 if and only if

$$E_{11/22}+E_{22/11}-2E_{12/12}=0\ , \tag{55}$$

where / followed by indices denotes covariant differentiation with respect to those indices.

Recalling that the total strain $\mathbf{E}$ admits the representation

$$\mathbf{E}=(\lambda-\nu\epsilon)\mathbf{e}_{1'}\otimes\mathbf{e}_{1'}+\epsilon\mathbf{e}_{2'}\otimes\mathbf{e}_{2'}\ ,$$

and that ϵ is the elastic stretch determined by the known stress $\mathbf{T}_\circ$, the unknown fracture strain field λ can be found by solving the differential equation (55).

In Fortunato (2010) the author finds the explicit solution of this differential equation in terms of $g_\circ$. The solution is

$$\lambda=\frac{z(1+g_\circ^2)}{1+g'_\circ\vartheta^2}+\nu\epsilon+g_\circ^2\epsilon$$

where z is the solution of the differential equation

$$z_{,22} = \frac{p}{1 + g_\circ \vartheta^2}$$

p being a specified function of f, g, that is of $g_\circ$ (see (73), p.103 Fortunato (2010)).

Rectangular panels under elongation, flexure and shearing: examples In this section the solution of some peculiar cases is presented. A rectangular panel of normalized lengths and Poisson ratio $\nu = 0$, subject to three different combinations of the given displacements $\{U, V, \Phi\}$ is considered. The Euler equation is solved numerically for each of the three cases with a multi-shooting technique. In Figure 47 the fundamental partition, the minimizer $g(\vartheta^1)$, the compression rays and the principal stress levels are shown. In particular for the example of pure shearing the contour plot of the fracture λ, that is the only non vanishing component of the anelastic strain in Ω_2, is shown in Figure 48. Since the solution of the Euler equation is obtained numerically the optimal g, and the corresponding σ, are affected by numerical errors depending essentially on the integration scheme chosen. In the examples, an adaptive algorithm has been adopted: the function g is integrated over the interval $[\underline{\vartheta}^1, \overline{\vartheta}^1]$, by using a Gauss-Kronrod quadrature formula, from which an integral value (usually overestimated) and an error estimate are obtained. If the estimation is too big, the interval is divided in half and the integration is performed over each of the halves using the quadrature formula. If the total error is still too big, the interval with the biggest error is again bisected. The process is repeated until the desired precision is reached. For the integration scheme adopted the anelastic strain is always non negative all over Ω_2. This outcome gives an indication that the compression ray solution is the exact solution for the cases considered ($\nu = 0$).

4 Model *two* (ML)

In this section the main ingredients of the theory concerning model *two* for masonry materials, namely the Masonry-Like (ML) material, that is the $n > 1$ version of the 1d model introduced in Chapter 1, are presented. The constitutive assumptions, the balance equations and the boundary and initial conditions are given and the evolutionary boundary value problem for ML materials is formulated. A number of illustrative exact solutions and examples are discussed and a new technique for handling numerically the solution of specific ML problems, is introduced.

4.1 The equilibrium problem for ML materials

The crushing behaviour of masonry, that is its limited strength in compression, is modeled as perfectly plastic, then the crushing behavior of the material is assumed to be represented within the classical framework of a convex elastic domain coupled with the normality law, the yield surface being fixed in the stress space (no hardening or softening).

The initial-boundary value problem describing the quasi-static evolution of a NT elasto-plastic body occupying a bounded domain Ω with boundary $\partial\Omega$ is then considered.

The first to propose and analyse this model for masonry materials were Lucchesi and Zani (1996).

Plastic behaviour is described in terms of strain rates and the problem is not merely a BVP but rather an evolutionary problem. The evolution is assumed to be quasi-static, that is, to occur so slowly that inertial effects may be ignored.

The initial-boundary value problem in two dimensions. Again I assume small strains and restrict to 2d problems.

Time dependent data are considered, such as the fields $\mathbf{b}(\mathbf{x},t)$ (body forces per unit volume), $\underline{\mathbf{s}}(\mathbf{x},t)$ (surface tractions per unit area), and $\underline{\mathbf{u}}(\mathbf{x},t)$ (surface displacements):

$$\mathbf{b}:\ (\mathbf{x},t)\in\Omega\times[0,\underline{t})\to\mathbf{b}(\mathbf{x},t)\in V^2\ ,$$

$$\underline{\mathbf{s}}:\ (\mathbf{x},t)\in\partial\Omega_N\times[0,\underline{t})\to\underline{\mathbf{s}}(\mathbf{x},t)\in V^2\ ,$$

$$\underline{\mathbf{u}}:\ (\mathbf{x},t)\in\partial\Omega_D\times[0,\underline{t})\to\underline{\mathbf{u}}(\mathbf{x},t)\in V^2\ ,$$

with $T=[0,\underline{t})$ the time interval in which the evolution is considered and $\underline{t}$ the final instant of the evolution. Usually it is assumed that

$$\mathbf{b}(\mathbf{x},0)=0\ ,\ \underline{\mathbf{s}}(\mathbf{x},0)=0\ ,\ \underline{\mathbf{u}}(\mathbf{x},0)=0\ .$$

We consider that the body Ω is composed of NT material, that is the stress $\mathbf{T}$ is negative semidefinite ($\mathbf{T}\in Sym^-$).

We further assume that the stress cannot be arbitrarily large but is confined to belong to a bounded convex set K of Sym containing the origin. Then the interior of K $\cap Sym^-$ is the elastic region:

$$\mathbf{T}\in \mathrm{K}\cap Sym^-\ , \tag{56}$$

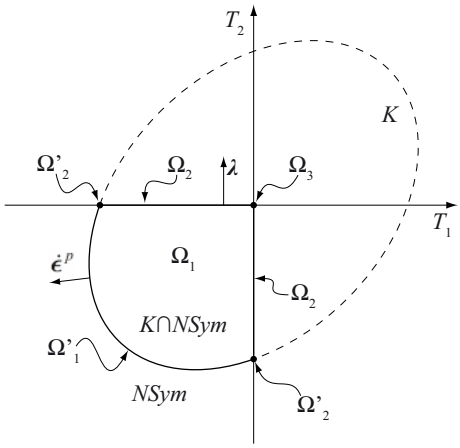

Figure 49. Section of the Elastic Domain in the stress space Sym with the plane $T_{12} = 0$.

while its boundary is the yield surface. Notice that K $\cap Sym^-$ is convex but need not to be smooth. The boundary of K may be represented by a level set of a function f, called the crushing function, so that

$$\mathrm{K} = \{\mathbf{T} \in Sym \ : \ f(\mathbf{T}) \leq 0\} \ .$$

For simplicity I consider

$$f(\mathbf{T}) = \tilde{\Phi}(\mathbf{T}) - \frac{\sigma_\circ^2}{2E} \ , \tag{57}$$

where $\tilde{\Phi}$ is the strain energy density of the isotropic NENT material, expressed as a function of the stress $\mathbf{T}$, and $\sigma_\circ$ is the crushing stress in uni-axial compression; that is the boundary of K is a level set of the free energy of the NENT material. In Figure 49 the intersection of the elastic domain with the plane $T_{12} = 0$, is depicted.

Under the small strain hypothesis, the total deformation is again described by the tensor $\mathbf{E}$, and an additive decomposition of the total strain can be considered in the form

$$\mathbf{E} = \mathbf{E}^* + \mathbf{E}^p \ , \tag{58}$$

where $\mathbf{E}^p$ is the plastic strain. Notice that now $\mathbf{E}^*$ represents the reversible part of the deformation, in turn composed itself of two parts:

$$\mathbf{E}^* = \mathbf{E}^e + \mathbf{E}^a \ , \tag{59}$$

the elastic part being linearly related to the stress $\mathbf{T}$:

$$\mathbf{E}^e = \mathbf{A}\left[\mathbf{T}\right] \ . \tag{60}$$

For the latent anelastic part (a measure for fracture) of the reversible strain, again normality to the cone Sym^- is assumed

$$(\mathbf{T}' - \mathbf{T}) \cdot \mathbf{E}^a \leq 0 \ , \forall \mathbf{T}' \in Sym^- \ . \tag{61}$$

For the time rate $\dot{\mathbf{E}}^p$ of the plastic strain the associative flow rule

$$(\mathbf{T}' - \mathbf{T}) \cdot \dot{\mathbf{E}}^p \leq 0 \ , \forall \mathbf{T}' \in \mathrm{K} \ , \tag{62}$$

is considered.

Notice that the reversible part of the strain $\mathbf{E}^*$ can still be derived by an energy density:

$$\mathbf{T} = \frac{\partial \Phi}{\partial \mathbf{E}^*} \ .$$

In the isotropic case the form of the energy density Φ can be constructed explicitly in terms of the eigenvalues e_1^*, e_2^* of $\mathbf{E}^*$ (here $e_1^* < e_2^*$ is assumed). In the case of generalized plane stress this form is

$$\Phi = \begin{cases} 0 \ , & e_1^* \geq 0 \text{ and } e_2^* \geq 0 \ , \\ \frac{1}{2} E (e_1^*)^2 \ , & e_1^* < 0 \text{ and } e_2^* \geq -\nu e_1^* \ , \\ \frac{1}{2} \frac{E}{1-\nu^2} \left((e_1^*)^2 + (e_2^*)^2 + 2\nu e_1^* e_2^* \right) & e_1^* < 0 \text{ and } e_2^* < -\nu e_1^* \ , \end{cases} \tag{63}$$

E, ν being the Young modulus and the Poisson ratio. Notice that the stress $\mathbf{T}$ derived from Φ satisfies identically the unilateral restriction (30), that is there is no need to impose it as a constraint.

Energy formulation, internal variables. The problem is described in terms of the total strain and of the recorded history of mechanical behaviour, by introducing as an internal variable the total plastic strain $\mathbf{E}^p$. If I consider that the form of $\Phi(\mathbf{E} - \mathbf{E}^p)$ is prescribed and that $\mathbf{T} = \frac{\partial \Phi}{\partial \mathbf{E}^*}$, the instantaneous values of $\mathbf{T}$ are known if $\mathbf{E}$ is given and the entire process

of plastic strain is known. Obviously $\mathbf{E}^p = \int_0^t \dot{\mathbf{E}}^p dt$, and $\dot{\mathbf{E}}^p$ is described by the flow rule (62).

Notice that, based on the ML model, fracture strains are reversible and are perfectly recoiled upon load inversion. Crushing strains, by contrast, cannot be healed and, being totally irreversible, can either stay or grow. In other words, smeared fractures cannot cancel crushing strains; the two mechanisms being completely independent.

4.2 Numerical minimization strategy

The numerical method I adopt to solve approximately the BVP for NENT materials is to search for the minimum of the potential energy (26) and is based on the direct minimization of such a functional through a descent method. The search is carried out in the subset of the set of statically admissible displacements K defined by the C° displacement fields obtained by employing a standard finite element approximation based on a triangular finite element discretization $\Pi^h(\Omega)$ of the domain Ω, where h denotes the mesh size. This kind of discretization excludes discontinuities in $\mathbf{u}$, that is, real cracks. The reason for considering such a simplification is twofold:

Firstly, I believe that fractures in NENT materials will appear smeared within the domain if the loads are safe (that is they are not collapse loads) in the sense specified in *Subsection* 2.9.

Secondly, in limit cases in which the loads approach the collapse limit the fracture strain may accumulate in narrow bands indicating the occurrence of real cracks in the limit.

Descent methods for NENT materials. The convenience of descent methods, favoured in recent years by the widespread availability of computational power, is recovered in the case of unilateral and non-smooth energy shapes. In the specific case of NENT materials the method is particularly indicated since the problem becomes unconstrained, the potential energy is a convex function of its arguments and the method of descent is insensitive to *zero-energy modes* (source of major troubles with standard FEM based on updated stiffness matrices, see Alfano et al. (2000)).

Several numerical tests performed on simple problems, for which the exact solutions are known, show the competitiveness of the descent approach with respect to more classical techniques. Some of these benchmark problems are reported in what follows, a larger number of examples can be found in the recent paper by Angelillo et al. (2010). Comparisons with numerical solutions obtained by other developing codes (see Lucchesi and Zani (2008)) and commercial programs (Abaqus, 6.12) indicate that the descent method

seems to be the right choice to overcome the difficulties which are inherent to the NT constraint.

The energy functional E is approximated with the function $\widetilde{E}(\{u_h\})$ of the nodal displacements $\{u_h\}$:

$$\widetilde{E}(\{u_h\}) = -\sum_r L_r \underline{\mathbf{s}}(\mathbf{x}_r)\cdot\mathbf{u}_r - \sum_m \mathbf{f}_m\cdot\mathbf{u}_m - \sum_n A_n \mathbf{b}(\mathbf{x}_n)\cdot\mathbf{u}_n - \sum_q A_q \Phi(\mathbf{x}_q) \tag{64}$$

where $\mathbf{u}_r$ is the displacement at the midpoint $\mathbf{x}_r$ of the r-th edge of length L_r on $\partial\Omega_N$, $\mathbf{u}_m$ the displacement of the m-th mesh node where the concentrated force $\mathbf{f}_m$ is applied, $\mathbf{u}_n$ the displacement at the Gauss point $\mathbf{x}_n$ of the n-th mesh triangle with area A_n, and $\mathbf{x}_q$ the Gauss point of the q-th mesh triangle of area A_q, where the strain energy density Φ is evaluated for integration. In the discretized version (64) of the potential energy, all the displacements $\mathbf{u}_j$, as well as the strain energy density $\Phi(\mathbf{x}_q)$ of the q-th triangle, are clearly explicit functions of the nodal displacements $\{u_h\}$, via the linear shape functions of a standard triangular mesh.

The iterative procedure adopted to minimize the function (64) is based on a step-by-step minimization method. Let us denote $\{u_h\}_j$ the nodal displacements at the j-th minimization step. The force acting on the mesh nodes is given by the negative gradient of the energy $\mathbf{f}_j = -\nabla_j \widetilde{E}$. The descent method implemented computes the current velocity $\mathbf{p}_j$ employing the nodal forces at the current and previous step as

$$\mathbf{p}_j = \eta_j \mathbf{p}_{j-1} + \mathbf{f}_j \ ,$$

where the scalar η_j is

$$\eta_j = Max\left\{\frac{\mathbf{f}_j\cdot(\mathbf{f}_j - \mathbf{f}_{j-1})}{\mathbf{f}_{j-1}\cdot\mathbf{f}_{j-1}}, 0\right\} \ ,$$

in the Polak-Ribiere version of the conjugate gradient method, and

$$\eta_j = \frac{\mathbf{f}_j\cdot\mathbf{f}_j}{\mathbf{f}_{j-1}\cdot\mathbf{f}_{j-1}} \ ,$$

if the Fletcher-Reeves variant of the method is employed (the Polak-Ribiere method is usually adopted in the applications reported herein).

If the nodes of the mesh are constrained, the velocity $\mathbf{p}_j$ is projected onto the tangent space of the constraint equations to obtain the compatible velocity $\mathbf{p}_j^*$. The velocity $\mathbf{p}_j^*$ gives the direction for the minimization motion while obeying all the constraints imposed on the nodes. The nodal displacement $\{u_h\}_j$ is computed as

$$\{u_h\}_j = \{u_h\}_j + \kappa_j \mathbf{p}_j^* \ ,$$

where κ_j is the amplitude of the minimization step in the direction of $\mathbf{p}_j^*$ and is computed via a line search method[16] to minimize the energy $\widetilde{E}(\{u_h\})$ in the direction of the velocity $\mathbf{p}_j^*$. The iteration process stops when a suitable norm of the energy gradient becomes sufficiently small (for the decrease conditions see for example (Kelley, 1999)).

Descent methods for ML (dissipative) materials. When considering ML materials, that is, adding to the NENT model a crushing strength criterion (of elasto-plastic associative type), it seems that the proposed numerical technique, based on energy minimization (extremely efficient for unilateral materials) should be abandoned. The elastoplastic behavior is indeed inherently path-dependent: the stress state at time t depends, in general, on the whole strain history in the interval $T = [0, \underline{t})$ rather than on the strain at time t. Then the equilibrium problem for such a material is essentially a dissipative evolution problem whose solution cannot be obtained by simply minimizing an energy functional. The proposed technique can still be applied to this evolutive problem considering the exact trajectory as the limit of a sequence of minimum problems. This is done by discretizing the time interval into steps and updating the energy in a suitable way. The evolutive problem is then approximated as a sequence of a discrete number of minimizing movements. The evolutive solution is obtained as the limit of the discrete evolution by letting the time step go to zero (see De Giorgi (1996) for the general formulation, Mielke and Ortiz (2008) for the convergence proofs in the general case of rate independent materials and Dal Maso et al. (2004) in the specific case of perfect elastoplasticity).

The time interval $T = [0; \underline{t})$ is discretized into k subintervals by means of the instants $0 = t_\circ \leq t_1 \leq .. \leq t_i \leq .. \leq t_k = \underline{t}$. The idea is approximate the exact trajectory $(\mathbf{u}(t), \mathbf{T}(t), \mathbf{E}^a(t), \mathbf{E}^p(t))$ (which solves the initial-boundary value problem defined above), with a sequence of states obtained by solving, at each time step t_i, the minimum problem for a suitably defined, updated energy functional, characteristic of an evolving hyper-elastic NT material. To model perfect plasticity in compression, I assume a linearly-growing extension of the strain energy function defined in (63), beyond the yield surface defined in (57) (see Figure 50).

[16] The line search method calculates the energy for several values of the scale factor κ_j (doubling or halving each time) until the minimum energy is passed. The optimum scale is then calculated by quadratic interpolation.

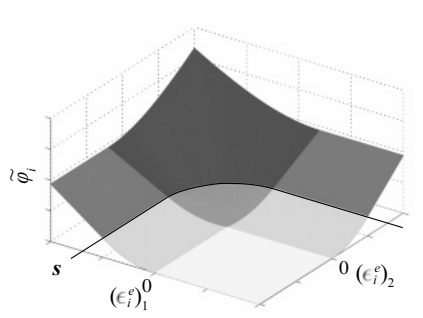

Figure 50. Linear prolongation of the strain energy beyond the crushing limit.

Namely, at any time step t_i, the functional form implemented in the finite element code is

$$\widetilde{\Phi}_i(\mathbf{E}_i^*) = \begin{cases} 0\ , & (e_1^*)_i \geq 0\ ,\ (e_2^*)_i \geq 0\ , \\ \frac{1}{2}E(e_1^*)_i^2\ , & (e_1^*)_i < 0\ ,\ (e_2^*)_i \geq -\nu(e_1^*)_i\ ,\ f(\mathbf{E}_i^*) \leq 0\ , \\ \alpha\sqrt{\frac{1}{2}E(e_1^*)_i^2} + \beta\ , & (e_1^*)_i < 0\ ,\ (e_2^*)_i \geq -\nu(e_1^*)_i\ ,\ f(\mathbf{E}_i^*) > 0\ , \\ \varphi((e_j^*)_i) & (e_1^*)_i < 0\ ,\ (e_2^*)_i < -\nu(e_1^*)_i\ ,\ f(\mathbf{E}_i^*) \leq 0\ , \\ \alpha\sqrt{\varphi((e_j^*)_i)} + \beta & (e_1^*)_i < 0\ ,\ (e_2^*)_i < -\nu(e_1^*)_i\ ,\ f(\mathbf{E}_i^*) > 0\ , \end{cases}$$

where

$$\varphi((e_j^*)_i) = \frac{1}{2}\frac{E}{1-\nu^2}\left((e_1^*)_i^2 + (e_2^*)_i^2 + 2\nu(e_1^*)_i(e_2^*)_i\right)\ ,$$

$(e_1^*)_i, (e_2^*)_i$ $((e_1^*)_i < (e_2^*)_i)$ are the principal values of $\mathbf{E}_i^*$, and the elastic strain at time t_i is given by the difference between the total strain $\mathbf{E}_i$ at the same time step and the plastic strain $\mathbf{E}_{i-1}^p$ inherited from the previous solution step, that is $\mathbf{E}_i^* = \mathbf{E}_i - \mathbf{E}_{i-1}^p$; by using this relation $\widetilde{\Phi}_i(\mathbf{E}_i^*)$ can be expressed as a function of $\mathbf{E}_i$ and becomes $\widehat{\Phi}_i(\mathbf{E}_i)$. The constants

$$\alpha = \sqrt{\frac{2}{E}}\sigma_\circ\ ,\ \beta = -\frac{\sigma_\circ^2}{2E}$$

are introduced to preserve the C^1 regularity of $\widetilde{\Phi}_i(\mathbf{E}_i^*)$. A representation of $\widetilde{\Phi}_i(\mathbf{E}_i^*)$ in the space of principal elastic strains is depicted in Figure 50.

The descent procedure finds the minimum of the total potential energy at time t_i, defined as

$$E_i(\mathbf{u}_i) = -\int_{\partial\Omega_N} \underline{\mathbf{s}} \cdot \mathbf{u}_i - \int_\Omega \mathbf{b} \cdot \mathbf{u}_i + \int_\Omega \widehat{\Phi}(\mathbf{E}_i(\mathbf{u}_i)) \,, \tag{65}$$

via a finite element discretization of the domain and descent minimization. The solution at the previous loading step is used as the initial condition for the minimization of the function

$$\widehat{E}(\{u_h\}) = -\sum_r L_r \underline{\mathbf{s}}(\mathbf{x}_r) \cdot \mathbf{u}_r - \sum_m \mathbf{f}_m \cdot \mathbf{u}_m - \sum_n A_n \mathbf{b}(\mathbf{x}_n) \cdot \mathbf{u}_n - \sum_q A_q \widehat{\Phi}(\mathbf{x}_q) \tag{66}$$

representing the finite element approximation of the total potential energy (65), as in the case of NENT materials (see (64)). At each step i, the minimization of the function $\widehat{E}(\{u_h\})$ is performed via the descent method described previously for NENT materials.

A plastic strain update is then performed at each Gauss point. The yield condition $f(\mathbf{E}_i^*) = 0$ defines, in the space of principal reversible strains $\mathbf{E}^*$, a curve whose position vector is $\mathbf{y}$, of coordinates $\{y_j\}$. It is useful to give a parametric description $\mathbf{y}(\gamma)$ of the yielding curve in the space of principal elastic strain, γ being the parameter. The return mapping algorithm, according to the principle of minimum dissipation imposed by the assumption of associated plasticity (Ortiz and Simo, 1986), consists in finding the value of the parameter giving the minimum distance (in the energy norm) of the current elastic strain $\mathbf{E}_i^*$ from the curve $\mathbf{y}(\gamma)$:

$$min_\gamma \Phi(\mathbf{y}(\gamma) - \mathbf{E}_i^*) \,.$$

This minimum problem can be easily formulated as

$$\frac{d}{d\gamma}\Phi(\mathbf{y}(\gamma) - \mathbf{E}_i^*) = 0 \,,$$

that can be solved for γ, at each Gauss point, via the Newton–Raphson method. The tensor of plastic strain rate $\dot{\mathbf{E}}^p$ at time t_i is coaxial to the reversible strain tensor $\mathbf{E}_i^*$, therefore the principal components $(\Delta e_j^p)_i$ (with j=1,2) of the plastic strain increment $\Delta\mathbf{E}_i^p$ (i.e., the discrete version of $(\dot{\mathbf{E}}^p)_i$) are simply computed as

$$(\Delta e_j^p)_i = (e_j^*)_i - y_j(\gamma_i^\circ) \,.$$

Once the plastic strain has been updated in the global reference frame, i.e. $\mathbf{E}_i^p = \mathbf{E}_{i-1}^p + \Delta\mathbf{E}_i^p$ (a backward Euler finite difference scheme), the

energy density dissipation at the given Gauss point, at time step t_i, can be computed as

$$D_i = \widehat{\Phi}(\mathbf{E}_i, \mathbf{E}^p_{i-1}) - \widehat{\Phi}(\mathbf{E}_i, \mathbf{E}^p_i) = \widehat{\Phi}(\mathbf{E}_i, \mathbf{E}^p_{i-1}) - \frac{1}{2}\mathbf{T}_i \cdot \mathbf{A}[\mathbf{T}_i]$$

from which one sees that the plastic strain increments produce energy loss.

4.3 Numerical examples

The ability of descent methods to approximate the solution of boundary value problems for NENT and ML materials is tested in the paper (Angelillo et al., 2010) in two ways: the numerical solutions are compared first with some simple exact solutions, then with some experimental results; finally the numerical solutions obtained with our code for more complex boundary value problems concerning masonry facades are presented. Here I report some of those results.

Example 1: Simple Flexure. In Angelillo et al. (2010), we solved numerically the problem of Flexure (whose exact solution is described in Subsection 3.7) both for the isotropic NENT material and for the isotropic ML material, by putting $\nu = 0$, $H = B = 2$ m.

For the first case (NENT material), we assumed for the Young modulus $E = 660$ MPa; the value of the rotation was set to $\Phi = 0.001$ radiants. To test convergence a sequence of structured discretizations of decreasing mesh size h was considered. By introducing the normalized mesh size h/D, D being the diameter of the domain, the four values $\sqrt{2}\{1/16, 1/32, 1/64, 1/128\}$ were considered. In Figure 51a, the contour plot of the maximum principal fracture strain obtained with the finest mesh, is reported. Fractures are non-zero in the region indicated as Ω_3 in Figure 38b, and their distribution suggests that the numerical solution is close to the rigid-block displacement represented in Figure 51b, which can be thought of as an energetically-equivalent alternative to the two analytical solutions described in *Subsection* 3.7 (see also Figure 39).

The numerical experiment was repeated for a ML panel by assuming for the maximum compressive stress in uniaxial compression, the value $\sigma_\circ = 19.8$ MPa. The value of the given rotation $\Phi = 0.006$ radiants is selected in such a way that, for the exact solution, the strip $y > B/4$ is forced into the yielding regime. For this value of Φ the exact stress solution is

$$\mathbf{T}_\circ = \begin{cases} -\sigma_\circ \mathbf{e}_1 \otimes \mathbf{e}_1 \ , \ y \geq B/4 \ , \\ -4\sigma_\circ \frac{y}{B} \mathbf{e}_1 \otimes \mathbf{e}_1 \ , \ B/4 > y \geq 0 \ , \\ 0 \ , \ 0 > y \ , \end{cases}$$

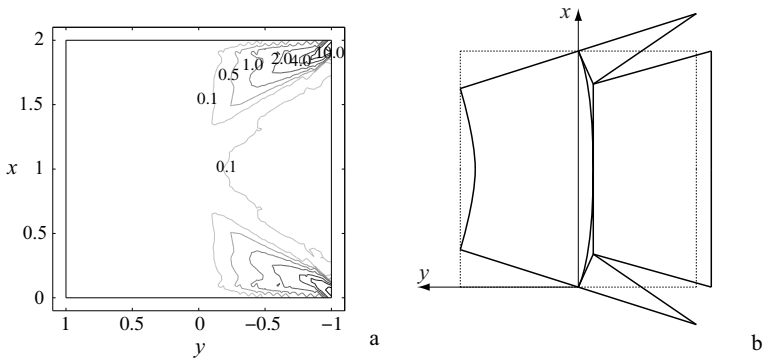

Figure 51. Numerical solution of the flexure problem for an isotropic NENT material. In (a): maximum fracture strain [$\times 10^{-3}$.]. Deformation on the right and rigid-block displacement on the right, close to the solution obtained numerically through descent.

Again the same sequence of discretizations of decreasing mesh size is considered. Figure 52a shows the computed isostatic curves for the finest mesh. They are very close to being vertical lines as expected. In Figure 52b the contour plot of the computed maximum compressive stress (solid lines) is comapared with the exact solution (dash-dotted lines). The numerical solution shows, graphically, good qualitative accuracy. The maximum fracture strain is reported in Figure 52c, and it can be noticed that the fracture distribution in the strip $y < 0$ (region Ω_3 in Figure 38b) is similar to the one observed in the NENT material (see Figure 51a). The distribution of fracture strain in the Ω_2 region resembles closely the crushing vertical fractures that appear in the experiment shown in Figure 52d.

For this example,both for the NENT and ML materials, we performed a numerical convergence study on the stress, by considering the sequence of discretizations of decreasing mesh size h described above. In Figure 53 a plot of the approximation error for the stress

$$e_h = \frac{\|\mathbf{T}_h - \mathbf{T}_{circ}\|_{L^2}}{\|\mathbf{T}_h\|_{L^2}} ,$$

versus the dimensionless mesh size h/D ($\mathbf{T}_0$, $\mathbf{T}_h$, being the exact stress solution snd the stress field computed for the mesh of size h) is reported. A linear convergence of the method is obtained in both cases.

Example 2: Pure relative shearing. The simple rectangular panel depicted in Figure 54 subject to a given relative horizontal translation of the bases (of value $2U$) and vanishing tractions on the lateral sides is considered.

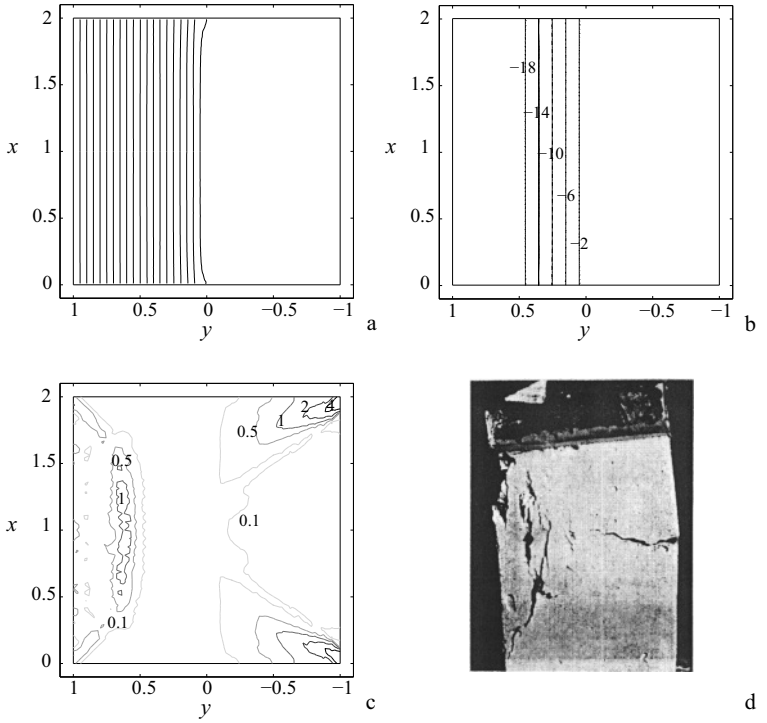

Figure 52. Numerical solution of the flexure problem for an isotropic ML material. In (a), (b): isostatic lines of compression and contour plot of the minimum principal stress (the other principal stress is almost zero). In (c): contour plot of the maximum anelastic strain component (fracture strain). Flexure test on a masonry panel (courtesy G. Castellano): (d).

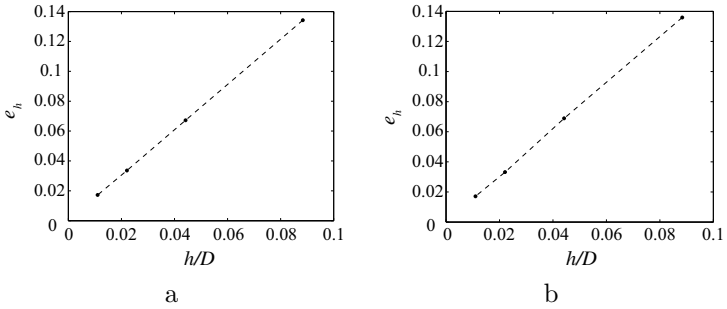

Figure 53. Flexure: convergence diagram. In (a): NENT material; in (b): ML material.

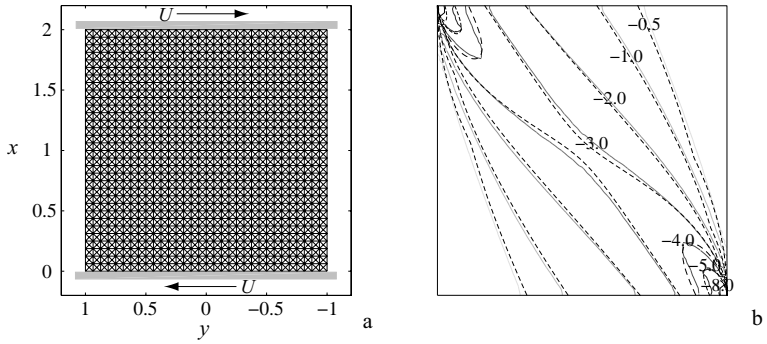

Figure 54. Pure relative shearing of a NENT panel. In (a): boundary conditions and mesh used in the numerical simulation. In (b): Comparison of the minimum principal compressive stress levels corresponding to the numerical (solid lines) and exact solution (dotted lines).

NENT material. The material parameters and the geometry are the same adopted in the previous *Section*. The value $U = 1$mm is considered. In Figures 54 and 55 the numerical solution is compared with the semi-analytical solution described in *Subsection* 3.8.

The distribution of the maximum compressive stress, the fracture strain, and the form of the isostatic lines computed numerically for the NENT panel are in good agreement with the results of the semi-analytical method of Fortunato (2010), as summarized in Figures 54 and 55.

ML material. The numerical experiment was repeated for a ML panel, by assuming the same material parameters adopted for the NENT material and putting for the limit stress: $\sigma_\circ = 19.8$ MPa. The value of the displacement at the boundary, $U = 1$ mm, previously considered, is small enough to give very limited yielding (mainly located in the vicinity of the corners, and is used as the first step in the discretized loading of the ML panel, whose evolution and crushing spreading is followed approximately, as the relative shearing U is gradually increased, by discretizing the real trajectory into steps.

In Figure 56 three stages of the evolving solution are reported. As the boundary displacement increases, a diagonal band, uniaxially and uniformly compressed at the limit stress of 19.8 MPa, forms progressively, and the isostatic lines of compression (compression rays) become more and more parallel.

The contour plots in Figure 57 represent the maximum fracture strain, which concentrates on two sub-diagonal lines, and the maximum plastic

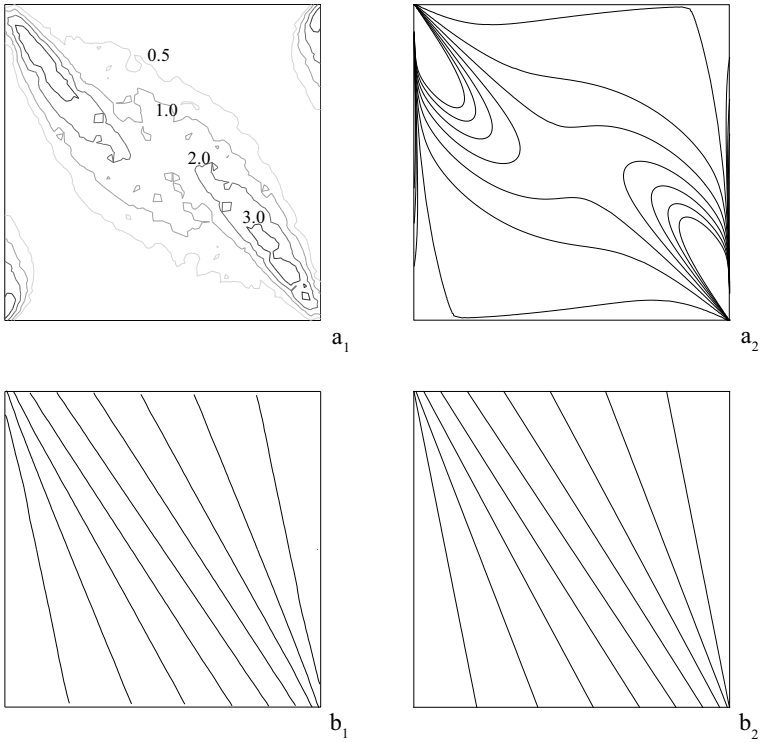

Figure 55. Pure relative shearing of a NENT panel. Fracture strain for the numerical: (a) and for the exact: (b) solutions. Compression rays for the numerical: (c) and the exact: (d) solutions.

strain, which concentrates at the constrained boundary, near two opposite corners. Concentration of plastic strain is expected, due to the assumed perfect plasticity of the material.

In Figure 58, a plot of the energy as a function of the step-wise increment of the boundary displacement U is reported, where: black circles denote the energy level of the computed solution at the beginning of the time step i, open circles denote the energy level due to the loading increment, and diamond marks denote the energy level reached after convergence.

Therefore the upward jump in energy represents the effect of updating the given disploacement from the value at time i to the one at time $i + 1$; the jump back of the energy is the effect of the numerical minimization of the updated energy, and the last smaller drop is the effect of the numerical

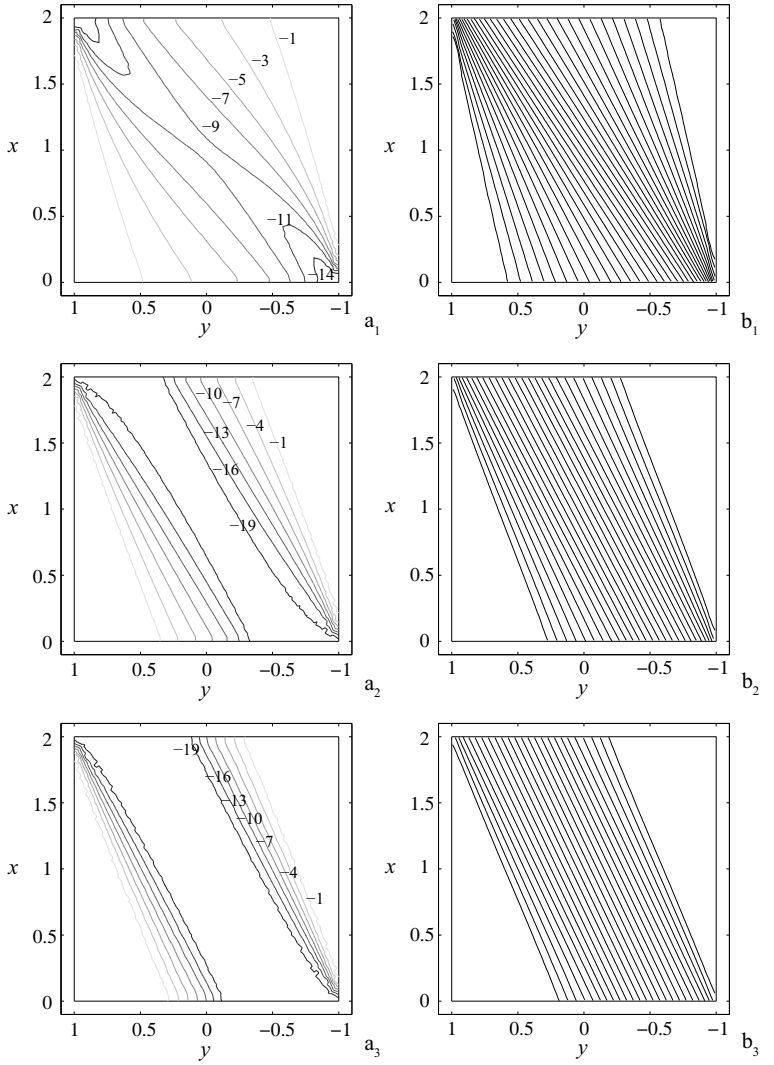

Figure 56. Pure shearing of a ML panel. Evolution of the contour plot of the minimum principal compressive stress and of the compression rays at three steps of the loading process.

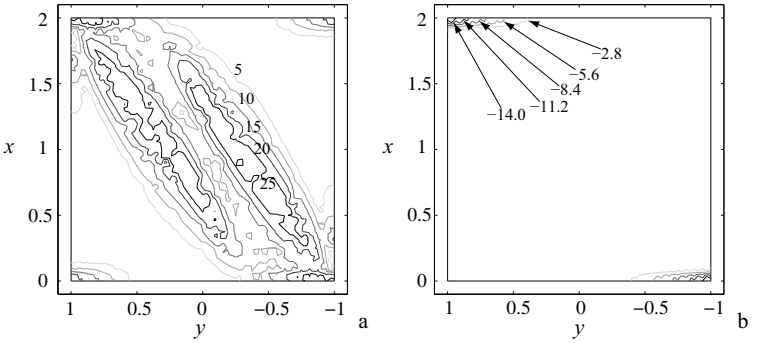

Figure 57. Pure shearing of a ML panel. Contour plot of the maximum principal fracture strain: (a), and minimum plastic strain: (b), for the final value of the relative displacement.

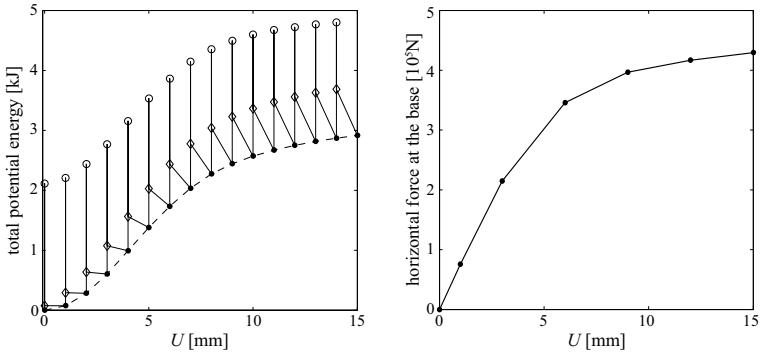

Figure 58. Pure shearing of a ML panel. Energetics.

update of the plastic strain that gives the approximate solution at time $i+1$.

This energy loss represents energy dissipation due to plastic work, and gives evidence of spreading of plastic deformation as the load is increased. The dashed line (that is the envelope of the solution points) represents the numerical approximation to the exact time history of the total potential energy of the body. In Figure 58b the push-over plot, that is the evolution of the horizontal component of the computed reaction at the base (horizontal force) as the displacement U increases, is depicted. The shear force plateaus, as expected for a perfectly plastic structure approaching collapse.

Validation against experimental tests. Here the ML material model is validated against independent sets of experimental results from Benedetti

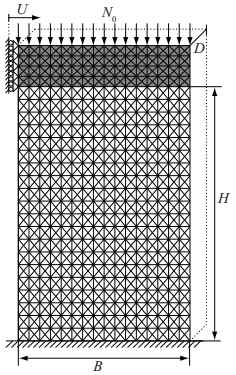

Figure 59. Loading scheme in the experiments by Benedetti and Steli (2008) and Eucentre (2010)

and Steli (2008) and Eucentre (2010), performed on different types of masonry. Figure 59 reports the constraints and the load scheme used in the numerical analysis to simulate the experimental setup.

A masonry panel of width B, height H, and thickness D is fixed to the ground at the bottom and to a steel beam at the top (the gray strip in Figure 59). A uniform load is distributed at the top part of the steel beam and the horizontal load is applied in incremental steps by imposing the horizontal displacement U of the left edge of the steel beam. Neither Benedetti and Steli (2008) and Eucentre (2010) report measurements of the Poisson's ratio, and because of that $\nu = 0$ is assumed in the simulations, since, parametric studies, not reported here, show that the simulated force-displacement curves, under shear, manifest very low sensitivity to the Poisson's ratio. The graphs in the top row of Figure 60 compare the numerical simulations and the experimental results for specimens (1A-08,2C-03) of the experiments by Benedetti and Steli (2008). In these tests, the masonry is composed of crushed stones and injected crushed stones. Our model reproduces quantitatively the substantial features of the measured force-displacement curves, with a slight overestimation of the force for higher levels of the horizontal displacement U.

The graphs of Figure 60c,d report the comparison between experimental data and numerical simulations for the specimens CS00, CS02, and CT01 of (Eucentre, 2010), all composed of stone masonry. Specimen CS00 differs from the other two because the mortar has been reinforced with 20% sand in mass fraction. This might explain the flatness of the force-displacement curve for experiment CS00 which is very well captured by the model. The

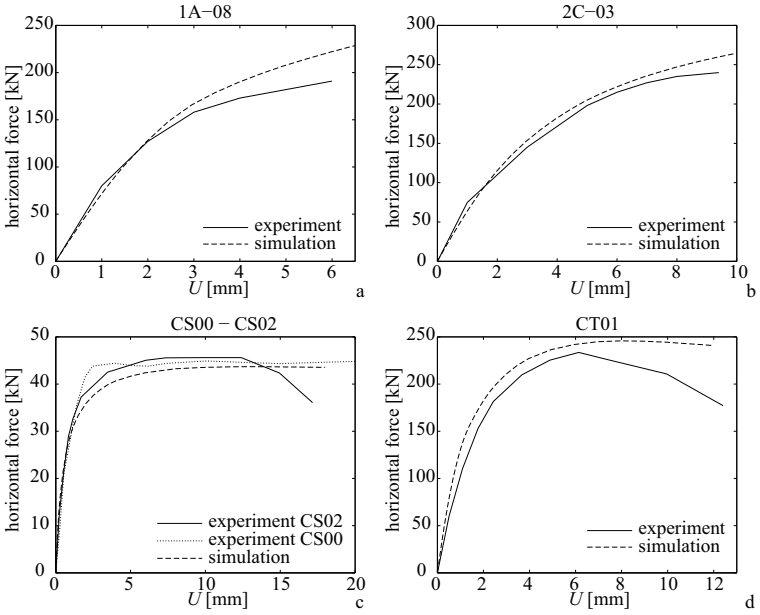

Figure 60. Comparison of numerical simulations with the experimental results of Benedetti and Steli (2008) (1A-08,2C-03) and Eucentre (2010) (CS00-CS02, CT01)

marked reduction of the horizontal force at higher levels of the displacement U might be due to softening effects induced in the masonry by the unreinforced mortar, an effect that is not captured by the ML model as presented here.

Example 3: Masonry walls with regular openings. In this section I apply the ML material model to simulate the response of a simple two-storey facade to vertical loads, seismic loads, and differential foundation subsiding. The geometry of the facade, the applied loads, and the boundary conditions are summarized in Figure 61a.

The facade is provided, above the openings, with 25 cm-thick wood beams and is assumed to be made of tuff and mortar of good quality. Wood is modeled as elastic, with Young's modulus $E = 11$ GPa, Poisson's ratio $\nu = 0.35$, and density $\rho = 800$ kg/m^3. For the tuff wall we assumed a Young's modulus $E = 0.66$ GPa, Poisson's ratio $\nu = 0.2$, density 1800 kg/m^3, and compression limit $\sigma^\circ = 1.98$ MPa. The whole structure is assumed to be 0.5 m thick.

Working loads. Working loads are represented by the weight of masonry

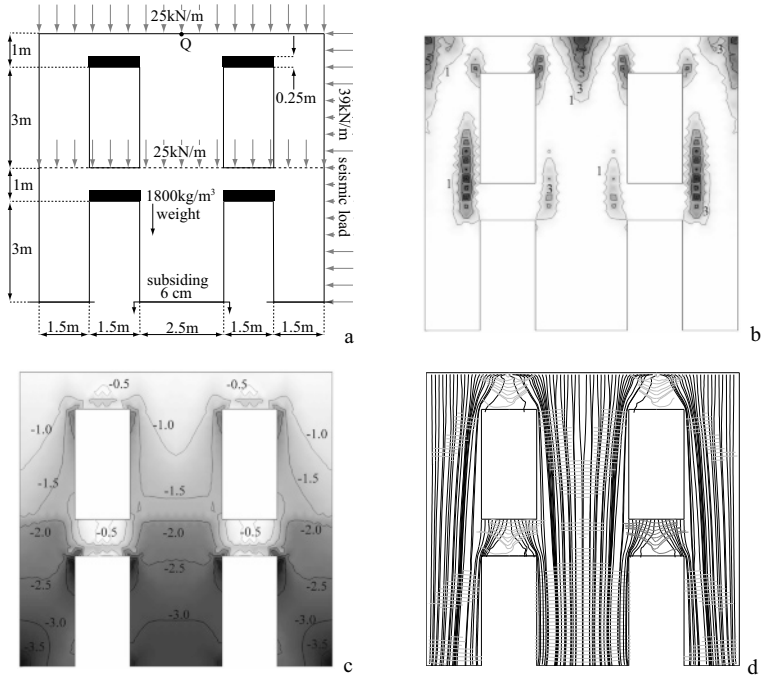

Figure 61. Masonry wall with openings. Loading schemes: (a). Numerical results for vertical loads: b,c,d. Contour plot of maximum principal fracture strain: (b). Minimum principal stress: (c). Isostatic lines: (d)

and the force transmitted by the floors (25 kN/m); the results of the simulation are reported in Figure 61b,c,d. The structure sustains the working loads without detectable crushing. The value of the maximum stress at the base of the wall is about 0.35 MPa. The partition of the domain can be inferred from Figure 61d: in Ω_1 both families of isostatic lines are depicted; in $Omega_2$ the family of isostatic lines corresponding to zero stress are not reported.

Horizontal loads. We simulated the response of the facade to a uniform horizontal force per unit length of 39 kN/m, distributed on the right side of the structure and superimposed to the structure subject to working loads (see Figure 61a). The total horizontal load is equivalent to 70% of the weight of the structure and is applied in ten steps. This kind of loading can be adopted to simulate seismic loads if horizontal ties or connections are present. Crushing strain accumulates in very localized regions near the

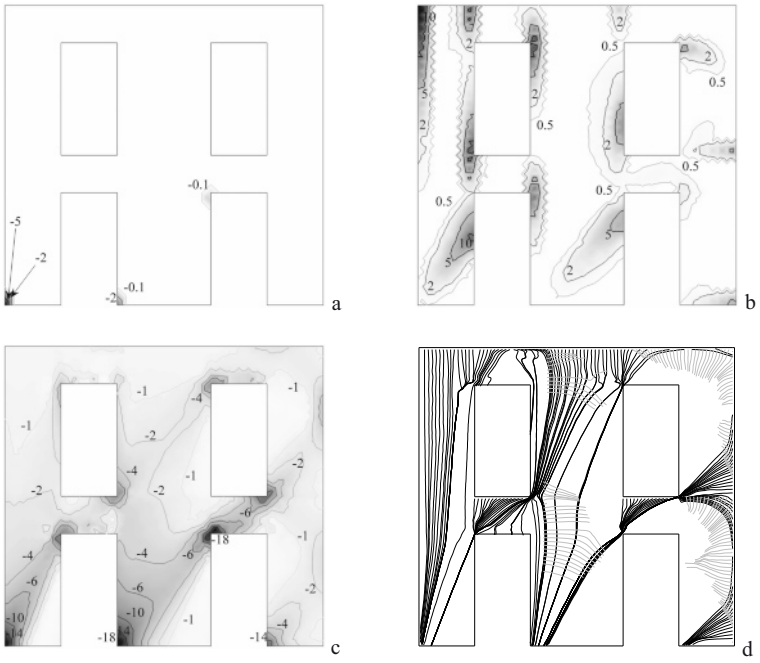

Figure 62. Numerical results for vertical and horizontal loads. Contour plot of maximum principal plastic strain: (a). Contour plot of maximum principal fracture strain: (b). Minimum principal stress: (c). Isostatic lines: (d)

corners (see Figure 62a). The formation of a compressed diagonal truss element, in the panels in between the openings, is evident from Figures 62c and 62d.

The force-displacement curve, depicted in Figure 64, shows that the structure is approaching collapse for the maximum horizontal load applied.

Differential foundation subsiding. A 6 cm subsiding of the base of the central wall is imposed in fifteen steps.This action is superimposed to the effect of working loads. The structure shows a peculiar kinematical effect, consisting in a vertical displacement of the central wall and an outward rotation of the lateral walls around the corner points of the bases, where the plastic strain concentrates (see Figure 63).

The computed vertical component of the reaction of the central wall drops from about 390 kN to 240 kN after the subsiding. This computation indicates that the vertical loads migrate from the central panel to the lateral ones. Such a stress redistribution is also highlighted from the com-

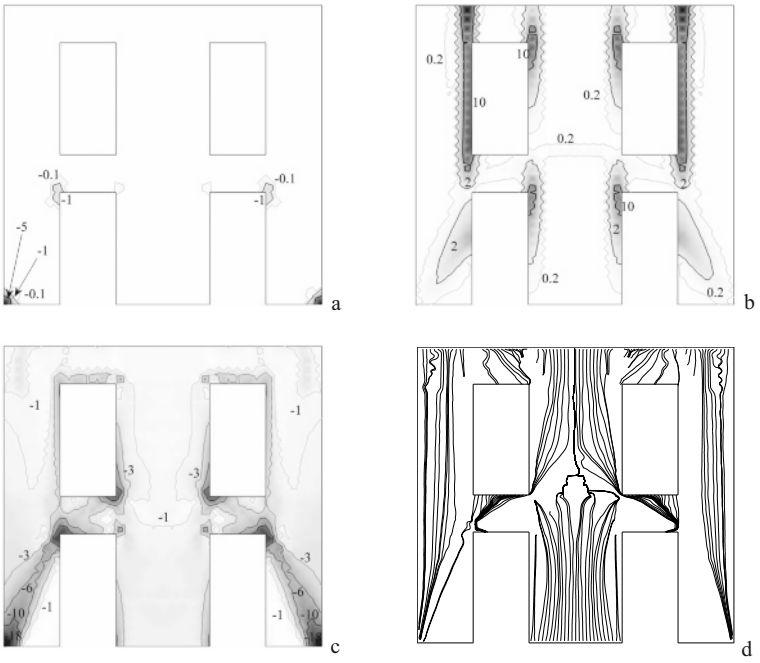

Figure 63. Masonry walls with openings under the effect of vertical loads and a vertical settlement of the central pier: mumerical results. Contour plot of maximum principal plastic strain: (a). Contour plot of maximum principal fracture strain: (b). Minimum principal stress: (c). Isostatic lines: (d)

parison of the isostatic lines depicted in Figure 63d with the ones reported in Figure 61d.

Bibliography

Dassault Systemes Abaqus, ver. 6.12 `http://www.3ds.com/fileadmin/PRODUCTS/SIMULIA`

G. Alfano, L. Rosati and N. Valoroso. A numerical strategy for finite element analysis of no-tension materials. *Int. J. Numer. Methods Eng.*, 48 (3): 317–350, 2000.

L. Ambrosio, N. Fusco and D. Pallara . *Functions of bounded variation and free discontinuity problems, Clarendon Press.* 2000.

M. Angelillo and A. Fortunato. Compatibility of loads and distortions for unilateral materials. *In preparation.*

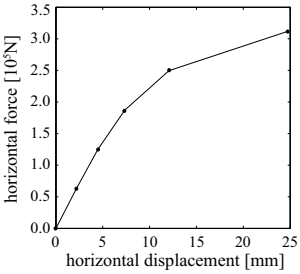

Figure 64. Masonry walls with openings under vertical and horizontal loads: shearing force versus roof displacement

M. Angelillo and L. Giliberti. Statica delle strutture murarie. *Giornale del genio Civile*, 1988 (in Italian).

M. Angelillo and R.S. Olivito. Experimental analysis of masonry walls loaded horizontally in plane. *Masonry International*, 8 (3):91–100, 1995.

M. Angelillo and F. Rosso. On statically admissible stress fields for a plane masonry-like structure. *Quarterly Of Applied Mathematics*, 53 (4):731–751, 1995.

M. Angelillo, L. Cardamone, and A. Fortunato. A numerical model for masonry-like structures. *Journal of Mechanics of Materials and Structures*, 5:583–615, 2010.

M. Angelillo, E. Babilio, and A. Fortunato. Singular stress fields for masonry-like vaults. *Continuum Mechanics And Thermodynamics*, 2012.

M. Angelillo, A. Fortunato, M. Lippiello, and A. Montanino. Singular stress fields and the equilibrium of masonry walls. *Meccanica*, under revision, 2013.

A. Benedetti and E. Steli. Analytical models for shear-displacement curves of unreinforced and frp reinforced masonry panels. *Constr. Build. Mater.*, 22 (3):175–185, 2008.

E. Benvenuto. *An Introduction on the History of Structural Mechanics Part II: Vaulted Structures and Elastic Systems, Springer-Verlag.* Springer Verlag, 1991.

G. Dal Maso, A. De Simone, and M.G. Mora. Quasistatic evolution problems for linearly elastic perfectly plastic materials. *Arch. Rat. Mech. Anal.*, 2004.

E. De Giorgi. Congetture riguardanti alcuni problemi di evoluzione. *Duke Math. J.*, 81(2):255–268, 1996.

G. Del Piero. Constitutive equation and compatibility of the external loads for linear elastic masonry–like materials. *Meccanica*, 24:150–162, 1989.

G. Del Piero. Limit analysis and no–tension materials. *Int. J. Plasticity*, 14:259–271, 1998.

F. Derand. *L'architecture des voutes, Cramoisy.* 1643.

C. L. Dym and I. H. Shames. *Solid Mechanics: a variational approach, Mc Graw Hill.* 1973.

M. Epstein. On the wrinkling of anisotropic elastic membranes. *J. Elast.*, 55:99–108, 1999.

Eucentre. Prove murature. 2010. URL `http://www.eucentre.it/provemurature`.

A. Fortunato. Elastic solutions for masonry-like panels. *J. Elas.*, 98:87–110, 2010.

M. Giaquinta and E. Giusti. Researches on the equilibrium of masonry structures. *Arch. Rational Mech. Analysis*, 88:359–392, 1985. ISSN 0950-2289.

E. M. Gurtin. *The linear theory of elasticity, in Handbuch der Physik, band VIa/2, Springer-Verlag.* 1972.

J. Heyman. *The stone skeleton: structural engineering of masonry architecture.* Cambridge University Press, 1995.

S. Huerta. Arcos, bovedas y cupulas. geometria y equilibrio en el calculo tradicional de estructuras de fabrica. *Report: Instituto Juan de Herrera*, 2004 (in Spanish).

S. Huerta. The analysis of masonry architecture: a historical approach. *Arch. Sc. Review*, 51(4):297–328, 2008.

C. T. Kelley. *Iterative Methods for Optimization", Frontiers in Applied Mathematics 18, SIAM.* 1999.

E. Kreyszig. *Introductory Functional Analysis with Applications, John Wiley.* 1989.

C. Padovani M. Lucchesi and N. Zani. Masonry-like solids with bounded compressive stress. *Int. J. Solids Struct.*, 33 (14):1961–1964, 1996.

M. Šilhavý M. Lucchesi and N. Zani. Singular equilibrated stress fields for no-tension panels. In *Lecture Notes in Applied and Computational Mechanics, 23, Springer*, pages 255–265, 2005.

G. Pasquinelli M. Lucchesi, C. Padovani and N. Zani. *Masonry constructions: mechanical models and numerical applications, Lecture Notes in Applied and Computational Mechanics 39, Springer.* 2008.

E. H. Mansfield. Tension field theory. In *Proc. 12th Int. Cong. App. Mech., M. Hetenyi and W. G. Vincenti (eds.), Springer*, 1969.

E. H. Mansfield. *The bending and stretching of plates, Cambridge University Press.* 1989.

E. Mery. Memoire sur l'equilibre des voutes en berceau. *Annales des pontes et chausees*, 1 (2):50–57, 1840.

A. Mielke and M. Ortiz. A class of minimum principles for characterizing the trajectories and the relaxation of dissipative systems. *ESAIM Control Optim. Calc. Var.*, 14 (3):494–516, 2008.

M. Ortiz and J. C. Simo. An analysis of a new class of integration algorithms for elastoplastic constitutive relations. *Int. J. Numer. Methods Eng.*, 23 (3):353–366, 1986.

D. J. Steigmann. Tension–field theory. *Proc. R. Soc. Lond. A*, 429:141–173, 1990.

R. Temam and G. Strang. Functions of bounded deformation. *Arch. Rat. Mech. Anal.*, 75 (1):57–73, 1994. ISSN 1980.

S. Timoshenko and J. N. Goodier. *Theory of elasticity, Mc Graw Hill.* 1951.

Y. W. Wong and S. Pellegrino. Wrinkled membranes ii: analytical models. *J. Mech. Mater. Struct.*, 1:27–60, 2006.